

See discussions, stats, and author profiles for this publication at: <https://www.researchgate.net/publication/266201748>

Water Stability and Adsorption in Metal–Organic Frameworks

ARTICLE *in* CHEMICAL REVIEWS · SEPTEMBER 2014

Impact Factor: 46.57 · DOI: 10.1021/cr5002589

CITATIONS

67

READS

382

3 AUTHORS, INCLUDING:



Nicholas Burch

Georgia Institute of Technology

8 PUBLICATIONS 135 CITATIONS

[SEE PROFILE](#)



Himanshu Jasuja

Georgia Institute of Technology

16 PUBLICATIONS 471 CITATIONS

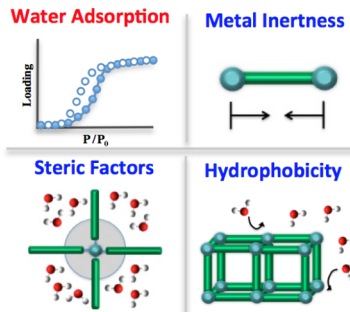
[SEE PROFILE](#)

Water Stability and Adsorption in Metal–Organic Frameworks

Nicholas C. Burtch, Himanshu Jasuja, and Krista S. Walton*

School of Chemical & Biomolecular Engineering, Georgia Institute of Technology, 311 First Drive NW, Atlanta, Georgia 30332, United States

Supporting Information



5.2. Approaches to Impart Water Stability

6. Concluding Remarks and Outlook

Associated Content

Supporting Information

Author Information

Corresponding Author

Notes

Biographies

Acknowledgments

Abbreviations

References

AC

AE

AF

AF

AF

AF

AF

AF

AF

AG

CONTENTS

1. Introduction
 - 1.1. Defining Water Stability
 - 1.1.1. Experimental Characterization Methods
 - 1.1.2. Practical Definitions
 - 1.2. Classical Definition of Isotherm and Hysteresis Types
 - 1.3. Water Adsorption Behavior in Traditional Adsorbents
2. Water Adsorption in MOFs
 - 2.1. Single Component Water Vapor Adsorption
 - 2.1.1. Flexible Behavior
 - 2.2. Multicomponent Adsorption
 - 2.2.1. CO₂
 - 2.2.2. Other Gases and Vapors
 - 2.3. Aqueous Phase Adsorption
 - 2.4. Computational Tools for Understanding Water Adsorption
3. Structural Factors Governing Water Stability
 - 3.1. Thermodynamic Stability
 - 3.1.1. Metal–Ligand Bond Strength
 - 3.1.2. Lability with Water
 - 3.2. Kinetic Stability
 - 3.2.1. Hydrophobicity
 - 3.2.2. Steric Factors
4. Existing MOFs and Their Stability
 - 4.1. Thermodynamically Stable
 - 4.2. High Kinetic Stability
 - 4.3. Low Kinetic Stability
 - 4.4. Unstable
5. Steps to Develop Next-Generation Water-Stable MOFs
 - 5.1. Fundamental Insight into Breakdown Mechanisms
 - 5.1.1. Experimental Techniques
 - 5.1.2. Computational Techniques

A

B

B

B

C

D

E

K

M

M

O

P

Q

T

T

U

V

V

V

W

W

X

X

X

AA

AA

AA

AB

1. INTRODUCTION

The ability to synthesize porous metal–organic frameworks (MOFs) with prescribed structural features (Figure 1) has led to



Figure 1. Flexible assembly process of MOFs from metal nodes and organic linkers.

intense interest in the materials for selective adsorption processes. The hybrid nature of MOFs provides an almost infinite set of building blocks that can be manipulated to target specific adsorption behavior by introducing open metal sites and functional groups into the structure, or by further modulating the properties by postsynthetic modification.^{1–6} To date, much of the experimental and theoretical research on MOF applications has centered on adsorption simulations and measurements, and MOFs have shown high loadings and selectivities for various target gases. Investigations of gas storage (hydrogen/methane) and carbon dioxide capture from flue gas have been a particular focus.^{7–10}

MOF behavior in the presence of water is a topic of significant importance when considering these materials for adsorption applications. Water vapor is ubiquitous in various industrial streams and must be accounted for when selecting adsorbents for adsorption separation and purification systems (Figure 2). Natural gas streams are often saturated with water vapor that must be removed to ppm levels before use or storage.¹¹ Water vapor is also present in most air pollution control problems

Received: May 14, 2014

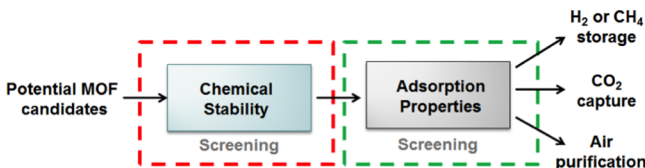


Figure 2. Importance of water stability for real world MOF applications.

including the removal of volatile organic chemicals and toxic industrial chemicals.^{12,13} In air separation units, the air compressor outlet often contains up to 40% relative humidity (RH) that adsorbs strongly on the adsorbent used in the system and interferes with the process.¹⁴ Water vapor is also a major component of industrial flue gas (~10%) and cannot be neglected when examining adsorbents for CO₂ capture. Significant water vapor is also present in biofuel streams, and the dehydration step can require an energy level that exceeds the amount of energy that is ultimately released by the combustion process.¹⁵ Clearly, when considering new materials for adsorption separation systems, the stability and behavior of an adsorbent in humid environments is a critical property that must be considered along with the more obvious high adsorption loadings and selectivities for the target molecule.

The water sensitivity of certain MOFs has been well-documented, and stability in process environments is widely considered to be a major challenge for the field from an applications perspective. One of the first water adsorption isotherm studies for MOFs appeared in the literature in 2002. Only 2–3 studies per year were reported after that until 2012, when studies began appearing at a much more rapid pace. MOFs receiving the most attention over the past decade include Cu-BTC (HKUST-1), MIL-100, MIL-101, MIL-53, MOF-74/CPO-27, UiO-66, and ZIF-8. In this work, we review the totality of the water adsorption literature for MOFs, including experiments, simulations, multicomponent systems, and characterization. A particular emphasis will be given to defining the different types of stability and the structural features that control the behavior.

Since 2012, as more researchers have begun to address water adsorption and/or humidity exposure in MOFs, several features have emerged as being critical contributors to MOF stability. These features include the basicity of the organic ligand, the extent of coordination between the metal and ligand, and shielding of coordination sites by functional groups. MOF performance in humid environments can be a decisive factor in the ability to use these materials as adsorbents, and understanding the parameters that contribute to this sensitivity is critical for elevating MOFs to the applied level. With the high quantity and diversity of MOF structures, it is reasonable to expect that while some structures are unstable in the presence of water vapor, a considerable number of stable MOFs must also exist.

Water stability will be a defining topic in determining whether real-world applications are realized using MOFs. In this first comprehensive review on the subject, we will provide the reader with a complete overview of water adsorption behavior in metal–organic frameworks and, from this information, develop a set of structural criteria for classifying this behavior and the subsequent effects on stability. In the remaining portions of section 1, we will define the characterization methods used to quantify water stability, discuss the limitations of the various approaches, describe isotherm and hysteresis types, and compare water adsorption behavior in MOFs with zeolites and activated

carbons. Section 2 discusses water adsorption experiments in MOFs for single component and multicomponent water vapor, and for the liquid phase. Computational tools for understanding water adsorption will also be introduced. The remaining sections will focus on a full classification of features that contribute to water stability (section 3), including thermodynamic and kinetic factors, applying these classifications to existing MOFs (section 4), and discussing synthetic techniques and approaches for understanding and improving the water stability of future MOFs (section 5). Section 6 will provide an outlook on the current state of MOF water stability as a whole.

1.1. Defining Water Stability

1.1.1. Experimental Characterization Methods. The simplest method for determining the stability of a crystalline material is to expose it to a prescribed amount of water vapor and compare the post-exposure powder X-ray diffraction pattern to the pristine sample. This method works well as a first-pass evaluation of stability, but a sample with an unchanged PXRD pattern can still display a significant loss in porosity and surface area or additional amorphous character not captured by this technique. Thus, measuring nitrogen adsorption on the water-exposed MOF at 77 K and calculating the BET surface area are important follow-up methods to more thoroughly determine if the MOF is stable or not. Furthermore, if the MOF is being considered for aqueous phase applications, one should also investigate whether the sample exhibits mass loss after filtration due to partial dissolution of the solid phase. However, each of these simple methods provides no information on the mechanisms involved in the structural stability or instability, and more sophisticated techniques are required to obtain this insight. These will be discussed in detail in section 5.

The carrier gas used to introduce water vapor into the system should also be carefully considered. The choice of carrier depends on the type of information the investigator is trying to obtain. If the goal is to understand stability after exposure to ambient conditions, then air should be used as a carrier. If the goal is to truly isolate the impact of water adsorption on the structure, then inert carrier gases (N₂, He) are a reasonable choice. Another option is to perform the water adsorption measurements by introducing a set partial pressure of water vapor into a system under vacuum. Such measurements will yield a true adsorption isotherm for water without any unnecessary interference from a carrier gas. The choice of carrier gas versus no carrier gas is generally dictated by the type of instrument employed in the measurements.

1.1.2. Practical Definitions. Within the context of adsorption applications, a person asking the generic question “is the material water-stable?” generally wants to know if they can handle the material in laboratory air, expose it to reasonable amounts of humidity, and expect the structure to remain porous. Thus, the simple PXRD and BET surface area test described above, using air as the carrier, is adequate for determining the stability. However, there are different levels of water stability that are needed for different applications. For example, adsorbents used in single-pass filters need only remain stable for a single feed step until the cartridge is saturated. On the other hand, other adsorption separation systems (e.g., flue gas treatment, air separation, gas purification) will require that the material return as closely to its original form as possible at the end of each cycle. Liquid phase separations present even more stringent stability needs, and many MOFs that show good stability under humid environments degrade completely in aqueous systems. Thus, it is

Table 1. Minimum Testing Conditions and Characterization Guidelines Needed To Ascertain the Stability of MOFs for Select Applications

Application	Testing Conditions	Postcharacterization
Gas or Vapor Phase		
One-Time Use		
single-pass cartridge (gas mask or air filter)	prolonged stability in ambient air	PXRD and BET analysis
Multiple Use		
industrial separations (CO_2 , O_2 , H_2 , etc.)	cyclic exposure to relevant gas mixture; subsequent regeneration via pressure or temperature swing	PXRD and BET analysis; change in cyclic adsorption capacity
gas storage (CH_4 , H_2 , CO_2)	prolonged stability under relevant storage conditions	PXRD and BET analysis
membrane or thin films	prolonged stability under relevant application conditions	PXRD and BET analysis; SEM, TEM, or AFM surface analysis
Aqueous Phase		
catalysis, drug delivery, liquid separations, etc.	immersion and stirring under relevant aqueous conditions	PXRD and BET analysis; solid phase mass loss after sample filtration

important to understand the range of stability in MOFs to facilitate proper selection of materials depending on the intended application. For this reason, we present minimum characterization guidelines in Table 1 to be used by researchers seeking to make claims as to the suitability of their materials for certain applications. It should also be noted that many gas adsorption applications involve gases such as SO_x , NO_x , etc., that may also contribute to the instability of the MOF framework. The effect of acid gases on the structural integrity of MOFs is an important topic, but one that has not been studied as in-depth as water effects and, thus, is outside the scope of this review.

1.2. Classical Definition of Isotherm and Hysteresis Types

Recommendations on the definition of adsorption isotherm and hysteresis types were outlined by an IUPAC report in 1985.¹⁶ A new IUPAC task group has been recently convened and charged with revising this 1985 report to update classifications of pore size, isotherm types, and hysteresis loops. This new report is not yet available but should be released in late 2014 or early 2015.¹⁷ For the purposes of this review, we will adhere to the 1985 classifications as shown in Figure 3.

Three isotherm types are associated with reversible adsorption: types I, II, and III. Type I isotherms are concave to the pressure axis and approach a limiting adsorption saturation loading as the relative pressure (P/P_0) approaches 1. Adsorbents displaying type I isotherms are typically microporous with strong

adsorbate–adsorbent interactions. The saturation value is controlled by the accessible pore volume. Type II isotherms are typically obtained from nonporous or macroporous materials and are characterized by unrestricted monolayer–multilayer adsorption. The type III isotherm is essentially the inverse of the type I isotherm. The adsorption is reversible, and the isotherm is convex to the pressure axis. This is a relatively uncommon adsorption isotherm type that results when the adsorbate–adsorbate interactions are much stronger than adsorbate–adsorbent interactions.

The type IV isotherm is irreversible and is characterized by a hysteresis loop that is associated with capillary condensation occurring in mesopores ($>20\text{ \AA}$ diameter). The low-pressure region of the isotherm follows similar adsorption mechanisms as the type II system. It is important to note the difference between capillary condensation and pore filling, as these are sometimes used interchangeably. According to the IUPAC definition, capillary condensation occurs when a liquid-like phase fills the empty pore space remaining after multilayer adsorption has completed on the walls/surfaces of a mesoporous material. Capillary condensation is distinct from micropore filling, which occurs in materials with pore diameters $<20\text{ \AA}$ and is often completely reversible as in the case of type I isotherms.

Type V isotherms are generally uncommon. The adsorption branch is controlled by similar mechanisms as type III isotherms (weak adsorbent–adsorbate interactions), but hysteresis is observed upon desorption. Lastly, type VI isotherms indicate stepwise multilayer adsorption on a uniform nonporous surface. Typical examples of this type are argon or krypton adsorbed on graphitized carbon black at 77 K.

Hysteresis types have also been classified (Figure 3), but these classifications appear in the literature less often than isotherm types. True hysteresis is typically associated with capillary condensation in mesoporous materials and can exhibit a wide range of shapes. The two extremes of hysteretic behavior are the H1 and H4 hysteresis types. In H1, the adsorption and desorption branches are almost vertical and approximately parallel over a large range of adsorption loadings. Type H4 hysteresis loops remain almost horizontal and parallel over a large relative pressure range. Types H2 and H3 fall between these two extremes. For some microporous materials, it is possible that the hysteresis loop will never “close”, with appreciable adsorbate loadings remaining in the pore space at a concentration or pressure near zero. In this case, high temperature will be needed to fully desorb the molecules. This behavior was traditionally associated with swelling of nonrigid porous structures or with

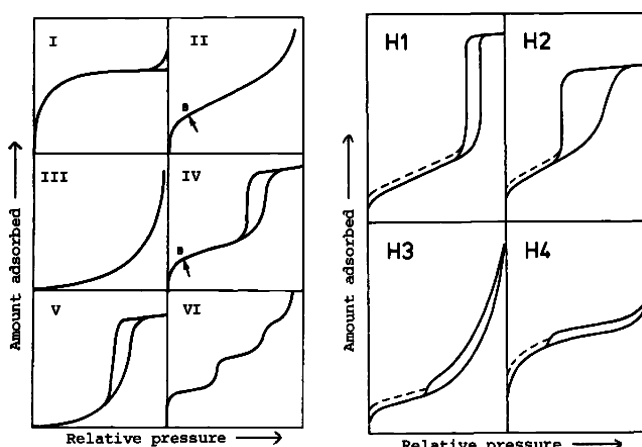


Figure 3. IUPAC classification of adsorption isotherm (left) and hysteresis (right) types. Reprinted with permission from ref 16. Copyright 1985 Wiley-Blackwell.

irreversible adsorption of molecules in pores of approximately the same size as the molecule.

The majority of metal–organic frameworks are microporous, and adsorption of many permanent gases follows the expected type I isotherm classification. However, MOFs are also known to exhibit unusual hybrids of the isotherm types. For example, MOFs with larger pores can display a type III isotherm shape at low pressure that then transitions into a type I isotherm with the expected “knee” in the curve at higher pressures. Flexible MOFs show even more varied isotherm behavior, such as the adsorption behavior observed in MIL-53 materials.¹⁸ In this case, the isotherm may resemble the type IV case, but the adsorption mechanisms are quite different than the cases originally described as type IV. The updated IUPAC report to be released later this year should address these differences.

For a porous material with good stability, the shape of the water vapor isotherm can provide direct information on the hydrophobicity or hydrophilicity of the material. A classical definition of a hydrophilic material is a substance with high affinity for water, but when applied to porous materials, this definition becomes less clear. For example, mesoporous silicas such as MCM-41 and SBA-15 are classified as hydrophobic but actually adsorb more water than microporous zeolites, which are largely hydrophilic. This seemingly conflicting behavior can occur because the water adsorption loadings are dictated by pore volume. For adsorbents, it is generally accepted that the hydrophilicity of a material can be determined on the basis of the selectivity of the material for water over other components in a mixture. Water adsorption loadings at low pressure can also be used to determine relative hydrophobicity among adsorbents. As shown in Figure 4, the hydrophilicity of adsorbent (a) is greater

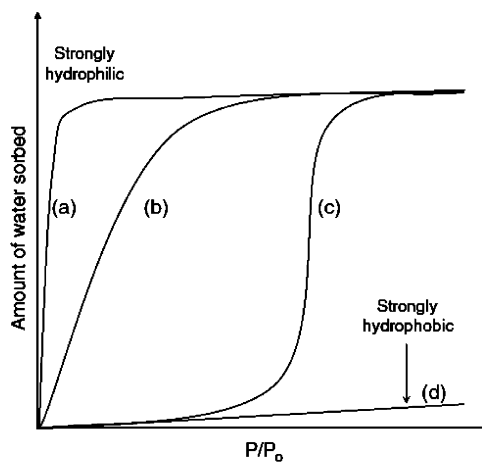


Figure 4. Water adsorption isotherms for adsorbents with different hydrophilicities near room temperature over the 0–1 P/P_0 domain. Reprinted from ref 19, Copyright 2008, with permission from Elsevier.

than adsorbent (b) due to the sharpness of the type I isotherm for (a). On the other hand, adsorbent (c) exhibits a type V isotherm with very low water adsorption throughout the low-pressure region, suggesting weak hydrophobicity, but eventually adsorbs similar loadings as adsorbents (a) and (b); this indicates similar pore volumes among the three materials. Adsorbent (d) is strongly hydrophobic and adsorbs very little water over the entire relative pressure range.

1.3. Water Adsorption Behavior in Traditional Adsorbents

In general, there are no perfectly hydrophobic adsorbents because most surfaces will contain a nonzero quantity of hydrophilic adsorption sites. These sites are introduced from defects, impurities, or dopants, and are present in various forms in both zeolites and activated carbons. Silica gel is one of the most well-studied silica-based adsorbents for water adsorption behavior.¹⁹ It is known to exhibit a type V water isotherm, but silanol groups present on the surface can hydrogen bond with water, leading to hydrophilic adsorption behavior. Tuning the functional groups during synthesis provides a method for tuning the hydrophilicity of the final adsorbent. Water loadings approach 45 wt % at 100% RH and 25 °C for commercial silica gels.²⁰

Zeolite molecular sieves such as the commercially important faujasite (FAU) and LTA aluminosilicates are well-known hydrophilic adsorbents due to extra-framework charge-balancing cations and frameworks that are electrostatically charged. Because of this abundance of preferred adsorption sites, water adsorption isotherms are typically of the type I form. For example, MgA (LTA structure) adsorbs approximately 42 wt % water at saturation.²¹ However, these strong adsorption sites also make it difficult to desorb the water. Zeolites are often dehydrated at temperatures exceeding 200 °C due to the strong adsorbent–water interactions. This capacity is also a function of the cation size. NaA possesses the same LTA ring size as MgA, but the replacement of two Na^+ cations by the smaller Mg^{2+} cation enlarges the accessible pore volume and leads to a 50% increase in water adsorption capacity (42 wt %) compared to NaA (29 wt %).²¹ These same water adsorption trends are observed for alkali metal exchanged ZSM-5 zeolites. Mesoporous materials including MCM-48, SBA-15, KIT-1, etc., show type V water isotherms (Figure 5).¹⁹ The pressure at which the onset of

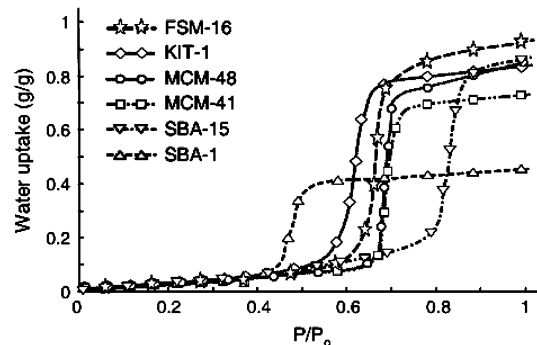


Figure 5. Water adsorption isotherms at 298 K for adsorbents with different mesoporous silicas. Reprinted from ref 19, Copyright 2008, with permission from Elsevier.

capillary condensation occurs is dictated by the pore size of the material. Saturation capacities are generally higher than those measured for microporous zeolites. For example, SBA-15 adsorbs 81 wt % water at 90% RH and 25 °C.²² Activated carbons also show type V behavior unless they possess highly oxidized surfaces, which cause the material to exhibit type IV behavior instead.^{11,23}

MOFs are often compared to microporous zeolites in terms of gas adsorption behavior, and many similarities can be observed between open metal site behavior of MOFs and exchangeable cations in zeolites. These similarities do not in general extend to hydrothermal stability as zeolites are well-known to display

excellent water stability over a broad temperature range compared to MOFs. This point is not particularly surprising because zeolites are purely inorganic materials and should display better stability than the inorganic–organic MOF structures. Nevertheless, even zeolites have hydrothermal stability limits, and aluminosilicates such as HZSM-5 and SBA-15 can undergo dealumination under steaming at elevated temperatures, leading to structural changes.^{24,25} A full assessment of water adsorption behavior in zeolites and silicas is outside the scope of this review. The reader is instead referred to a comprehensive review by Ng and Mintova.¹⁹

2. WATER ADSORPTION IN MOFS

2.1. Single Component Water Vapor Adsorption

As discussed in section 1.2, the shape of an adsorption isotherm can provide important details on the strength and type of interaction between the adsorbate molecule and adsorbent surface. However, to ascertain these details from the isotherm, the adsorbent must maintain its structure during the measurement. This section will highlight water adsorption behavior in MOFs possessing good to moderate structural stability.

Bülow and co-workers published one of the earliest studies of water adsorption in MOFs in 2002, including the first water adsorption isotherm reported for HKUST-1 (Cu-BTC).²⁶ HKUST-1 is a well-known open-metal site MOF that possesses a bimodal pore size distribution.²⁷ The main pore diameter is approximately 9 Å, and the smaller pockets are about 6 Å in diameter. The coordinatively unsaturated copper sites are accessible from the main pore only, rendering it hydrophilic compared to the small pores that are surrounded by benzene rings. In 2009, Kaskel and co-workers published a more in-depth study of water adsorption in HKUST-1, along with several other MOFs.²⁸ Consistent with Bülow and co-workers,²⁶ they found that HKUST-1 exhibits a water isotherm of approximately the type I form. The open metal sites adsorb water preferentially into the hydrophilic main pore at low relative pressure (P/P_0), and the MOF eventually achieves a saturation loading of approximately 25 mol/kg (45 wt %). This behavior is analogous to that of microporous zeolites as shown in Figure 6. Zeolites 5A and 13X display type I water isotherms with saturation capacities of approximately 15 mol/kg (29 wt %).²⁹ The lower saturation capacities of the zeolites relative to HKUST-1 are a consequence

of lower pore volumes. However, nitrogen adsorption analysis showed that the water-exposed HKUST-1 loses approximately 50% of the original surface area. Liang et al.³⁰ and Schoenecker et al.³¹ also reported similar behavior for water adsorption in HKUST-1.

Henninger et al.^{32,33} performed water adsorption cycling studies on HKUST-1 and, consistent with previous equilibrium isotherm studies, found that severe degradation occurs over the various cycles. After 20 cycles of water adsorption between 40 and 140 °C, 53% of the capacity was lost. However, Li and Yang showed that HKUST-1 is stable at 40% RH for 7 days in air.³⁴ DeCoste et al. performed detailed aging studies of HKUST-1 along with Mg-MOF-74, which decomposed under all conditions.³⁵ Consistent with the work of Li and Yang,³⁴ they found that HKUST-1 shows no structural change after exposure to 40% RH at 40 °C for up to 14 days. However, at 40 °C and 90% RH, the PXRD looks similar to the decomposed 25 °C sample, and the porosity and surface area are completely lost. This stability behavior can be better understood through a 2011 solid state NMR study, which followed the structural changes upon exposure to water.³⁶ HKUST-1 was found to maintain structural integrity with water content up to 0.5 mol equiv with respect to copper, but decomposition occurred at higher water content.

The MIL-100 series of materials has also been extensively studied for water adsorption and cyclic stability.^{28,37–41} Three isostructures have been the main focus of these studies: MIL-100(Fe), MIL-100(Cr), and MIL-100(Al). The framework is a three-dimensional system of mesopores formed from octahedra of M^{3+} trimers ($M = Fe, Al, Cr$) connected by oxygen atoms from the 1,3,5-benzenetricarboxylate (BTC) ligand. This structure possesses mesopores of 25 and 29 Å that are accessible through microporous windows of 5.5 and 8.6 Å, respectively.⁴² MIL-100(Fe) possesses a BET surface area of approximately 2000 m²/g and a pore volume of 1.0 cm³/g.³⁷ The water isotherm for MIL-100(Fe) is known to exhibit well-defined steps at approximately $P/P_0 = 0.25, 0.40$, and 0.45 before fully saturating at 0.8 g/g. MIL-100(Cr) exhibits similar behavior, and the isotherm resembles type VI form. The standard synthesis uses HF, but Kitagawa et al. synthesized two other types of MIL-100(Cr) using HCl or H₂SO₄ instead of HF to introduce different counterions into the pore system.³⁸ The water isotherms display similar steps as the HF version, but the slope of the curve differs. MIL-100(Cr) shows almost an identical isotherm shape to MIL-100(Fe)²⁸ and saturates around 0.8 g/g as well. At relative pressures below 0.25, adsorption occurs around the hydrophilic open metal sites. At higher relative pressures, capillary condensation occurs in steps associated with filling of the smaller mesopore first and subsequent filling of the larger pore. Full saturation is reached at relative pressures >0.5 .

Jeremias et al.³⁷ evaluated MIL-100(Al and Fe forms) as water adsorbents for heat pump or adsorption chiller applications. These MIL materials are synthesized under harsh conditions, where the pH is equal to 0.6 or 1, and temperature is 210 or 150 °C for MIL-100(Al) and MIL-100(Fe), respectively. So, good water stability could be expected. MIL-100(Al) exhibits a similar isotherm shape as the Fe version, but full saturation capacity is lower. In this study,³⁷ the measured pore volume for MIL-100(Al) is 0.65 cm³/g compared to 0.87 cm³/g for the Fe form, even though the materials are isostructural. The smaller pore volume for the Al version could be due to incomplete activation/removal of unreacted ligand. Isosteric heats of adsorption for the Fe and Cr versions of MIL-100 were found to be approximately

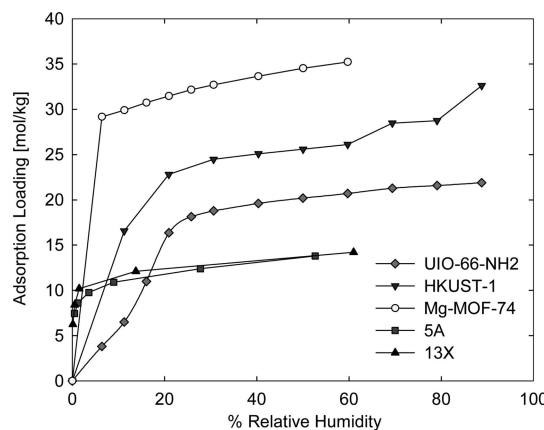


Figure 6. Water adsorption isotherms for UIO-66-NH₂, HKUST-1, and Mg-MOF-74 compared with zeolites 5A and 13X from the work of Wang et al.,²⁹ all at 298 K. Reprinted from ref 31. Copyright 2012 American Chemical Society.

48 kJ/mol for both.^{28,38} These values compare favorably with silica gel, which exhibits an isosteric heat of 47.6 kJ/mol for water.⁴³

Hydrothermal cyclic stabilities were assessed for both MIL-100(Al) and MIL-100(Fe) using 5.6 kPa of water in argon as carrier.³⁷ The samples were cycled between 40 and 140 °C for 40 cycles at 5 h per cycle, as shown in Figure 7. Porosity and surface

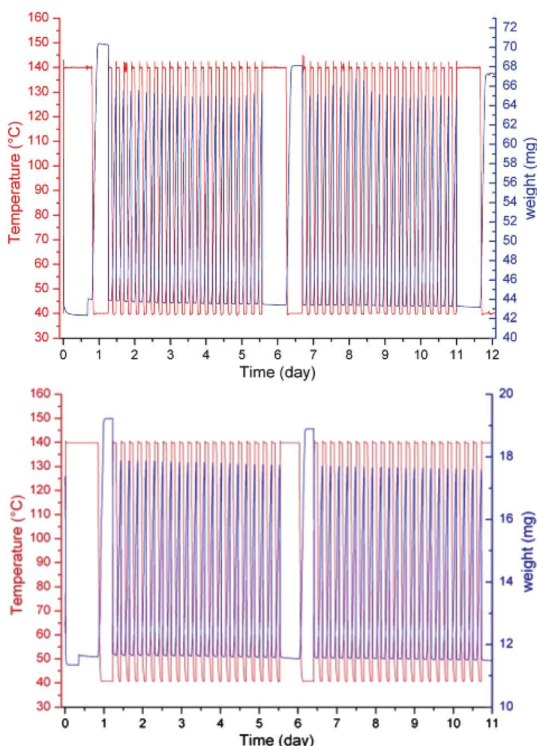


Figure 7. Temperature profile and load signal of the MIL-100(Al, upper, and Fe, lower graph) cycling experiment, acquired at $p = 5.6$ kPa. Reprinted with permission from ref 37. Copyright 2012 Royal Society of Chemistry.

area remained essentially unchanged after the 40 cycles, with only 2–6% loss in surface area, and the loss in water capacity was negligible. Pirngruber et al. showed that MIL-100(Cr) also exhibits good cycling stability for water in a N₂ carrier.³⁹ Seo et al. evaluated MIL-100(Fe) as a water adsorbent for dehumidification systems.⁴⁴ Consistent with other studies, MIL-100(Fe) has remarkable stability to water vapor at elevated temperatures and also maintains stability after boiling in water for up to 7 days.⁴⁴ The highly charged trivalent metals (M^{3+}) used to assemble the structure lead to a strong metal–ligand bond that results in excellent stability. At 30 °C, MIL-100(Cr) adsorbs water with a loading that is approximately 2.5 times higher than NaX and SAPO-34, which are commercially used water adsorbents. The cycling rates, usually controlled by the desorption step, were found to be much faster for the MIL-100 materials compared to commercial zeolites and silica gel, which could provide great advantages for dehumidification applications. De Lange et al. studied water adsorption using a combined experimental/simulation approach and found that, at low loadings, MOF–water interactions dominate, and water–water interactions dominate at higher loadings.⁴⁵ MIL-125-NH₂ is synthesized from titanium(IV) isopropoxide and also displays high stability and reproducible adsorption and desorption isotherms after many water isobar cycles.^{46–48}

MIL-101(Cr) is a mesoporous MOF⁴⁹ with two types of cages of 29 and 34 Å diameter that are accessible through 12 and 16 Å openings. The supertetrahedral unit is made up of three chromium trimers that are connected through terephthalate linkers (BDC). The surface area of this material exceeds 4000 m²/g, and it possesses among the largest pore volumes of MOF materials. MIL-101(Cr) exhibits a strong type V water isotherm, indicating poor interaction energy between water and the MOF.^{28,33,50–52} A hysteresis loop of type H2 is also observed. Capillary condensation occurs at a relative pressure of approximately 0.4. Similar to MIL-100(Cr), MIL-101(Cr) is highly stable and even maintains its BET surface area and PXRD pattern after immersion in boiling water for 1 week.^{44,53} Consistent with its large pore volume, MIL-101(Cr) can adsorb a remarkable 1.3 g/g of water at saturation and 25 °C.^{28,33,51} The isotherm behavior for MIL-101(Cr) matches closely to that of SBA-1,¹⁹ which is a mesoporous silica with pores of 21 Å diameter. Capillary condensation for both materials occurs at approximately 40% RH. However, the saturation capacity is much higher for MIL-101(Cr) (1.3 g/g) compared to SBA-1 (0.45 g/g) due to differences in pore volume; SBA-1 has a pore volume of approximately 0.8 cm³/g. Kusgens et al. point out that, even with this remarkable uptake of water, which presumably fills the pore space, calculating pore volume using water will always result in a value that is smaller than the pore volume calculated from N₂ adsorption at 77 K.²⁸ The reason is because water adsorbs first on hydrophilic sites within the MOF, similar to zeolites. The water molecules then cluster with each other through H-bridging to form smaller water clusters. As these clusters grow, they eventually join with the clusters on the other side of the pore. However, unfilled space remains around the hydrophobic area. Thus, pore volume calculation based on this will not account for the full space. Nevertheless, it can be a good measure of hydrophobicity and hydrophilicity because a strongly hydrophobic material will show almost zero pore volume when calculated on the basis of water.

Ehrenmann et al. evaluated MIL-101(Cr) for heat pumps/adsorption chiller applications and found that this is one of the most promising MOFs for such applications.⁵⁰ After 40 cycles, the material maintained 96.8% of the initial loading. The BET surface area of the cycled sample only decreased by 0.5% relative to the untreated sample. The heat of adsorption was determined from TG/DSC to be 46.0–47.2 kJ/mol, which compared well with a previous estimation²⁸ of 45.13 kJ/mol determined from the Clausius–Clapeyron equation. Note that these values are lower compared to MIL-100, which is expected because MIL-101 is a larger-pore material than MIL-100. Akiyama et al. evaluated the effect of functional groups on water adsorption behavior in MIL-101(Cr).⁵¹ This MOF was made using BDC functionalized with three different groups: NO₂, NH₂, and SO₃H. The parent and functionalized materials had surface areas of 3124, 2146, 2509, and 1920 m²/g, respectively. The functional groups take up pore space, so it is not surprising that the surface area decreases slightly with functional group size. At saturation, the water loadings follow the surface area trends. With the exception of the NO₂ group, the functionalized versions undergo pore filling at lower relative pressures compared to the unfunctionalized form because these are hydrophilic groups that will attract the water at lower relative pressure (Figure 8). Water can be desorbed at 353 K without need of high vacuum. In general, these MOFs load more than 4 times the maximum loading of conventionally used zeolites in this application.³³ However, capillary condensation occurs at relative pressure >0.35, which may reduce the working

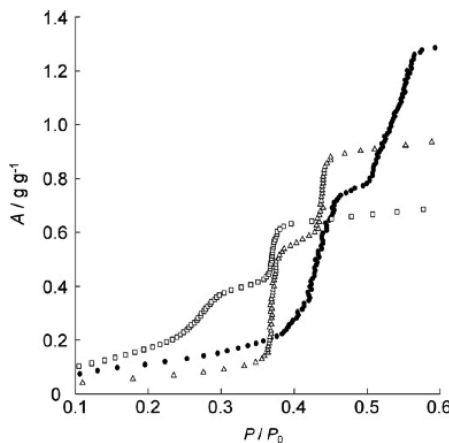


Figure 8. Water adsorption isotherms at 298 K for desolvated MIL-101(Cr) (●), MIL-101-NH₂(Cr) (△), and MIL-101-SO₃H(Cr) (□). Reprinted from ref 51, Copyright 2012, with permission from Elsevier.

capacity within a cyclic process. Nevertheless, MOFs offer an advantage over zeolites due to the ability to more easily vary the hydrophilicity of the framework. Seo et al. also showed that MIL-101(Cr) is a promising candidate for dehumidification applications due to very high water loadings and cyclic stability.⁴⁴ Khutia et al. examined NH₂ and NO₂ functionalized MIL-101(Cr) along with versions that were approximately 78 mol % functionalized.⁵² The goal of adding these groups was to shift the pore filling from P/P_0 of 0.4 to lower relative pressures. The NH₂ samples maintained good stability after 40 adsorption/desorption cycles with only 6.3% loss in surface area (BET). However, the NO₂ version lost about 25% for the fully functionalized material and 20% for the 78% functionalized material. This surface area loss after water adsorption cycles was attributed to the electron withdrawing capability of this group that decreases the inertness of the chromium–carboxylate coordination. In general, these groups do not shift the capillary condensation step appreciably because MIL-101(Cr) pores are so large; one would need much bulkier functional groups to truly affect the condensation step's location.

Kaskel and co-workers have presented water adsorption behavior for a variety of MOFs known as "DUT" materials. DUT-4 (Al(OH)(2,6-NDC)) is assembled by aluminum coordinated to six oxygen atoms in an octahedral manner, where the octahedron is slightly distorted. Hydroxyl groups axially bridge the octahedral. Resulting chains are connected by the 2,6-naphthalenedicarboxylate (2,6-NDC) linker forming a 3D network with channels of $8.5 \times 8.5 \text{ \AA}^2$ in diameter. The material is hydrophobic and adsorbs almost no water until a relative pressure of 0.4.²⁸ It is stable under ambient conditions but will decompose after exposure to humidity >40% and after exposure to liquid water. Comotti et al. also synthesized an Al-NDC material using 1,4-NDC and water as solvent instead of DMF.⁵⁴ This material has two square channels with diameters of 7.7 and 3 Å, respectively. This MOF exhibits a perfect type V isotherm, with pore filling occurring at a relative pressure of 0.4. A strong hysteresis loop resembling the H2 form was also observed, even though those are mainly classified for mesoporous materials that undergo capillary condensation. The well-defined adsorption and desorption isotherms give good indication that the material is stable. Additionally, since the MOF was synthesized in water, it could be expected to display good water stability. Bon et al. presented DUT-51, which was synthesized using bent

dithienothiophene and Zr⁴⁺ or Hf⁴⁺.⁵⁵ The addition of benzoic acid to the reaction as a modulator facilitates the formation of an 8-connected cluster, leading to a new framework that adopts the reo topology. The BET surface areas are 2335 and 1859 m²/g for DUT-51(Zr) and DUT-51(Hf), respectively. The water adsorption isotherm of DUT-51(Zr) exhibits type V form, with pore filling occurring at $P/P_0 > 0.45$, and hysteresis was observed. DUT-67, -68, -69 were also recently synthesized using Zr or Hf but with 2,5-thiophenedicarboxylate as the ligand.⁵⁶ DUT-67 is isostructural to DUT-51. All 3 materials exhibit good structural stability. Water isotherms (Figure 9) show that DUT-67 begins

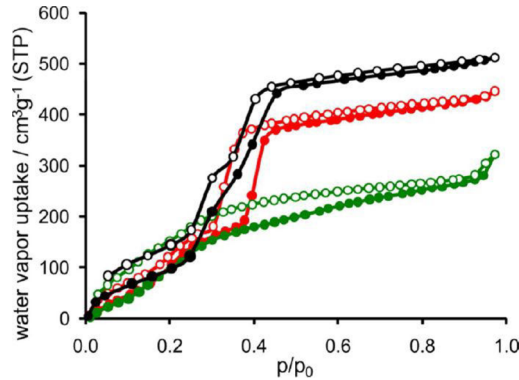


Figure 9. Water vapor adsorption (solid symbols) and desorption (open symbols) isotherms at 298 K of zirconium-based MOFs: black, DUT-67; red, DUT-68; green, DUT-69. Reprinted with permission from ref 56. Copyright 2013 American Chemical Society.

pore filling by a relative pressure of only 0.2, which is earlier than the isostructure DUT-51. However, the pore diameter of DUT-67 is smaller than that of DUT-51, so the earlier pore filling is expected. The isotherm is similar to type IV for both DUT-67 and DUT-68, but DUT-69 exhibits an isotherm approaching type I. However, of the three, only DUT-67 appears to have been nearly fully activated. The other two materials show much lower BET surface areas than expected from geometric calculations. Thus, the water adsorption saturation capacities cannot be compared effectively. DUT-69 is microporous with 5 Å pores, and the type I is expected. DUT-67 has pores of 14.2 Å diameter, and DUT-68 has 27.2 Å diameter pores (which do not seem to be fully open in the activated form). Bon et al. also recently synthesized DUT-52, -53, and -84 using Zr⁴⁺ and Hf⁴⁺ and 2,6-NDC.⁵⁷ DUT-52 is isostructural to UiO-66.⁵⁸ DUT-53 has four linker molecules omitted from the 12-connected SBU. DUT-84 has 6 linkers omitted from the SBU, which causes the topology to switch to a 2D structure. Surface areas are 1399, 1097, 782, and 637 m²/g for DUT-52(Zr), DUT-52(Hf), DUT-53(Hf), and DUT-84(Zr), respectively. These materials are all microporous with pore limiting diameters of 4.26, 8.48, and 7.57 Å for DUT-52, -53, and -84, respectively. Water isotherms are shown in Figure 10. The zirconium forms of DUT-52 and DUT-53 display very similar water isotherms, with low adsorption below $P/P_0 = 0.3$ and then a step in the isotherm develops. The isotherm resembles the water isotherm reported for UiO-66.³¹ DUT-84 has no pronounced step, even though it has a pore limiting diameter that is smaller than DUT-53.

Reinsch et al. presented a family of Al-based isostructures known as CAU-10.⁵⁹ These materials are synthesized in aqueous solvent using the isophthalic acid linker functionalized with CH₃, OCH₃, NO₂, NH₂, or OH. Al is 6-coordinated with oxygen in this compound, and the pore diameters of the resulting material are 7

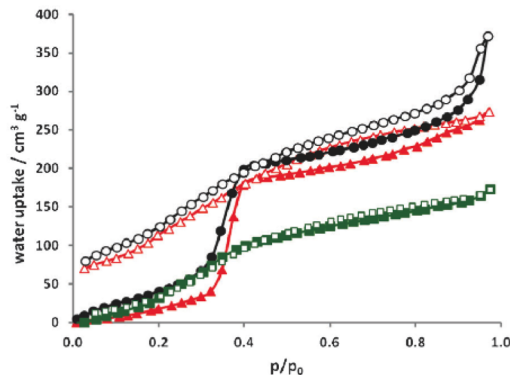


Figure 10. Water vapor physisorption isotherms measured at 298 K: DUT-52(Zr) (black circles), DUT-53(Hf) (red triangles), and DUT-84(Zr) (green squares). Closed symbols, adsorption; open symbols, desorption. Reprinted with permission from ref 57. Copyright 2013 Royal Society of Chemistry.

Å for the parent structure and slightly smaller for the functionalized versions. As shown in Figure 11, these 6 MOFs

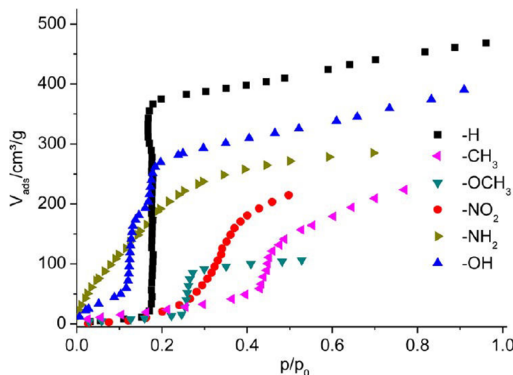


Figure 11. Water vapor isotherms at 298 K for CAU-10-X structures. Reprinted with permission from ref 59. Copyright 2012 American Chemical Society.

display very diverse water adsorption behavior as a function of polarity and size of the functional group. The unfunctionalized CAU-10-H exhibits a type V isotherm, with pore filling occurring around $P/P_0 = 0.2$. However, CAU-10-NH₂ displays a type I water isotherm, and CAU-10-OH is also more hydrophilic compared to the parent material. CAU-10-CH₃ and -OCH₃ are both more hydrophobic than the parent structure as evidenced by the low water adsorption and pore filling at higher relative pressures compared to CAU-10-H. All of these materials maintain crystallinity according to PXRD patterns examined before and after water exposure, but surface areas were not measured postexposure.

Another highly coordinated oxygen-coordinated MOF was reported by Taylor et al.⁶⁰ CALF-25 is a barium-tetraethyl-1,3,6,8-pyrenetetraphosphonate compound, where Ba is 9-coordinated to oxygen from the phosphonates. The 3D material forms channels with diameters of 4.6×3.9 Å² and has a surface area of $385 \text{ m}^2/\text{g}$. CALF-25 appears to be stable at 90% RH up to 353 K according to PXRD results. The water isotherms were measured at temperatures over the range 298–353 K, and all exhibit type III forms. This behavior implies strong hydrophobicity of the pore space, and the stability is attributed to kinetic protective effects of ethyl groups that line the channels.

This kinetic stability is further supported by the fact that CALF-25 breaks down in boiling water. In other work, Čelić et al. presented a zinc trimesate material that is synthesized in a water/ethanol mix.⁶¹ The material Zn₂(BTC)(OH)(H₂O)1.67H₂O is assembled from 1D chains that are made up of ZnO₂(OH)₂ tetrahedral and ZnO₄(OH)(H₂O) octahedral units connected to each other by corner-shared μ_3 -hydroxy bridging groups. These units are further connected by carboxylate groups of BTC moieties to form an extended 3D structure with two types of parallel channels. Only one of the channel types is open, and has a pore diameter of approximately 5 Å. This material exhibits a type I water isotherm due to preferred interactions with the open zinc sites, and reaches a saturation loading of 10 mol/kg (0.18 g/g). The MOF is stable after boiling in water and after 40 cycles of water adsorption. The robustness of the framework is attributed to the geometry of the SBU and connectivity to the structure, where 50% of all zinc atoms are located in an octahedral environment. Ligand displacement is not as favorable for this arrangement compared to the typical tetrahedral Zn–oxygen-based MOFs such as MOF-5^{62–67} and MOF-177.^{63,68,69}

MOFs constructed with nitrogen containing ligands (pyrazoles, pyridines, etc.) tend to exhibit better stability than MOFs assembled from carboxylic acid functionalities. The material known as Zn(BDC)(DABCO) or “Zn-DMOF” is a pillared MOF constructed with Zn-BDC forming 2D sheets that are connected to each other in the third dimension using 4-diazabicyclo[2.2.2]-octane (DABCO). Lee et al. performed a water adsorption study on Zn-DMOF and found no appreciable water adsorption up to relative pressure of 0.4,⁷⁰ and then the MOF is unstable after that point.⁷¹ Tan et al. examined the stability of Cu, Zn, Ni, and Co versions of DMOF using IR, Raman, and PXRD under controlled humidity levels.⁷² They found that, for Zn- and Co-DMOF, DABCO is displaced first and the 2D sheets remain intact. Zn-DMOF has been shown to reassemble to its original 3D structure when DABCO is added back in solvent.⁷³ The Ni version was the most stable of all variations whereas the Cu-O-C bond was found to hydrolyze in the Cu-based structure. Uemura et al. looked at a nitro-functionalized BDC version of Zn-DMOF and found that the structure also shows decomposition and is more hydrophilic than Zn-DMOF.⁷⁴ Jasuja et al. extended this study and evaluated the water adsorption behavior of Zn-DMOF with BDC functionalized with hydroxy, dichloro, naphthalene, anthracene, and tetramethyl groups.⁷⁵ It was found that, for groups that have favorable interactions with water, the MOF degrades at lower humidities compared to the parent DMOF. On the other hand, the nonpolar groups (tetramethyl, anthracene) prevent hydrolysis with the zinc coordination sites to make the structures completely stable. In fact, DMOF-TM can undergo multiple water adsorption cycles without losing structural integrity, but the MOF decomposes completely upon soaking in liquid water (Figure 12).⁷⁶

As shown in Figure 13, the MOFs with these groups adsorb large quantities of water but display approximately type V isotherms, although no hysteresis is observed. DMOF-TM adsorbs 20 mol/kg (0.36 g/g) of water. MOFs made with half TM-BDC and half BDC or with NDC undergo partial decomposition, with 32% and 26% loss in BET surface area, respectively. This study shows that stability can be adjusted up and down, depending on the choice of functional group. Jasuja et al. also showed the impact of catenation and basicity (pK_a) of the pillared ligand on water stability.⁷⁷ Catenation is the interpenetration or interweaving of two or more identical and

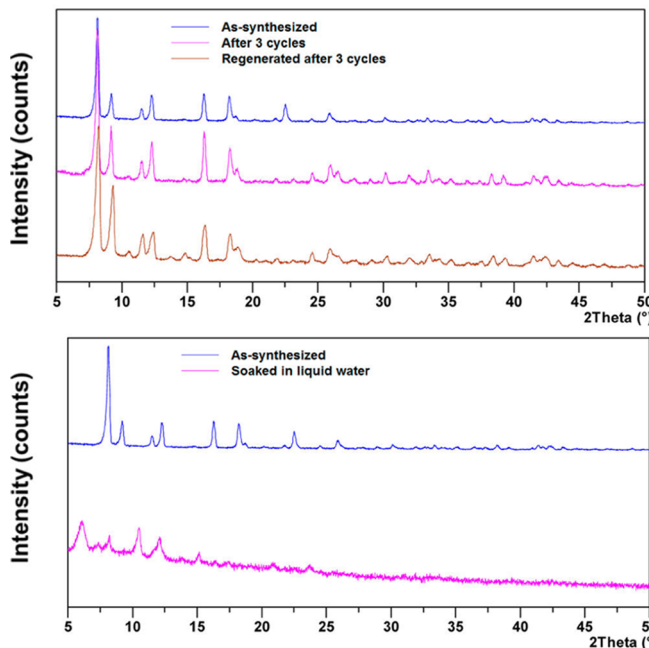


Figure 12. PXRD patterns for DMOF-TM before and after cyclic water vapor adsorption measurements up to 90% RH at 298 K (top) and before and after exposure to liquid water (bottom). Reprinted with permission from ref 76. Copyright 2013 American Chemical Society.

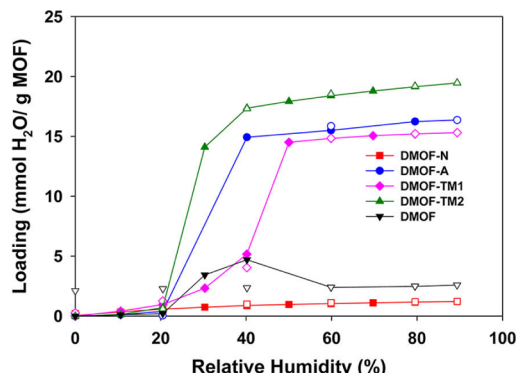


Figure 13. Water vapor adsorption/desorption isotherms at 298 K for desolvated compounds DMOF-N, DMOF-A, DMOF-TM1, and DMOF-TM (closed symbols, adsorption; open symbols, desorption). Lines connecting adsorption points are to guide the eye. Reprinted with permission from ref 76. Copyright 2013 American Chemical Society.

independent frameworks. This work showed that water-stable MOFs can be obtained through catenation even when the pillar ligand has lower basicity (pK_a value). After 90% relative humidity (RH) exposure, in a comparison of DMOF with MOF-508 (which is catenated DMOF where DABCO has been replaced by 4,4'-bipyridine or BPY), MOF-508 is stable due to its 2-fold interpenetration that prevents significant water adsorption. In contrast, in a comparison of the noncatenated isostructural pillared MOFs DMOF-TM (Zn-TMBDC-DABCO) and MOF-508-TM (Zn-TMBDC-BPY), MOF-508-TM is unstable because BPY has a lower pK_a and is less rigid than DABCO.⁷⁷

Other pillared MOFs such as those reported by Kondo et al. are made from Cu-PZDC (2,3-pyrazinedicarboxylate), with the pillared linker being PYR (pyrazine), BPY, or BPE (*trans*-1,2-bis(4-pyridyl)ethylene).⁷⁸ All three MOFs have essentially 1D pores of 6×4 , 6×9 , or $6 \times 11 \text{ \AA}^2$ and display type I isotherms.

Water adsorption saturation capacities increase with pore size/volume and are 12, 17, and 27 wt %, respectively. The water isotherms are completely reversible with no hysteresis observed, which is indicative of physisorption in a microporous material. Hou et al. presented two isostructural MOFs assembled from Ni^{2+} or Co^{2+} and the ligand 3,5-di(pyridine-4-yl)benzoic acid.⁷⁹ These porous MOFs are formed by a building unit in which each metal atom is coordinated by 3 pyridine nitrogen atoms from 3 distinct ligands and 3 oxygen atoms from 2 distinct ligands. The resulting frameworks are 2-fold interpenetrating networks. The water vapor isotherm shows multiple steps, with the first step occurring at 8% RH and the second step occurring slightly later at 19% RH. The saturated loading is approximately 150 cc/g (0.12 g/g). The structure is microporous and cannot adsorb N_2 at 77 K but does adsorb CO_2 at 195 K. PXRD patterns remained unchanged after water exposure, but the porosity was not further confirmed. Padial et al. presented a Ni-pyrazolate-based series of MOFs that are hydrophobic and display type V isotherms.⁸⁰ The mixed carboxylate/pyrazolate systems are sensitive to moisture, but the bipyrazolate-based MOFs are very hydrophobic and have high stability. Consistent with other porous materials, pore filling of water occurs at pressures that increase with the pore size of the material. One of the MOFs was functionalized with CH_3 and CF_3 , and these showed increasing hydrophobicity over the unfunctionalized version. A variety of other MOFs involving mixed coordination modes (oxygen and nitrogen) similar to the pillared MOFs have shown good stability in the presence of water, with adsorption behavior following the expected trends based on hydrophobicity, pore size, and surface area.^{81–89}

Triazole-based MOFs have also exhibited good water stability. For example, the fully nitrogen-coordinated MAF-2, made from Cu^{2+} and the ligand 3,5-diethyl-1,2,4-triazole, is completely hydrophobic, with no water adsorption even at 100% RH, but it readily adsorbs alcohols with type I isotherms and loadings of, e.g., 0.2 g/g for ethanol below 0.2 P/P_0 .⁹⁰ Similarly, FMOF-1 synthesized from Ag^+ and 3,5-bis(trifluoromethyl)-1,2,4-triazolate is highly hydrophobic and adsorbs no water while adsorbing appreciable amounts of alkanes and aromatics.^{91,92} JUC-110, synthesized from Cd^{2+} and (S)-4,5,6,7-tetrahydro-1*H*-imidazo[4,5-*c*]pyridine-6-carboxylate, possesses square 1D channels with diameters of 5 Å. Cd is 4-coordinated with two nitrogens from amino groups, two nitrogens from imidazole rings, and two oxygens from carboxylate groups. This microporous MOF exhibits a type I water isotherm as expected and saturates at a loading of approximately 5.3 mol/kg (0.09 g/g).⁹³ The structure maintains its integrity and also survives boiling water. Burd et al. reported the synthesis of two microporous isoreticular bipyridine-based MOFs coordinated with CuSiF_6 as a pillar.⁹⁴ The smaller pore material, which possesses 8 Å pores, exhibits an approximate type V isotherm, but condensation occurs at very low P/P_0 with saturation loadings of 0.2 g/g water adsorption. The larger pore MOF, with 10.6 Å pores, exhibits an isotherm that is similar to a modified type V form, but the pore-filling step is shifted to the right, where almost no water adsorbs below a relative pressure of 0.1, but then a knee in the isotherm is observed at 0.3 P/P_0 , and it has a saturation loading similar to the smaller MOF.

Several other examples of stable, nitrogen-coordinated MOFs have also been reported. For example, Rosi and co-workers have synthesized Co-adeninate materials known as “bioMOFs”.⁹⁵ One version, bioMOF-14, synthesized using adeninate with valerate groups maintained its crystallinity after 1 month in liquid water, indicating a high thermodynamic stability. Wade et al.

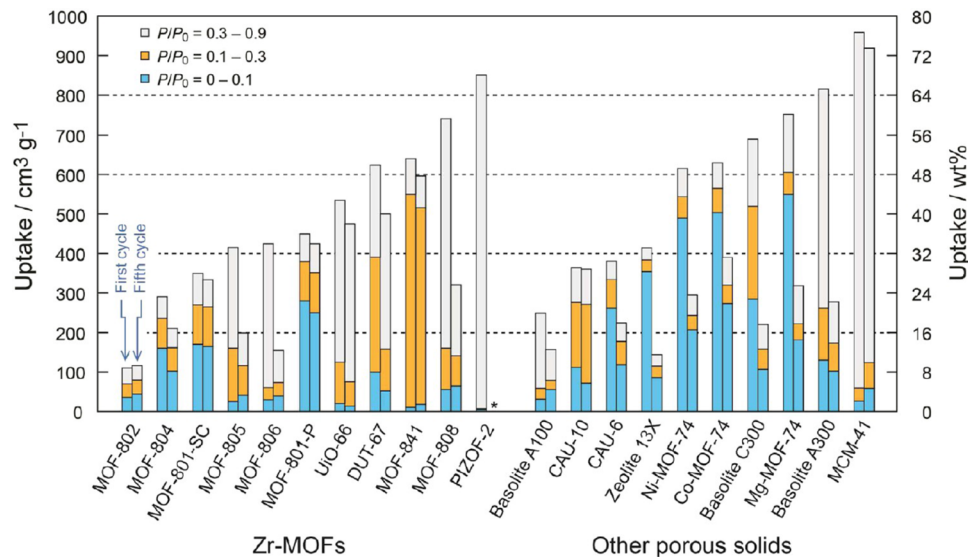


Figure 14. Water capacities in different pressure ranges for Zr-based MOFs (left) and other representative materials (right) at 298 K. Left and right bars represent the first and fifth cycles, respectively. For MOF-801-SC, uptake capacities of first and second cycles were presented. An asterisk (*) indicates no data. Reprinted with permission from ref 110. Copyright 2014 American Chemical Society.

presented a large-pore MOF (16 Å channels) synthesized from $\text{Zn}(\text{NO}_3)_2$ and pyrazolate ligands. This material exhibits a type V water isotherm.⁹⁶

The highly stable UiO-66 was reported in 2008⁵⁸ and has been the focus of intense study in the adsorption separations community. This MOF is synthesized by ZrCl_4 and BDC, which forms 12-coordinated zirconium–oxo clusters in its defect-free form. The material possesses micropores of approximately 6 Å diameter. Water adsorption in UiO-66 displays a reversible type V isotherm, which indicates that the material is weakly hydrophobic. The pore-filling step occurs near 20% RH with very little adsorption below this point, and the saturation loading is approximately 20 mol/kg (0.36 g/g).^{31,35,41,97,98} When the MOF is synthesized with functional groups on the BDC ligand, including NH_2 , NO_2 , etc., the adsorption loadings increase at low pressure due to the enhanced interactions with water, leading to an isotherm that approaches a type I shape.^{31,97} Nonpolar functional groups such as dimethyl- and monomethyl-BDC decrease water adsorption loadings.^{99,100} Water adsorption cycles have also been performed for UiO-66, and it was shown to maintain porosity and surface area after 6 cycles at 298 K.⁴¹ Extended isostructural versions of this material have also been reported in the literature.^{58,101–103} Hupp and co-workers developed a new family of materials based on the NU-1000 material using solvent-assisted ligand incorporation (SALI).¹⁰⁴ They used this method to attach perfluoroalkane carboxylates on Zr_6 nodes of NU-1000. NU-1000 possesses mesoporous channels lined with –OH groups. Water isotherms were measured at 298 K in helium carrier. NU-1000 and SALI-1, -3, -7, and -9 show decreased water adsorption as a function of increasing chain length. On the basis of PXRD patterns, the materials are all stable after water exposure.

Zeolithic imidazolate frameworks (ZIFs) first reported by Yaghi and co-workers in 2006 exhibit among the highest stabilities known for MOFs.¹⁰⁵ ZIF materials possess a metal–imidazolate–metal angle of 145°, very close to that found in the Si–O–Si bonds of many zeolites. ZIF-8 possesses ZnN_4 tetrahedra connected by imidazolate linkers to form 11.6 Å cages

that are accessible through approximately 3.4 Å windows. This material is strongly hydrophobic and displays a type III water isotherm where negligible water is adsorbed until pore filling occurs above 80% RH.^{28,106–109} The water adsorption is reversible, and the material maintains its porosity and surface area after exposure. By carefully varying the ZIF-8 crystal size from 0.4 μm to 15.8 and 324 μm, Zhang et al. showed the non-negligible effect the hydrophilic –N–H functionality introduced by the terminated imidazolate linkers on the surface can have on the water adsorption behavior.¹⁰⁸ The water vapor adsorption properties of the ZIF-71 and ZIF-90 structures possessing the dichloroimidazole and imidazole-2-carboxaldehyde ligands were also investigated by Zhang et al., and it was found that ZIF-71 is also strongly hydrophobic and adsorbs very little water even when exposed to water up to 100% RH at 308 K.¹⁰⁶ However, while ZIF-90 possesses the same SOD topology as in the case of ZIF-8, the presence of hydrophilic carbonyl groups in the imidazolate linkers gives the material a weakly hydrophobic type V isotherm with a saturation loading of 18 mol/kg (0.32 g/g). The pore-filling step in this structure occurs near 30% RH.

The diverse range of water adsorption behaviors present in MOFs also make them promising candidates for an array of applications ranging from thermal batteries and low temperature heating and cooling applications to dehumidifier and water delivery applications. Yaghi et al. recently presented three criteria to be considered in the selection of high performing materials for such applications.¹¹⁰ In addition to possessing good water stability, these criteria include the presence of steep, well-defined pore condensation at a low relative pressure, high uptake to allow maximum working capacity, and facile recyclability of the material during water adsorption. In this study,¹¹⁰ the performances of 20 metal–organic frameworks and 3 other porous materials (Figure 14) were evaluated according to this criteria to identify two top-candidate Zr-based MOFs, MOF-801-P and MOF-841. Both structures are formed from the $\text{Zr}_6\text{O}_4\text{(OH)}_4\text{(-CO}_2\text{)}_n$ secondary building unit with fumaric acid as the linker in MOF-801-P and 4,4',4'',4'''-methanetetracyl-tetrabenzonic acid as the linker in MOF-841. These materials

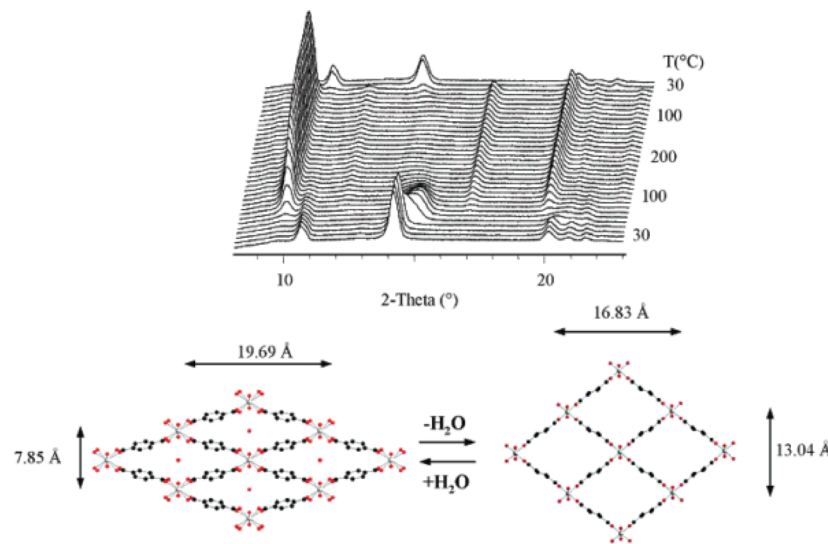


Figure 15. Schematic representation of the reversible hydration–dehydration of MIL-53(Cr), bottom. PXRD pattern of MIL-53(Cr) under air (for a better understanding, a 2θ offset is applied for each pattern), top. Reprinted with permission from ref 113. Copyright 2002 American Chemical Society.

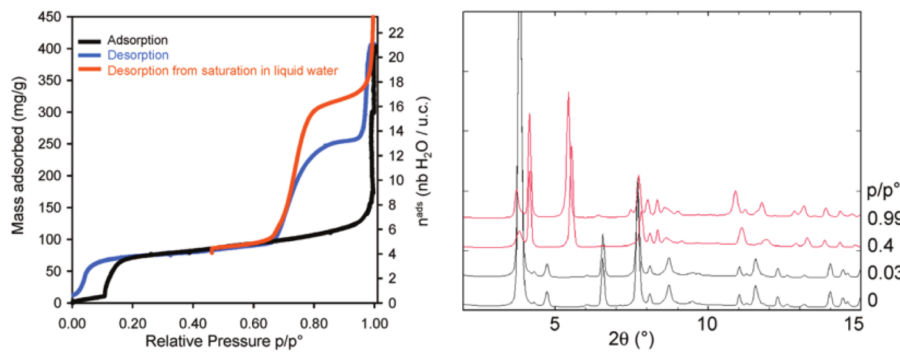


Figure 16. Adsorption and desorption isotherms for water in MIL-53(Cr) at 298 K, left. PXRD patterns for MIL-53(Cr) at different water vapor pressures, right. Reprinted with permission from ref 114. Copyright 2010 American Chemical Society.

were found to be optimal due to their appropriate pore size that is small enough to condense water at low relative pressures but still large enough to allow large water loadings and facile regeneration. The authors also performed diffraction studies on MOF-801 to determine the location of adsorbed water molecules and elucidate the important role intermolecular hydrogen bonding networks plays in stabilizing water clusters in the cavities of the MOF. By carefully considering the relative pressure at which water capture and release occur in the process of interest, a similar approach can be used by future researchers to identify further promising materials for specific target applications.

These highlighted studies show that the water adsorption behavior in stable, rigid MOFs aligns closely with the well-known adsorption behavior in carbons, zeolites, and mesoporous silicas. Microporous MOFs with open metal sites or functional groups that interact well with water display type I water isotherms, similar to cation-containing zeolites (e.g., 13X; 4A). In the absence of these hydrophilic sites, microporous MOFs display weakly hydrophobic behavior, with little or no adsorption in the low concentration region and commencement of pore filling at relative pressures of 0.2–0.4. MOFs with large pores (>20 Å diameter) exhibit type V isotherms that mimic those seen in mesoporous silicas (e.g., SBA-15), with capillary condensation occurring at a relative pressure dictated by the pore size. We also note from these studies several important features that correlate

with water-stable MOFs: (i) highly coordinated metal nodes, (ii) high basicity of the ligand (Zn-imidazoles vs Zn-BDC), (iii) shielding of the coordination site. We will expand upon these ideas in section 3.

2.1.1. Flexible Behavior. While most MOFs display water adsorption behavior that is similar to other porous materials, there are several notable cases that exhibit interesting adsorption behavior as a consequence of framework flexibility.^{18,111,112} Breathing is a flexible behavior that occurs when a material undergoes a reversible structural transition from a starting conformation to some new state(s) before returning back to its original form. On the other hand, gate-opening occurs when a material abruptly changes from a closed, nonporous form to a porous form at some nonzero pressure. From the isotherm alone, framework flexibility cannot be ascertained because the presence of characteristic adsorption steps or pronounced hysteresis that may indicate framework flexibility can also be caused by changes in adsorbate packing interactions (i.e., from mono- to multilayer adsorption) or even structural breakdown in the framework. As a result, in this section we only consider studies where there is direct crystallographic evidence indicating that a water-induced structural transition is in fact occurring within the framework.

The MIL-53 materials are the most well-studied MOFs that exhibit breathing behavior in the presence of water. Breathing in the highly stable MIL-53(Cr) structure was first reported by Serre et al. in 2002.¹¹³ They found that the as-synthesized MIL-

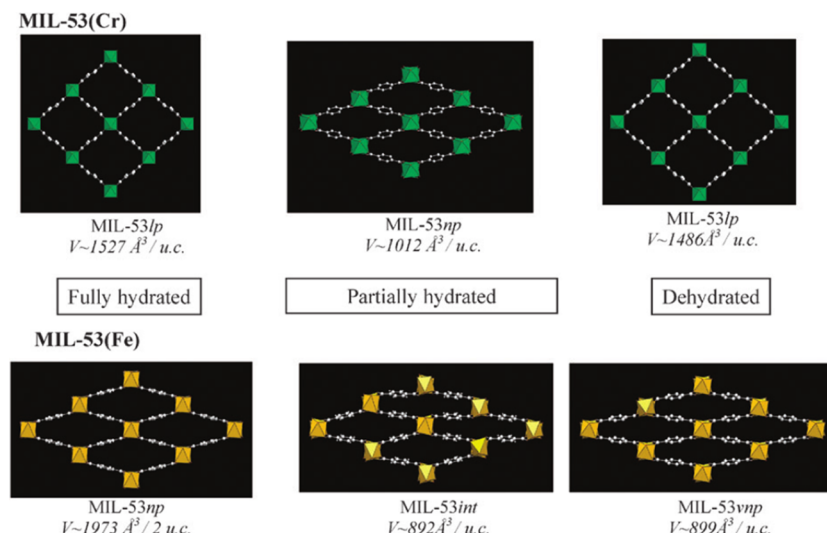


Figure 17. Comparison of the crystal structures of the MIL-53(Cr) (large pore and narrow pore versions) and MIL-53(Fe) (narrow pore, intermediate pore, and very narrow pore versions) upon water desorption. Reprinted with permission from ref 118. Copyright 2010 Royal Society of Chemistry.

53(Cr) material, after calcination, results in a wide pore form of the material. However, upon exposure to atmospheric water at room temperature the material transforms into a narrow pore form that can then be reversibly returned to its wide pore form upon subsequent water removal. This transition between the narrow and wide pore form creates a large change in unit cell dimensions of more than 5 Å in a single direction and was directly observed using variable temperature PXRD measurements (Figure 15). In subsequent work, Bourrelly et al. applied a variety of approaches including gravimetric adsorption, PXRD, microcalorimetry, and IR spectroscopy to further understand the MIL-53(Cr) breathing behavior.¹¹⁴ The water adsorption and desorption isotherms of the material along with PXRD patterns at different water vapor pressures at 298 K are shown in Figure 16. As mentioned in section 1.2, the adsorption and desorption isotherms of flexible materials cannot be fully described by the existing IUPAC classifications. In the case of MIL-53(Cr), the adsorption behavior of the material most closely resembles the two-step adsorption present in type IV isotherms; however, features not described by this classification are also present in the material such as an initial highly hydrophobic portion of the isotherm below $P/P_0 = 0.1$, which is due to MIL-53(Cr) being in its large-pore form. The PXRD patterns collected at different vapor pressures confirmed that the isotherm plateaus on the adsorption branch of Figure 16 correspond to a saturation of the porosity of the material in its narrow pore or large pore forms. The position of water molecules from the refined XRD data in the MIL-53(Cr) narrow pore form indicates two types of important host–guest intermolecular interactions in this conformation. These are hydrogen bonding interactions between water's oxygen atoms and the hydrogen atoms on the $\mu_2\text{-OH}$ groups in the framework, and hydrogen bonds between the protons on water and the oxygen atoms of the carboxylate groups on the ligand.

In 2004, Loiseau et al. discovered MIL-53(Al) to exhibit a breathing behavior in the presence of water as well.¹¹⁵ Similar to its chromium analogue, MIL-53(Al) also adsorbs water at room temperature to induce a reversible structural transition from its large pore form to its narrow pore form with a large corresponding reduction in pore volume. In its evacuated form the material has channel dimensions of $8.5 \times 8.5 \text{ Å}^2$, but upon

adsorption of one water molecule per aluminum, it transitions into a narrow pore form with $2.6 \times 13.6 \text{ Å}^2$ dimensions. Similar to MIL-53(Cr), hydrogen bonding interactions between water and the hydrophilic components of the framework were found to provide important host–guest interactions that stabilize its narrow pore form.

Modification of the MIL-53(Al) framework can also be used to modulate the flexibility of the material in the presence of water. Biswas et al. synthesized a series of functionalized MIL-53(Al) structures containing the BDC-X ligand ($X = \text{Cl}, \text{Br}, \text{CH}_3, \text{NO}_2, (\text{OH})_2$) and showed using vapor adsorption and variable temperature PXRD that only the dihydroxyl variation exhibits breathing behavior in the presence of water.¹¹⁶ Postsynthetic modification of MIL-53(Al) to form MIL-53(Al)-COOH with noncoordinating carboxylic acid groups was also used by Reimer et al. to yield a structure with a high degree of flexibility similar to the parent MIL-53(Al) material.¹¹⁷ MIL-53(Al)-COOH also assumes the narrow pore form after the adsorption of water under ambient conditions before again entering its large-pore form after water saturation or upon sample activation. This behavior was ascertained via temperature-dependent PXRD measurements and a vapor sorption isotherm at 298 K. The vapor sorption behavior of this material shows the characteristic two-step behavior with the first step progressing until $P/P_0 = 0.5$ with the material in its narrow pore form and each pore filled with one molecule each before reaching its hydrated large pore form and adsorbing a second water molecule.

Other MIL-53 materials (Fe, Ga) also exhibit breathing, and in these structures the critical role the metal identity plays in dictating the flexible behavior can be seen. Relative to the Cr version, MIL-53(Fe) is much less flexible (Figure 17) and exhibits a breathing behavior that results in only a 10% variation in the unit cell volume relative to the 40% variation present in MIL-53(Cr).¹¹⁸ Recently, Coudert et al. reported a detailed study into the energetics and thermodynamics of breathing in MIL-53(Ga) in the presence of water to understand why its behavior differs so greatly from MIL-53(Al).¹¹⁹ Contrary to the MIL-53(Al) behavior, MIL-53(Ga) exhibits a thermodynamically stable narrow pore form when evacuated under ambient temperatures. MIL-53(Ga) then shows an intermediate narrow-pore phase upon hydration that is similar to that found in MIL-

53(Fe). The stability of this narrow-pore phase under ambient temperatures in MIL-53(Ga) that is not present in MIL-53(Al) (or MIL-53(Cr)) was attributed to the more diffuse molecular orbitals of Ga compared to Al which result in a coordination sphere that can deform more easily. This property allows the benzene linkers in MIL-53(Ga) to more easily assume the more tightly packed narrow-pore orientation. In situ PXRD and IR measurements allowed the direct observation of this structural transition in the presence of water, and a series of water adsorption isotherms and isobars under various conditions were then used to construct a full pressure–temperature diagram of the structural transitions in the system (Figure 18).

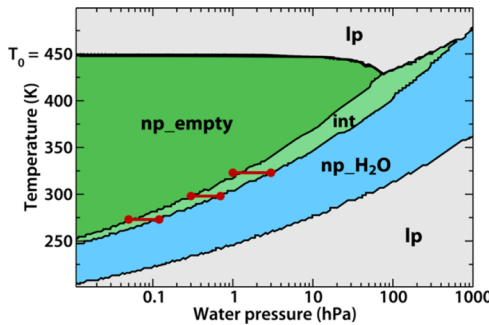


Figure 18. Water pressure vs temperature phase diagram of Ga-MIL-53, indicating the domains of stability of the different structures of the material. Red segments correspond to the experimental transitions. Reprinted with permission from ref 119. Copyright 2014 American Chemical Society.

A breathing structural transition in MIL-88B(Fe) has also been observed during the adsorption and desorption of water.¹²⁰ A distinct two-step change in the lattice parameters of the unit cell from PXRD measurements indicates that this breathing occurs and results in a unit cell volume change of 40%. Water isotherm measurements also captured this two-step structural transition with the steps in the isotherm closely corresponding with the step changes observed in the structure's lattice parameters from the PXRD measurements.

In the realm of gate-opening behavior, Fukushima et al. reported the presence of such structural transitions in a combination of two CID (CID = coordination polymer with an interdigitated structure) materials.¹²¹ These two flexible, interdigitated structures known as CID-5 ($\text{Zn}(\text{5-NO}_2\text{-ip})(\text{BPY})$) ($\text{5-NO}_2\text{-ip}$ = 5-nitroisophthalate) and CID-6 ($\text{Zn}(\text{5-MeO-ip})(\text{BPY})$) (5-MeO-ip = 5-methoxyisophthalate) were synthesized along with a series of mixed materials containing different ratios of the $\text{5-NO}_2\text{-ip}$ and 5-MeO-ip ligand denoted as CID-5/6 (with x in the range $0.06 < x < 0.92$). While CID-5 is nonporous in its evacuated form, at 298 K it exhibits gate-opening at a water pressure of 2.48 kPa after which it rapidly adsorbs almost 5 water molecules per unit cell (Figure 19). The CID-6 structure, however, does not display this same behavior and instead shows a near linear uptake of water throughout its entire isotherm. Furthermore, the CID-5 structure exhibits a large hysteresis because the structure remains in its porous form until very low desorption pressures near 0 kPa whereas CID-6 exhibits a much less pronounced hysteresis branch. Interestingly, the CID-5/6 mixed-ligand structures display character of both the CID-5 and CID-6 structures depending on the ratio of ligands incorporated, providing a direct means for tuning the gate-opening pressure, degree of hysteresis, and hydrophobicity of the materials in this

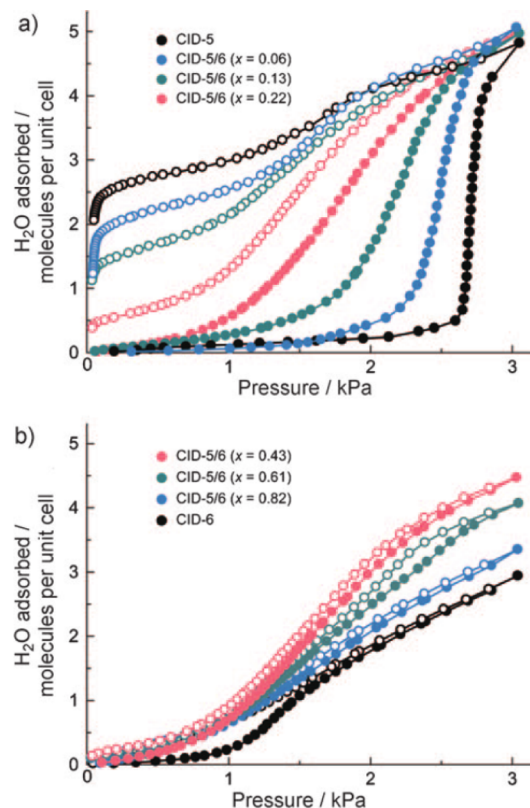


Figure 19. Adsorption isotherms (●) and desorption isotherms (○) of water at 298 K for (a) CID-5 and CID-5/6 ($x = 0.06–0.22$) and (b) CID-5/6 ($x = 0.43–0.82$) and CID-6. Reprinted with permission from ref 121. Copyright 2010 Wiley-VCH.

study. Recently, similar control over gate-opening behavior in the presence of water vapor was also demonstrated in series of mixed-ligand $\text{Al}(\text{BDC-OH})_x(\text{BDC-NH}_2)_{1-x}$ materials isostructural to MIL-53(Al).¹²²

2.2. Multicomponent Adsorption

In addition to stability effects, one must also consider the important effect water can have on the MOF's selective adsorption properties under the application's operating conditions. Among the limited multicomponent adsorption studies available in the literature, CO_2 is the most well-studied adsorbate due to strong interest in utilizing MOFs as adsorbents for reducing greenhouse gas emissions. However, because residual moisture will be present in nearly any adsorption application where the adsorbent is exposed to ambient air, it is critically important to consider the significant effect these trace amounts of water can have on the capacity and selectivity of the material under nearly all process operating conditions.

2.2.1. CO_2 . There has been particular interest in utilizing MOFs as postcombustion CO_2 capture materials because of the potential advantages they have over state-of-the-art aqueous amine-based solutions due to lower regeneration costs.^{123–127} Unless dehumidified, postcombustion flue gas will be fully saturated with water. In this section we discuss past studies that explore the effect water has on the CO_2 capacity and selectivity of a variety MOFs. Because certain structures may not be chemically stable under the water loadings investigated in the study, it can be difficult to decouple the effects due to competitive adsorption versus structural breakdown in the MOF. One must therefore also carefully consider the stability level (section 4) for

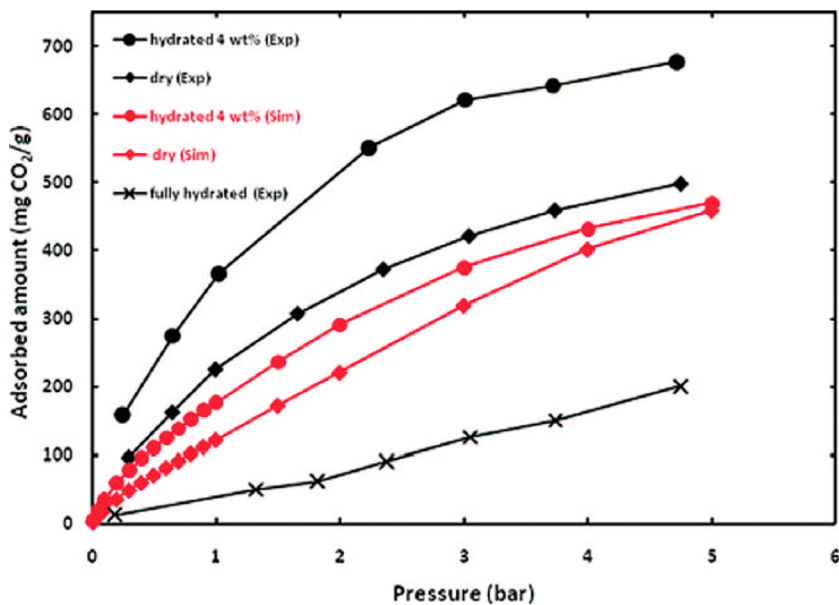


Figure 20. Experimental and simulated CO_2 isotherms at 298 K in HKUST-1 at different water contents. Reprinted with permission from ref 128. Copyright 2009 American Chemical Society.

each of the structures in this section in order to fully rationalize their multicomponent adsorption behavior.

In the majority of cases, water has a negative effect on the CO_2 selectivity and capacity of the material that becomes more pronounced as the water loading in the structure increases. Because CO_2 and water are both polar molecules, the same attributes that make MOFs attractive candidates for CO_2 capture can also make them prone to adsorbing large amounts of water that directly compete with CO_2 for the most favorable adsorption sites. Open metal site MOFs are among the most promising CO_2 capture materials due to the favorability of their coordinatively unsaturated metals as binding sites for adsorbates with higher multipole moments. Interestingly, HKUST-1 possesses a CO_2 uptake and selectivity that depends strongly on the precise water loading that is present in the structure. In a combined experimental and simulation study Snurr et al. showed that small amounts of preloaded water (4 wt %) enhance the equilibrium CO_2 uptake (Figure 20) and selectivity over N_2 and CH_4 in the material due to increased electrostatic interactions caused by the quadrupole moment of CO_2 interacting with the electric field created by bound water molecules at the open metal site. However, upon full saturation with water, significant drops in the CO_2 equilibrium capacity throughout the 0–5 bar range result.¹²⁸ A similar result was found in a subsequent computational study by Balbuena et al. exploring a variety of different water preloadings from 0 to 8 wt % in this same structure.¹²⁹ This positive effect at low water loadings followed by a large drop in performance at higher loadings has also been observed in a number of other equilibrium and dynamic adsorption studies on the HKUST-1 structure.^{39,41,130}

The M-MOF-74/M-DOBDC/M-CPO-27 MOFs are another set of structures with coordinatively unsaturated metals that exhibit extremely promising CO_2 capture properties, with the Mg-MOF-74 variation possessing the highest CO_2 affinity in the low-pressure regime that is most relevant to CO_2 levels in postcombustion flue gas.¹³¹ However, numerous experimental studies have shown that the presence of any moisture in the gas stream has a detrimental effect on M-MOF-74 CO_2 adsorption performance.^{130,132,133} In the case of Mg-MOF-74, which

possesses a higher dry capacity for CO_2 than the isostructural Zn, Ni, and Co structures, Matzger et al. showed that after exposure to 70% RH in CO_2/N_2 breakthrough experiments it undergoes the greatest decrease in performance of all variations and retains only 16% of its original CO_2 capacity after subsequent thermal regeneration.¹³² The CO_2 capture properties of the highly stable MIL-100(Cr) structure have also been explored under multicomponent breakthrough conditions with a similar decrease in performance after presaturating the breakthrough column with water.³⁹ The breakthrough performance of the promising SIFSIX-2-Cu-i and SIFSIX-3-Zn materials were also tested in various CO_2/N_2 and CO_2/H_2 binary mixtures and exhibited a slight decrease in performance in the presence of 74% RH.¹³⁴ Multiple simulation studies have predicted a similar performance decrease in the CO_2 capture properties of a diverse range of other MOF materials as well.^{135–139}

While the impact of water on CO_2 adsorption properties is generally negative, there are numerous cases where water has a minimal impact on the CO_2 capture properties of the material. For instance, Gascon et al.¹⁴⁰ found that MIL-53(Al)-NH₂ exhibited little change in its breakthrough profiles in a CO_2/CH_4 mixture in the presence of 0.042 bar water vapor, whereas Llewellyn et al.³⁹ found only a minor impact on the dynamic CO_2 capacity for the stable UiO-66 over 3–40% RH conditions in CO_2/N_2 mixtures. In the case of MIL-101(Cr), He et al. also discovered a retention of its experimental dynamic CO_2 capacity over the complete 0–100% RH range explored in CO_2/N_2 mixtures.¹⁴¹ In fact, via a mechanism similar to that observed in HKUST-1, molecular simulations have shown that the presence of terminal water molecules in the hydrated MIL-101(Cr) under low water loadings should also increase its affinity and selectivity for CO_2 over nonpolar molecules such as CH_4 .¹⁴² Computationally, water has been predicted to have a negligible effect on CO_2 capture properties in a wide range of other MOFs at low water loadings as well.^{139,143,144} The most remarkable water-induced increase in CO_2 uptake in a MOF was discovered in the MIL-100(Fe) structure where a 5× increase in its breakthrough capacity for CO_2 at 0.2 bar partial pressure is observed in samples pre-equilibrated with 40% RH.⁴¹ This increase in CO_2 uptake

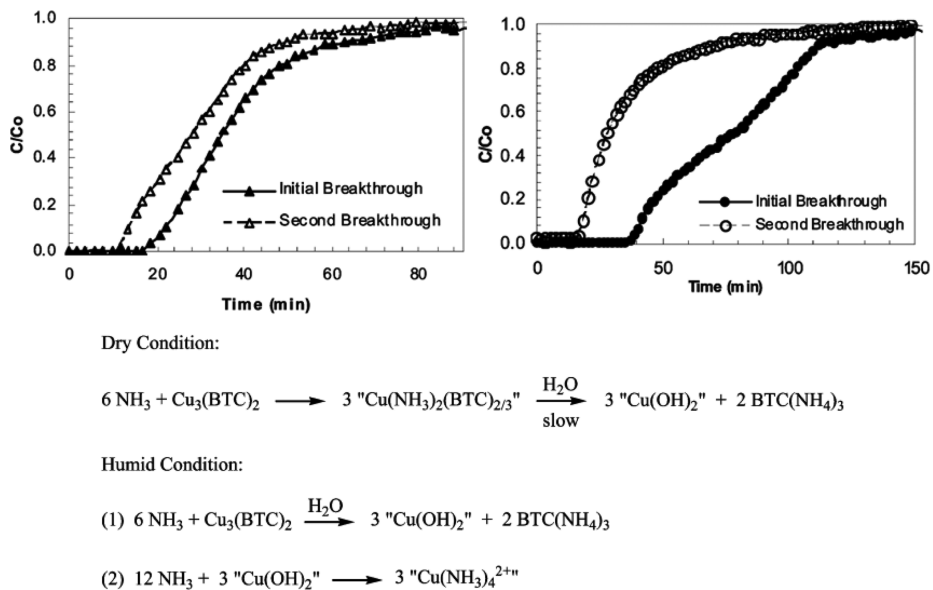


Figure 21. (Top) Experimental ammonia breakthrough curves for HKUST-1 under dry (left) and 80% RH (right) conditions at near ambient temperatures in air. (Bottom) Proposed reaction mechanisms for HKUST-1 under dry and wet conditions. Adapted with permission from ref 148. Copyright 2009 American Chemical Society.

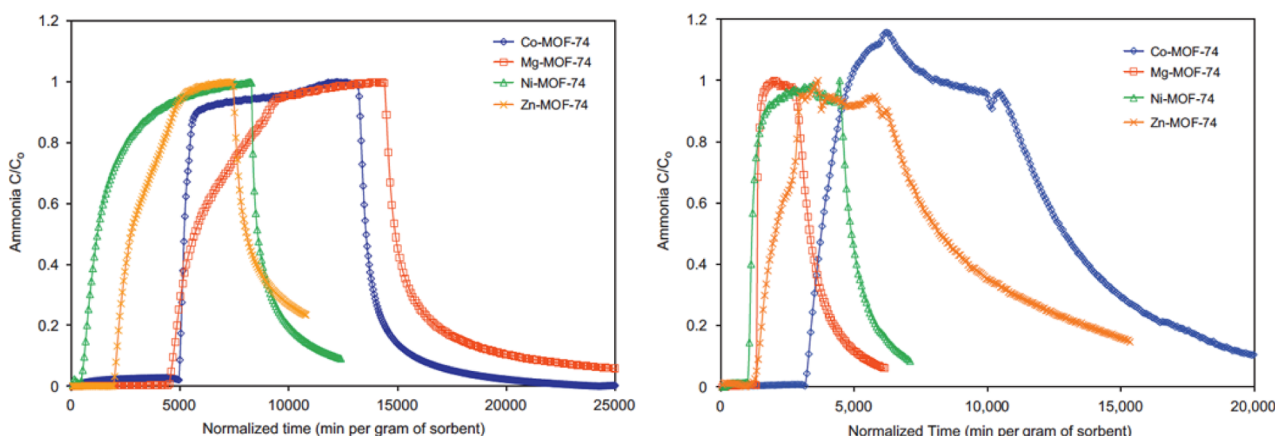


Figure 22. Experimental ammonia breakthrough and desorption curves for MOF-74 variations under dry (left) and 80% RH (right) conditions at 293 K in air. Reprinted from ref 149, Copyright 2011, with permission from Elsevier.

corresponds with a large decrease in adsorption enthalpy and was attributed to an increased solubility for CO_2 in the center of the pores as water adsorbs on the structure's Lewis acid metal sites.

Because adsorbent materials require both stability and CO_2 selectivity to be attractive candidates for CO_2 capture applications, strategies that simultaneously improve both of these attributes are of great interest in developing future materials. In this regard, ligand functionalization with methyl functional groups has been shown to be a promising approach for simultaneously improving both the moisture stability and low-pressure CO_2 affinity of structures.^{76,145} Postsynthetic modification has also been used with ethylenediamine in ZIF-8 to not only improve its CO_2 capacity and selectivity over N_2 but also reduce its H_2O adsorption capacity under single component conditions.¹⁰⁹ Core–shell structures where a more hydrophobic structure can serve as a protective layer for a more water-sensitive but CO_2 -selective core is yet another promising strategy for simultaneously increasing both the CO_2 selectivity and water stability of various structures.^{146,147}

2.2.2. Other Gases and Vapors. A limited number of breakthrough studies have explored MOF performance under humid conditions for the capture of various gases and vapors present in low concentrations in air. Among these studies, hazardous gas capture has been investigated the most extensively,^{80,148–155} with a particular interest in the ammonia capture performance of the MOF-74 and the HKUST-1 structures due to their open metal site properties.^{148–150}

In the HKUST-1 structure, Peterson et al. first explored the effect of moisture on its dynamic ammonia breakthrough performance via measurements under dry and 80% RH conditions in air.¹⁴⁸ The authors discovered that while the material's initial ammonia breakthrough performance is much stronger under humid as opposed to dry air conditions, during the second pass through the column there is a significant drop in HKUST-1's humid ammonia performance (Figure 21, top). This large decrease in capacity and breakthrough time in the presence of moisture was attributed to an irreversible loss of structure and porosity evidenced by PXRD, NMR, and N_2 adsorption measurements on the sample after the breakthrough runs.

Reaction mechanisms supported by ^1H MAS NMR data were also proposed to explain how moisture may accelerate the structural breakdown of HKUST-1 in the presence of ammonia (Figure 21, bottom). In subsequent work, Bonino et al. utilized a combination of PXRD, XAFS, IR, diffuse reflectance ultraviolet-visible-near infrared (DRUV-vis-NIR), and EPR techniques to further confirm the critical role moisture plays in promoting the irreversible breakdown of HKUST-1 in the presence of ammonia.¹⁵⁰ Interestingly, Nenoff et al. found that HKUST-1 also possesses properties that are relevant to nuclear energy industrial processes.¹⁵⁶ Despite the hydrophilic nature of the structure the authors found molecular iodine, a long-lifetime product that is released during the processing of spent nuclear fuel, is preferentially adsorbed over water in HKUST-1 under 1:1 $\text{I}_2:\text{H}_2\text{O}$ conditions. This behavior was attributed to the formation of hydrophobic I_2 barriers in the structure which reduce water's ability to adsorb into the pores. Calero et al. also showed through molecular simulation that selectively blocking the open metal sites in HKUST-1 with molecules such as acetone or dimethyl ether may be a promising approach for reducing the framework's water affinity in order to improve the alcohol–water separation performance of the structure.¹⁵⁷

In the case of M-MOF-74 (Co, Mg, Ni, Zn), the same moisture-induced enhancement in ammonia single-pass breakthrough performance present in HKUST-1 was not observed by Yaghi et al. in their measurements on the structures.¹⁴⁹ In this case, the presence of 80% RH in air significantly decreased the ammonia capacity of the structures (Figure 22) and, for the other adsorbates investigated in their study (cyanogen chloride, sulfur dioxide, and octane), resulted in a near complete loss of dynamic capacity for the molecules.

It is important to note that even if a structure is highly stable under humid conditions, the presence of basic or acidic gases in the mixture can result in behavior that causes an otherwise stable structure to breakdown. This was apparent in the work of Bandosz et al. investigating the breakthrough performance of UiO-66 for capturing the pollutant NO_2 under dry and 71% RH conditions in air.¹⁵² The authors found that UiO-67 had a better NO_2 breakthrough performance than UiO-66 under humid conditions and attributed this to the greater ability of NO_2 to dissolve and form acidic species in the larger pore space of UiO-67. On the basis of PXRD measurements on the samples after the breakthrough runs it is also likely that, in a manner similar to that observed in HKUST-1,¹⁴⁸ irreversible structural changes resulting from NO_2 chemisorption may play a role in the enhanced single pass breakthrough performance of the material as well.

The capture of the volatile organic compound diethylsulfide, a surrogate for the mustard gas chemical warfare agent bis(2-chloroethyl)sulfide, was explored in a series of seven MOFs based on Ni^{2+} hydroxo clusters bridged by different pyrazolate- and carboxylate-based ligands.⁸⁰ Dynamic adsorption profiles under dry and 80% RH conditions in an inert carrier identified a variation of these MOFs possessing the $-\text{CF}_3$ functional group that may possess a diethylsulfide capture performance comparable to that of a commercially available activated carbon material used in current filtering systems. In a separate study, the breakthrough performance of the $\text{Zn}_4\text{O}(\text{BDC})(\text{BPZ})_2$ and DUT-4 structures was investigated in 50% RH air streams containing 5 ppm of the biogas impurity octamethylcyclotetrasiloxane.¹⁵⁸ While this composition is not representative of those found in real biogas mixtures, the authors found that these

two MOFs significantly outperformed an activated carbon standard at removing this impurity from the mixture.

The limited range of adsorbates explored under multi-component conditions makes this a rich and largely unexplored area for future research. Furthermore, it should be noted that while the strong MOF–water interactions found in many structures are often considered a drawback for most real world applications, there are also scenarios where the selective adsorption of water in the structure is a desired attribute for the application. For example, in the MIL-88(Fe) structure it has been shown that the preferential adsorption of water over nitric oxide can be used to facilitate the controlled release of preadsorbed quantities of this biologically active target molecule from the structure.¹⁵⁹

2.3. Aqueous Phase Adsorption

Relative to the number of gas adsorption studies reported in the literature, the number of liquid phase adsorption studies in MOFs is much more limited. In this section we discuss only the subset of these liquid phase studies investigating the selective adsorption of components from the aqueous phase.

The liquid phase separation performance of adsorbents can either be evaluated via flow-through chromatographic experiments where the adsorbent is incorporated as the column's stationary phase or in batch experiments where the MOF is immersed in the liquid mixture. In the batch case, the adsorbent's uptake of the target molecule is often quantified via TGA or elemental analysis of the framework after adsorption equilibrium is reached or through appropriate spectroscopic or chromatographic techniques that indirectly quantify the adsorbent's uptake by measuring the decrease in concentration of the target species from the bulk solution.

The use of MOFs as adsorbents in separations relevant to industrial wastewater remediation is most prevalent in the literature, with the removal of toxic metals,^{160–165} drugs and pharmaceuticals,^{63,166–168} and other harmful pollutants^{67,169–186} having been explored. Among these studies, variations of the UiO, MIL, and ZIF materials have been studied most extensively for these applications due to their high chemical stability properties. Xu et al. demonstrated that the incorporation of free thiol groups on the BDC ligand in UiO-66 yields a remarkable 99.9% removal of $\text{Hg}(\text{II})$ from 10 ppm to below 0.01 ppm after immersing the structure in water for 12 h.¹⁶² Azzazy et al. also showed that the parent UiO-66 structure has promise for the visual detection and removal of trace amounts of $\text{Hg}(\text{II})$ along with other toxic metal ions such as $\text{Bi}(\text{III})$, $\text{Zn}(\text{II})$, $\text{Pb}(\text{II})$, and $\text{Cd}(\text{II})$ in water.¹⁶³ Within the MIL series of MOFs, the chromium-based MIL-100 and MIL-101 structures have shown promise for their pharmaceutical and drug adsorption properties^{63,167,168} as well as their ability to remove chloroaromatic pollutants from aqueous solutions.¹⁷³ ZIF-8 was also identified by Jiang et al. and Yang et al. to be a quick and effective adsorbent for the removal of toxic benzotriazole¹⁷² and tetracycline¹⁷⁴ pollutants from aqueous solutions. Numerous structures have also been identified as promising adsorbents for the removal of dye pollutants,^{175–185} a particularly important separation relevant to the remediation of wastewater streams from the textile industry.

The separation of alcohols from water represents a costly step in the production of bioalcohols where the identification of suitable adsorbents for the separation could result in significant savings over more energy-intensive distillation approaches.¹⁸⁷ However, very few studies have explored the liquid phase

performance of MOFs for performing this separation. While no liquid phase chromatography experiments were performed, Banglin et al. used single crystal XRD measurements and elemental analysis after immersion in a 1:1 water–methanol liquid mixture to identify a Cu-based structure that displays the exclusive adsorption of water over methanol under these conditions.¹⁸⁸ This behavior was attributed to a size exclusion mechanism where methanol molecules are unable to adsorb into the structure's narrow pores. The JUC-110 MOF was used as a stationary phase in various alcohol–water gas chromatography experiments and, based on its high chemical stability and gas-phase performance, should be considered another promising candidate material for separating alcohols under aqueous conditions.⁹³ The selective adsorption of water over common organic solvents (benzene, toluene, and tetrahydrofuran) has also been demonstrated in a Co-based MOF.¹⁸⁹

In the realm of chemical sensing, the aqueous phase detection of various analytes has been demonstrated by exploiting guest-induced changes in the luminescent properties of MOFs. Bein et al. showed that MIL-101(Al)-NH₂ can be used as an optical sensor for fluoride ion sensing through a mechanism where a fluorescent dye molecule is first entrapped in the structure and is then fluoresced in the presence of aqueous fluoride solutions that break down the framework in a controlled manner.¹⁹¹ This fluorescence response can be directly related to fluoride concentration to provide a highly sensitive and selective method for measuring aqueous fluoride concentrations in the presence of other anions. Yan et al. also showed that a cation exchange mechanism in MIL-53(Al) (Figure 23) creates a highly selective

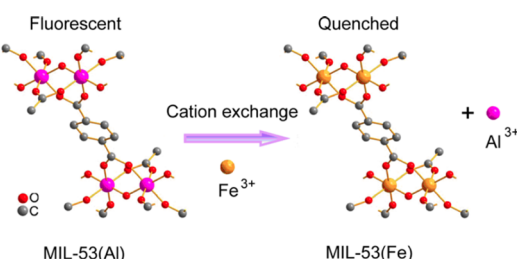


Figure 23. Schematic showing the cation exchange mechanism that allows the use of MIL-53(Al) as a fluorescent probe for Fe³⁺ sensing. Reprinted with permission from ref 190. Copyright 2013 American Chemical Society.

fluorescence response that allows the detection of Fe³⁺.¹⁹⁰ Zhou et al.¹⁹² and Bradshaw et al.¹⁹³ have also demonstrated that highly stable Zr-based MOFs can also exhibit pH-dependent fluorescent properties for sensing applications as well. The selective luminescent detections of various aromatic molecules,¹⁹⁴ anions,¹⁷⁸ and toxic metal species¹⁶¹ have also been demonstrated in other MOFs under aqueous conditions.

2.4. Computational Tools for Understanding Water Adsorption

This section reviews computational studies exploring the thermodynamics and transport properties of water adsorbed in MOFs. Comprehensive reviews discussing the theory and practical considerations of running such molecular simulations in crystalline materials are available in the literature,^{195–199} and only a brief overview of key points from these topics will be provided in this section. Molecular simulations can be performed in either the classical or quantum mechanical treatment. In the classical treatment, the electronic nature of the system is not

explicitly accounted for and the molecular interactions are instead expressed in terms of empirical force field functions that are parametrized to capture the physics of the system. For simplicity, these intermolecular interactions are often described solely in terms of the van der Waals interactions (via Lennard-Jones parameters) and electrostatic interactions (via point charges). For many simple systems, an accurate description of these interactions can be obtained via force fields that are generic or experimentally derived; however, for more complex systems, more accurate and reliable descriptions of these intermolecular interactions can be obtained through the use of force fields based on first-principles calculations.²⁰⁰ In quantum mechanical calculations, the electronic properties of the system are directly considered via an approximation to the Schrödinger equation. The specific quantum mechanical approximation chosen for the electrons can have a drastic impact on the accuracy and computational cost of the calculation, but in general, quantum mechanical calculations will require orders of magnitude more computational resources than classical simulations. As a result, modeling the dynamical and equilibrium properties of systems over long time scales is largely restricted to classical simulation techniques.

Water adsorption represents an equilibrium phenomenon that can be simulated via a classical simulation in the grand canonical Monte Carlo ensemble. In this method, water is allowed to transfer between an external bulk system with a specified chemical potential and temperature and a separate system containing the MOF. The adsorbed water amount is then obtained by considering the total amount of water adsorbed in the MOF after equilibrium is reached between the two systems. This is analogous to the common experimental scenario where the bulk phase pressure (related to chemical potential via an equation of state) and temperature are specified and the adsorption isotherm is obtained by measuring the gravimetric or volumetric changes to the system after equilibrium has been reached. On the other hand, the transport properties of water once adsorbed into the framework can be explored via molecular dynamics simulations. When considering MOFs for real world applications, this kinetic information can be equally as important as the equilibrium information available from adsorption isotherms. For example, in a pressure or temperature swing adsorption process, these kinetic diffusion rates govern the speed with which a single cycle of the process can be performed. In the case of membrane separations, the goal is to maximize both the diffusivity and adsorption affinity of the species being removed from the bulk mixture.

All classical simulations are performed on a MOF unit cell that, through the application of periodic boundary conditions,²⁰¹ is extended to represent the full crystal lattice. One important implication of these periodic boundary conditions is that only the infinite, perfect crystal structure is considered and experimental properties such as the internal defects and external surface area of the crystal are neglected. These effects can be non-negligible in hydrophobic MOFs such as ZIF-8 where, despite the very large internal to external surface area ratio of the crystal, hydrophilic –N–H moieties at the external surface due to the terminated imidazole linkers can adsorb significant amounts of water relative to the structure's hydrophobic interior.¹⁰⁸ The presence of linker defects in UiO-66 was shown to have a significant impact on its CO₂ adsorption properties²⁰² and likely has a similar effect on its water adsorption properties as well. The crystallographic positions of the framework atoms are often held rigid throughout classical simulations, but in cases where flexible force field models

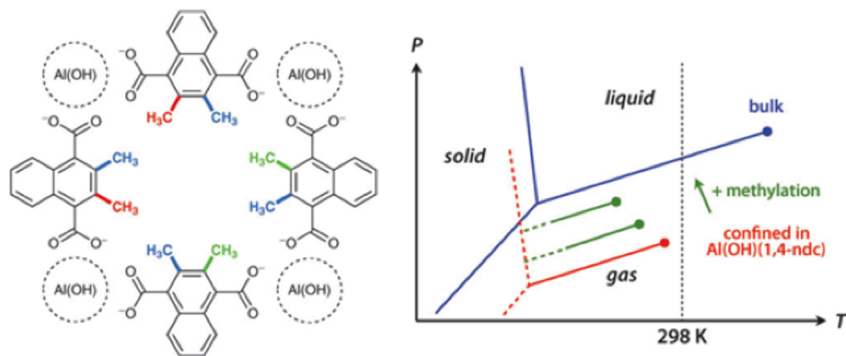


Figure 24. (Left) Schematic of the Al(OH)(1,4-NDC) pore structure and methyl positions for the three methylated variations studied in ref 215. Red indicates the two methyl groups per unit cell introduced in the first variation, green the additional two in the second variation, and blue the final two in the fully methylated structure. (Right) Schematic water phase diagram for Al(OH)(1,4-NDC) in the parent (red) and methylated (green) variations with reference to the phase diagram of bulk water (blue). Reprinted with permission from ref 215. Copyright 2010 Royal Society of Chemistry.

are available,^{145,203–208} framework motion can also be considered. Flexible framework simulations are much more computationally expensive but can be critically important in structures such as MIL-53(Cr)¹¹¹ where the framework exhibits reversible structural transitions in response to water adsorption. Water simulations are further complicated by the fact that the majority of MOFs are also chemically unstable in the presence of water. In this section, we only discuss studies into the thermodynamics and transport properties of relatively stable MOFs; in section 5.1.2, we discuss computational studies seeking to obtain mechanistic understanding into the reaction events occurring in unstable MOFs in the presence of water.

If they are able to correctly reproduce the physics of the experimental system, molecular simulations can provide molecular-level insight into structure–property relationships and adsorption mechanisms that are difficult or impossible to observe experimentally. Furthermore, experimental MOF synthesis and characterization can be both tedious and time-consuming to perform; molecular simulations can therefore be used to screen large numbers of existing MOFs for specific properties of interest²⁰⁹ as well as identify hypothetical, yet to be synthesized, MOFs that have extreme promise for certain applications and therefore merit attention as synthetic targets for experimentalists.²¹⁰ In this regard, the factors discussed in section 3 of this review are currently being used as criteria for ongoing efforts in our group to screen large numbers of structures for water stability. Grand canonical Monte Carlo simulations have become common practice for simulating H₂, CH₄, CO₂, and short-chain alkane adsorption properties due to the high accuracy they've shown at reproducing experimental isotherms.^{196,199,211} Unfortunately, this is not the case for water. Despite its well-studied and relatively simple triatomic structure, the wide range of chemical and physical properties resulting from water's fleeting hydrogen-bond networks is still poorly understood.²¹² In fact, among the dozens of classical water models developed in the literature over the past half-century, no single model can successfully reproduce the thermodynamic properties of water with great accuracy.²¹³ To further complicate matters, the H–O–H bond angle and dipole moment of water are also known to change upon adsorption in nanoporous materials.²¹⁴ There is always some trade-off between the computational cost and physical accuracy of the particular water model being used, and while water force fields designed to capture the complex multipoles and polarizability properties of water do exist, they require much greater computational costs than their simpler

analogues. However, given the dynamic properties of water when under confinement, flexible water models with electric-field-dependent properties are likely necessary to describe its complex interaction with structures possessing large electric fields (such as open metal site MOFs).

Water adsorption in zeolites with different silicon to aluminum ratios and defect properties has been actively studied in numerous past simulation studies.^{216–225} However, few studies have attempted to reproduce experimental water isotherms in MOFs. Fuchs et al. reported the first detailed molecular simulation study into the thermodynamics of water adsorption using the hydrophobic Al(OH)(1,4-NDC) MOF (Figure 24, left).²¹⁵ This structure contains 1D square channels of two different types; there are smaller channels containing the aromatic side group of the NDC ligand and larger 7 × 7 Å² channels that are not hindered by these groups. They were able to qualitatively capture the structure's type V experimental water vapor isotherm via grand canonical Monte Carlo simulations using a rigid framework model with DREIDING²²⁶ and UFF²²⁷ Lennard-Jones parameters. The authors chose the TIP4P-Ew model for water and then empirically scaled down the point charges assigned to the framework atoms until their simulations captured the type V nature of the experimental isotherm. Similar framework charge-scaling approaches are commonly employed when simulating water adsorption in hydrophobic zeolites where the adsorption behavior is also highly sensitive to the specific atomic charges being used.^{216,218,222,228} This complication arises from the fact that water force field models are parametrized to capture the properties of water molecules when in the bulk phase. Bulk water is a highly polarizing medium that will create larger dipole moments for individual water molecules than what exists in a more confined and less polarizing medium.²²⁹ Reducing framework atomic charges is therefore one approach to account for the weaker water–framework interactions that result from the lower molecular dipole moment of confined water.^{222,225,230} Water loading histograms and bidimensional free energy profiles at various vapor pressures were then used to identify a continuous adsorption phase transition in the Al(OH)(1,4-NDC) structure.²¹⁵ The water loading histograms suggest a continuous phase transition by showing a series of intermediate thermodynamic states containing some channels filled with water and other channels empty during the phase transition. In the alternative scenario of a first-order phase transition, these water histograms would depict two coexisting metastable states with all the pores either completely empty or full. The bidimensional free

energy profiles confirmed the presence of these intermediate states and also showed that the observed hysteresis during desorption exists because of free energy barriers between states that are much larger than kT . The authors then extended their analysis to include methylated derivatives of the Al(OH)(1,4-NDC) structure (Figure 24, left) in order to explore the effects of pore size and ligand functionalization on the thermodynamics of water adsorption. They found the onset of the type V isotherm increased to higher vapor pressures and the isotherms became less steep as the degree of functionalization increased, features attributed to the greater internal hydrophobicity introduced by the methyl groups. While the phase transitions in these methylated structures were still continuous in nature, the free energy barriers between intermediate states in these structures were lower than those in the parent structure, and no hysteresis was therefore observed during desorption. These trends were then summarized in a water phase diagram (Figure 24, right) to qualitatively capture both the shifts in vapor–liquid equilibrium and the supercritical nature of water within the different structures. Recently, Coudert et al. also explored how altering the topology and linker functionalization in various ZIF structures can be used to alter the water adsorption properties of these structures from a hydrophobic type V isotherm to a more hydrophilic type I behavior.²³¹

MIL-53(Cr) is a particularly interesting water-stable MOF due to its dynamic breathing behavior between its large pore (LP) and narrow pore (NP) conformations in the presence of water.¹¹³ Maurin et al.²²⁸ first examined the adsorption and diffusion properties of MIL-53(Cr) using the fixed-charge TIP-4P/2005²³² water model and a flexible framework model previously developed by Ferey et al.²⁰⁸ Molecular dynamics and grand canonical Monte Carlo simulations were used to obtain a microscopic understanding of how its breathing behavior between the LP and NP forms effects the hydrophobicity and water transport properties of the framework. Their simulations correctly captured the experimentally observed MIL-53(Cr) structural transitions from the LP to NP and then NP to LP at water loadings of roughly 2 H₂O/unit cell and 8 H₂O/unit cell, respectively (Figure 25). In previous work, Dubbeldam et al. also demonstrated that the LP to NP transition occurs at a water loading of exactly 2 H₂O/unit cell.²³³ The authors observed the LP form to be more hydrophobic than the NP form and confirmed this via water enthalpy and isotherm calculations on the two conformations.²²⁸ Water density distributions were also calculated to directly illustrate the stronger water–water interactions present in the more hydrophobic LP form versus the more predominant water–framework interactions present in the more hydrophilic NP form. They also found that the different water distributions in the LP and NP forms resulted in distinct water self-diffusion mechanisms throughout the structures. While the LP form exhibits a 1D type water diffusion mechanism that proceeds via a hopping sequence along adjacent μ_2 -OH groups in the pore, water diffuses in a slower and more continuous, single-file fashion through the center of the pores in the NP form.

Paesani et al.²³⁴ then explored the effects of electronic polarization on the behavior of adsorbed water in MIL-53(Cr) by comparing molecular dynamics results from fixed-charge water models with those obtained from the fully polarizable TTM3-F water model²³⁵ in a polarizable MIL-53(Cr) framework model. These simulations show that polarization plays a significant role in describing the qualitative spatial distribution of water molecules in the pores of MIL-53(Cr). In particular, the

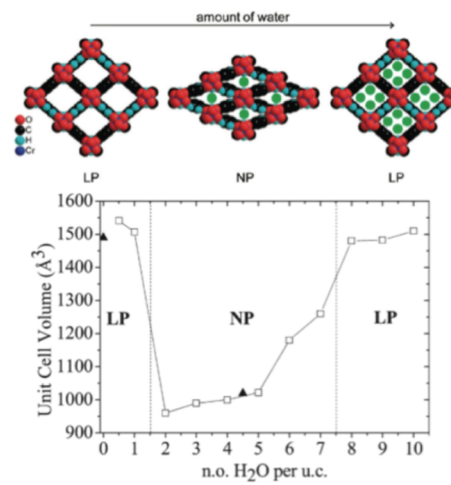


Figure 25. (Top) Breathing behavior in MIL-53(Cr) upon adsorption of water. (Bottom) Change in MIL-53(Cr) unit cell volume as the number of water molecules per unit cell increases. Open squares indicate results from molecular dynamics simulations at 300 K whereas closed triangles indicate available experimental values. LP denotes the large pore conformation, and NP indicates the narrow pore conformation. Reprinted with permission from ref 228. Copyright 2011 American Chemical Society.

nonpolarizable water models were unable to capture important variations in water dipole moments that existed in the polarizable water models, leading to the neglect of important many-body interactions between the framework and water atoms. Sholl et al. reached a similar conclusion in HKUST-1 where they found significant changes to the density functional theory (DFT) derived atomic charges as water moved through the framework.²³⁶ Only through a classical force field model with an added water–copper distance-dependent correction term could they properly account for the nonstatic nature of water's Coulombic interactions. These studies question the use of classical water models that treat electrostatic interactions in a purely static, nonpolarizable manner and suggest that more sophisticated water force fields may be necessary, especially in MOFs possessing open metal sites or other hydrophilic moieties. Nuclear quantum effects have also been shown to have a significant impact on the dynamical properties of water in MIL-53(Cr) in the narrow pore conformation where slower orientation dynamics result from the increased molecular volume of quantum H₂O molecules in the pores.²³⁷ Recently, the critical role the metal identity plays in determining the phase behavior of isostructural MIL-53 materials was elucidated by Coudert et al. via an analysis of the coordination chemistry and molecular orbitals in MIL-53(Ga) to explain why its breathing behavior is distinctly different from that of MIL-53(Cr).¹¹⁹

MOFs have also demonstrated properties that make them promising materials for proton conduction applications under hydrated conditions in fuel cells.^{122,238–253} The mechanism of proton transport in the presence of water in MIL-53(Cr) was explored in a recent computational study and suggested to proceed through a proton-hopping Grotthuss mechanism resembling a Zundel-like structure in the narrow pore form and an Eigen-like structure in the large pore form.²⁵⁴ While the proton mobility in this structure benefits from a lower free energy barrier to proton transfer relative to bulk water, this is counteracted by hydrogen bonding interactions between water and the μ_2 -OH groups in MIL-53(Cr) that suppress this mobility

by slowing the rearrangement of the hydrogen bonding networks in the pores. It was therefore noted that the incorporation of hydrophobic moieties, similar to those found in biological proton channels, is one possible strategy for increasing proton conductivity in MOFs.

Insight into the agglomeration behavior of water molecules under nanoconfinement is critical to the fundamental understanding of many biological and colloidal phenomena.²⁵⁶ The formation and stability of water clusters in the hydrophobic pores of FMOF-1 were recently investigated using DFT calculations combined with *in situ* spectroscopy techniques.²⁵⁵ The FMOF-1 framework contains Ag_4TZ_6 units linked by Ag(I) centers and possesses two different pore types, a main pore with $\sim 12.2 \times 6.3 \text{ \AA}^2$ channels lined with CF_3 groups and second, smaller pore that is $\sim 6.6 \times 4.9 \text{ \AA}^2$ in size.⁹² While no measurable water adsorption was detected in prior isotherm measurements on the structure,⁹² subsequent *in situ* IR spectroscopy identified the presence of water clusters in the larger cavities of the structure that are held together primarily by intermolecular hydrogen bonding interactions.²⁵⁵ At water vapor pressures lower than 3 Torr pentameric water clusters were observed, and as the vapor pressure increased, even larger water clusters formed. First principle DFT calculations within the FMOF-1 pore as the water cluster size increases from a dimer to pentamer structure (Figure 26) were performed to understand why these larger water

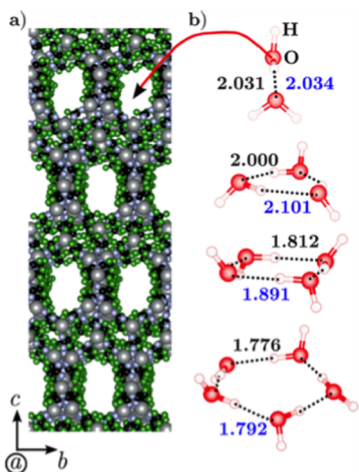


Figure 26. Orientation of water clusters in the pores of FMOF-1 after relaxation using density functional theory. Hydrogen bond distances in the gas phase (black) and inside FMOF-1 (blue) are shown in Å. Reprinted with permission from ref 255. Copyright 2013 American Chemical Society.

clusters are more favorable than the smaller ones, a phenomenon that was attributed to the increased adsorption energy due to greater nondirectional dispersive interactions in the larger water clusters. Analysis of the water modes during water desorption and interaction with coadsorbed methane also confirmed the relatively high stability of these pentameric clusters. In fact, DFT calculations indicated that the water clusters formed in the pores of FMOF-1 are even more energetically favorable than these same water clusters when present in the water gas phase.

3. STRUCTURAL FACTORS GOVERNING WATER STABILITY

In this section we present a conceptual flowchart (Figure 27) to understand the interplay of structural factors that govern water

stability in MOFs. This flowchart was developed on the basis of a comprehensive survey of past experimental studies involving MOF water exposure and subsequent characterization and presents relevant structural factors in terms of the simplest, most chemically meaningful properties of the framework. For example, rather than rationalizing stability trends in terms of overarching properties such as the geometry of the framework's secondary building unit, we instead present this in terms of simpler constituents such as the coordination number and identity of the atoms in the metal cluster. This more fundamental classification allows the understanding of water stability trends in a wide array of current and yet to be discovered MOF structural motifs using as few descriptors as possible.

The underlined factors in the ovals on the right side of Figure 27 identify the relevant structural characteristics governing MOF water stability in the thermodynamic or kinetic regime of the flowchart whereas the subpoints identify specific factors related to this structural characteristic that can be quantified directly from the structure's crystallographic information file (CIF) or via a molecular simulation with the CIF. These characteristics are organized in a hierarchical fashion with the most important factors in the flowchart at the top and those of decreasing importance toward the bottom. In other words, when interpreting Figure 27, if the characteristics at the top of the flowchart are met then a structure is expected to be thermodynamically stable and the factors below it need not be considered. However, if the uppermost factors are not met, one must then look further down the chart and take into account a combination of both the uppermost factors and the relevant factors below it to rationalize the structure's water stability.

3.1. Thermodynamic Stability

The key structural property common to thermodynamically stable MOFs is an inert metal cluster that renders it unfavorable for an irreversible hydrolysis reaction to occur. The oxygen in water is a nucleophile whereas the metal coordination centers in MOFs are electrophilic. If this metal center is not sufficiently inert, water can coordinate with the metal cluster and distort or destroy the MOF's crystal lattice. Computationally, the thermodynamic stability of a structure in the presence of water can be directly quantified by examining the free energy of the hydrolysis reaction via the following relationship:

$$\Delta G_{\text{hydrolysis}} = \Delta G_{\text{prod}(\text{MOF} + n\text{H}_2\text{O})} - \Delta G_{\text{react}(\text{MOF} + n\text{H}_2\text{O})} \quad (1)$$

In eq 1, ΔG_{prod} is the free energy of the coordination complex formed between the MOF and the water molecules after the hydrolysis reaction takes place and ΔG_{react} is the free energy of the MOF and the water molecules before the hydrolysis occurs. The practical challenges of performing such calculations are discussed in section 5.1.2. Experimentally, this stability can be inferred via prolonged exposure of the MOF to aqueous conditions and subsequent comparison of the sample's structural properties before and after water exposure via methods such as PXRD and BET surface area analysis.

3.1.1. Metal–Ligand Bond Strength. A metal–ligand coordination bond is the key feature that distinguishes MOFs from more chemically stable porous materials such as zeolites and activated carbons. As a weak point in the structure, the strength of this bond can be a strong indicator of the MOF's hydrolytic stability.⁶² While the MOF's enthalpy of formation from its constituent units can be used to predict the thermodynamic stability of the evacuated or solvated structure,^{257–259} this property will be of little value if the constituent

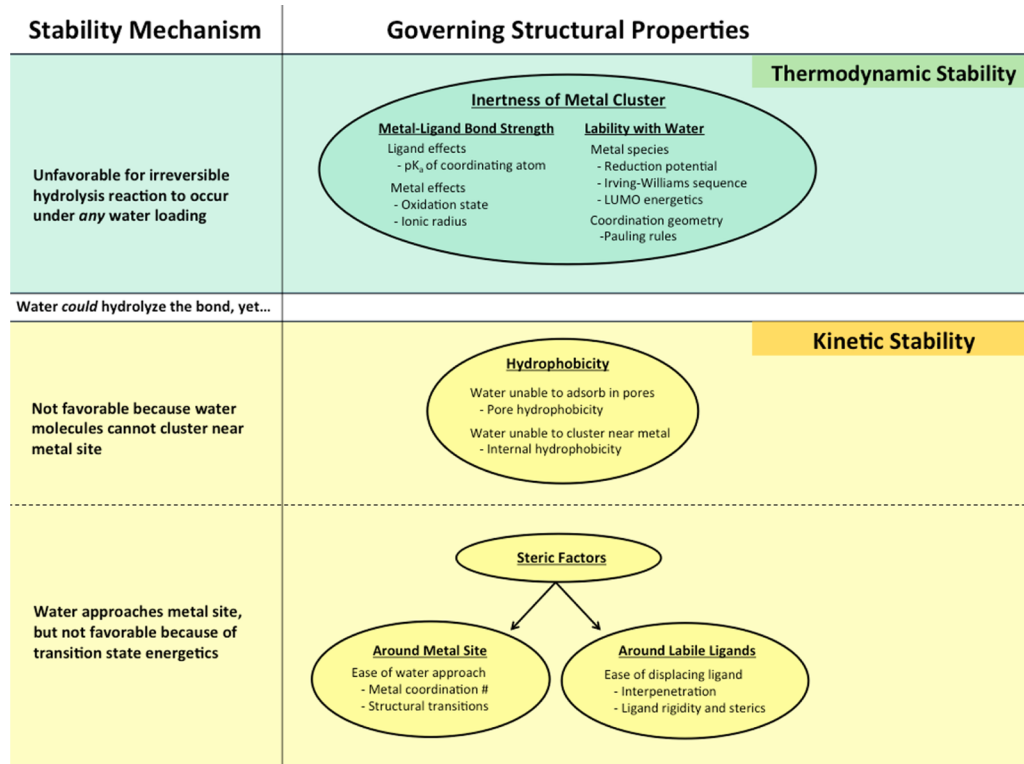


Figure 27. Flowchart of structural factors governing water stability in MOFs.

units do not correspond to the MOF's product state after the hydrolysis reaction. This point underscores the importance of performing further experimental and computational studies into breakdown mechanisms in MOFs (section 5.1).

Because MOFs are governed by Lewis acid–base coordination chemistry, the pK_a of the coordinating atom on the ligand can be used as a first-order approximation of the metal–ligand bond strength. This was first noted by Long et al. and used as a strategy in the synthesis of a series of highly stable Co-, Zn-, Ni-, and Cu-based MOFs containing the pyrazolate ligand (pK_a 19.8).^{260,261} Ligand pK_a is a particularly useful metric because it can be readily approximated with tools such as the SPARC ligand pK_a calculator²⁶² and used to predict the stability of novel structures before any synthesis attempt is made. The properties of the metal species will also play an important role in determining the metal–ligand bond strength, and factors such as the metal oxidation state and ionic radius also need to be taken into account. For example, MOFs containing the group IV metals Ti, Zr, and Hf in the +4 oxidation state, tend to correlate with high levels of chemical stability.^{35,47,55,56,101,103,192,263–266} However, while the isolated properties of the ligand and metal species can provide useful initial insight into the chemical stability of the resulting structure, a full understanding of the metal–ligand bond strength can only be obtained by considering the combined metal–ligand properties. For example, greater similarity between the ligand and metal's polarizability (as a hard or soft acid and base) will result in a more strongly binding coordination complex.²⁶⁷ At the most detailed level, factors related to the ease of atomic orbital overlap between the metal and ligand in their specific coordination geometry need to also be taken into account.

3.1.2. Liability with Water. While the metal–ligand bond strength alone can be used to rationalize the stability of the majority of chemically stable MOFs in the literature, the lability

of the metal cluster toward water must be considered to understand the stability of select cases. A comparative study of the MIL-53(Al,Cr) and MIL-47(V) structures found that the relative chemical stability of these frameworks (Cr > Al > V) is governed by the inertness of the metal center as opposed to the average metal–oxygen bond strength.²⁶⁸ The exceptional stability of MIL-53(Cr) thus arises from a large energy difference in the frontier orbitals of water and chromium. For similar reasons, the authors noted that Rh-based MOFs are expected to have exceptional chemical stabilities.

On the basis of the existing literature, we propose several guidelines that may be useful in the selection of further chemically stable MOFs based on this criterion. The Irving–Williams series describes the relative stability of first row transition series bivalent metal ions ($\text{Mn} < \text{Fe} < \text{Co} < \text{Ni} < \text{Cu} > \text{Zn}$)²⁶⁹ with a wide variety of ligands and can therefore be used as a guiding tool in the synthesis of stable structures. Work by LeVan and Matzger on the MOF-74 series suggests that the frameworks containing metal species that are weaker reducing agents tend to have stronger moisture stability,^{132,270} making the reduction potential of the metal another potentially useful predictor. Pauling's rules are used to determine the favored crystal structures of ionic crystals from the ratio of the cation and anion radius²⁷¹ and may be used as another useful guideline for determining whether ionic contributions favor an irreversible reaction to progress based on the coordination geometry of the hydrolysis product state. This concept was used in the work of Lopez et al.²⁷² to understand the ionic origins of the higher hydrolytic stability observed in the experimentally synthesized Be-based IRMOF-1 variation²⁷³ relative to its less stable Zn counterpart.

3.2. Kinetic Stability

While the free energy of a hydrolysis reaction governs the thermodynamic stability of MOFs, kinetic stability instead relies on a sufficiently high activation energy barrier, E_a , being present. The activation energy of a reaction depends not only on the product and reactant states but also the specific reaction pathway and transition states involved. As a result, quantifying the kinetic stability of structures using eq 2, below, is significantly more difficult to explore from a computational standpoint.

$$\Delta G_{Ea} = \Delta G_{TS(MOF+nH_2O)}^{\ddagger} - \Delta G_{react(MOF+nH_2O)} \quad (2)$$

In this equation ΔG_{TS}^{\ddagger} is the free energy of the hydrolysis reaction's transition state whereas ΔG_{react} is the free energy of the MOF and the water molecules before hydrolysis occurs. However, considering these kinetic factors is critically important to obtaining a full understanding of the varying levels of water stability in MOFs. As shown in Figure 28, even if a structure does

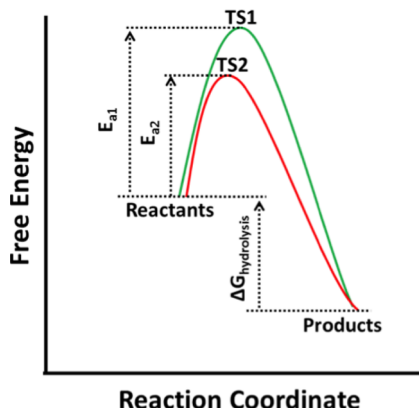


Figure 28. Reaction coordinate diagram highlighting the importance of kinetic factors in determining MOF water stability. While structures 1 (green) and 2 (red) have the same thermodynamic stability ($\Delta G_{\text{hydrolysis}}$), structure 1 is more stable under humid conditions due to kinetic factors that increase the activation energy barrier (E_a) needed to reach its transition state (TS).

not possess thermodynamic factors which make its metal center inert, the presence of kinetic factors such as hydrophobicity and ligand sterics can still increase the activation energy for hydrolysis to render the structure stable under humid conditions.

3.2.1. Hydrophobicity. A hydrolysis reaction can only progress if two distinct events occur. First, the water molecule must come sufficiently close to the metal to allow interaction between the electron orbitals on the electrophilic metal and nucleophilic water. Second, the energetics of this interaction must be great enough to overcome the activation energy barrier of the reaction. The necessity of this first event underscores the important role framework hydrophobicity can play in improving MOF water stability. It has been widely reported that MOF stability under humid conditions can be improved by incorporating hydrophobic fluorinated and alkyl functional groups on the ligand.^{60,64,65,84,91,95,274–276} This increase in stability may be due to two different types of hydrophobicity mechanisms. In the first case, pore hydrophobicity can prevent water from adsorbing into the pores.^{84,92} This stability mechanism can be verified by performing adsorption isotherms on the sample to confirm the hydrophobic groups exclude water from ever adsorbing into the structure. In the second case, internal hydrophobicity can result where water still adsorbs into

the pores but cannot cluster around the metal center and react.^{277,278} Shimizu et al. showed that nonpolar alkyl functional groups in CALF-25 allow the structure to adsorb appreciable amounts of water but remain water stable due to functional group shielding around the metal center.⁶⁰ The contribution that water clustering can play in promoting hydrolysis reactions in MOFs was highlighted in the separate works of Lopez et al.²⁷⁹ and Fuchs et al.²⁸⁰ who showed that only after water has formed clusters around the metal center can the metal–oxygen bond in IRMOF structures be hydrolyzed. Lopez et al. also demonstrated the importance of these effects by exploring how polar functional groups in the IRMOF series can improve their structural stability at low water contents by serving as basins of attraction which draw water away from the metal center.²⁷⁸

3.2.2. Steric Factors. Even if water molecules can come sufficiently close to the metal center, the presence of steric factors can reduce the reaction kinetics by providing a significant activation energy barrier to overcome. Despite the relatively low pK_a of carboxylate ligands, the high coordination number of the metal in the well-known Zr-based UiO-66 MOF helps make this structure highly stable even after adsorbing large amounts of water.^{35,47,62,103} This high coordination number also correlates with the stability observed in a range of other MOFs including the Zr-based MIL-140,¹⁰¹ DUT-51,67–69,^{55,56} PCN-56–59,222,224,225,^{192,263,264,266} and MOF-525,545,²⁶⁵ the Hf-based DUT-51,67–69,^{55,56} and the La-based LaBTB.²⁸¹ One rationale for the greater stability in these structures is that their high metal coordination numbers create a crowding effect that prevents water clusters from forming near the metal center. Additionally, even if a bond breakage event were to occur in these structures, their higher metal coordination number can result in a greater tolerance for hydrolysis before lattice collapse will occur by having a number of other bound ligands still available as support.

The ligand properties can also play a role in altering the activation energy barrier for hydrolysis reactions by affecting ligand rotational effects. The aromatic rings in MOFs can exhibit significant rotational dynamics that, in the case of UiO-66, are on the order of thousands of kHz near room temperature.²⁸² It has been suggested that UiO-67 with the 4,4'-biphenyldicarboxylate (BPDC) ligand is less stable than the BDC-based UiO-66 due to the greater torsional strain the BPDC linkers create around the metal cluster.⁹⁸ It has also been shown that, after water exposure, this structure is particularly prone to capillary-force-driven channel collapse during sample activation, and this instability can be mitigated via solvent exchange with a lower surface tension solvent.²⁸³ Steric factors around the ligand can also play an important role in determining the stability of many other MOF systems. A comparative study of Zn-based pillared MOFs demonstrated that catenation, which is the interpenetration of individual frameworks, can be used to obtain more water-stable MOFs even when the basicity of the pillar ligand is reduced.⁷⁷ This behavior is likely a result of the steric hindrances to ligand displacement that catenation provides by effectively locking the labile ligand in place within the framework. Ligand functionalization can have a similar impact as bulky functional groups can also sterically lock the labile ligands in place to prevent their irreversible displacement as well.

Structural transitions that occur in response to physical stimuli such as guest adsorption can affect MOF water stability by changing the sterics and accessibility for water around the metal center as well.^{18,111,284} For example, MOF breathing from the large to narrow pore conformation can allow water clusters²²⁸ to

come in closer proximity to the metal clusters, and the gate-opening effect can cause nonporous structures to form more porous variations that result in a sudden increase in the structure's water uptake. MIL-53(Cr)^{114,118,285} and DMOF^{203,286–288} are well-studied MOFs that show breathing behavior in the presence of polar vapors and MOFs such as Cu(4,4'-BIPY)(DHBC)₂²⁸⁹ ELM-11,²⁹⁰ and La(BTB)-(H₂O)²⁹¹ have shown a gate-opening effect during the adsorption of various gases.

4. EXISTING MOFS AND THEIR STABILITY

In this section we assign stability classifications to all MOFs that have been experimentally characterized after water exposure at the time of this Review. These classifications are given in Tables 3–6 and will be a valuable resource for researchers looking to evaluate existing MOFs for specific adsorption applications by allowing the quick identification of promising candidates based on the stability findings of past literature. The criteria for these classifications are presented in Table 2 and provide practical

confidence levels, the specific characterization techniques used and the number of independent studies that investigated the stability properties of the structure were considered. For example, if PXRD is the only technique used to characterize a MOF's stability after weeks in liquid water we can only place this structure in the thermodynamically stable category with a low confidence level. This is because, as discussed in section 1.1.1, PXRD provides only spatially averaged information about the long-range crystallinity of the structure and thus neglects critically important information related to loss of solid phase content due to sample solubility, additional amorphous character, and structural collapse occurring only at the crystal's surface that would still render the internal surface area inaccessible to adsorbates. It is therefore recommended that all structures placed in a certain stability category with a low confidence level be first characterized via porosity measurements after water exposure before further investigating the structure for a certain application. Depending on the target application, further stability tests exploring effects due to long-term aging or multiple regeneration steps should also be conducted on the structure. There are also cases where conflicting water stability results are reported by different research groups investigating the same structure. Such variations are inevitable and can be explained by an array of uncontrolled (but potentially important) factors ranging from the incorporation of varying defects or crystal size distributions within the sample during synthesis to differing activation conditions utilized during the sample preparation stage. For a comprehensive list of the experimental characterization results and rationales behind the confidence levels assigned to each of the structures reported in Tables 3–6, the reader is referred to the Supporting Information.

4.1. Thermodynamically Stable

We designate thermodynamically stable MOFs as those that do not exhibit structural breakdown after long-term exposure to aqueous conditions. Long-term exposure was classified as a time period of a week or greater in neutral, room temperature liquid water, or in cases where acidic/basic or high temperature conditions were present, a less stringent time period of only 1 day was required. From a stability standpoint, the MOFs in Table 3 therefore merit further consideration for a wide array of adsorption applications in which the adsorbent may face direct exposure to aqueous conditions. The thermal stability limits of these materials in the presence of water is one important property that still requires further exploration before considering these materials for certain applications. While JUC-110,⁹³ H₃(Cu₄Cl)₃-(BTTRI)₈,²⁹⁷ Zn(1,4-BDP),²⁶⁰ Zn(1,3-BDP),²⁶⁰ Ni₃(BTP)₂,²⁶¹ and Cu₂(TCMBT)(BPP)(μ₃-OH)²⁹⁸ have demonstrated stability under boiling water conditions, stability under steam conditions has only been explored for the MIL-96(Al),²⁹⁹ MIL-101(Cr),^{50,62} ZIF-8,⁶² and NOTT-300³⁰⁰ structures.

As discussed in section 3.1, the key structural feature common to thermodynamically stable MOFs is an inert metal cluster that makes it unfavorable for an irreversible hydrolysis reaction to occur under high water loadings. This characteristic is evident in all the structures assigned to Table 3 with a high confidence level (Bio-MOF-14, MIL-100(Cr), Ni₃(BTP)₂, and ZIF-8). Each of these structures possess either a strongly binding coordination ligand or, in cases where such a ligand is not present, a highly inert metal species (Cr³⁺). Among the remaining structures in this category these characteristics are also present with a few notable exceptions (PCMOF-5, NOTT-300). These exceptions can be rationalized by one of two possible explanations. One

Table 2. Criteria for Water Stability Classifications

thermodynamically stable	stable after long-term exposure to aqueous solutions: week or greater in pure water, day(s) in acidic/basic or boiling conditions <i>strong potential for a wide range of applications</i>
high kinetic stability	stable after exposure to high humidity conditions: decomposes after short exposure times in liquid water <i>strong potential for industrial applications with high humidity conditions</i>
low kinetic stability	stable under low humidity conditions <i>potential for applications with predried gas conditions</i>
unstable	quickly breaks down after any moisture exposure <i>potential for applications under moisture-free conditions</i>

guidelines for the highest level of water exposure that the target MOF can be expected to withstand under the application's operating conditions. While thermal stability is not explicitly addressed in the classification criteria, effects due to water exposure under harsher conditions such as elevated temperatures or acidic or basic environments were also considered. Depending on the application, the presence of acid gases such as SO_x, NO_x, and H₂S may also have a significant impact on MOF stability. Studies into MOF stability in the presence of acidic and basic gases are limited^{103,148,149,152,292–296} though such species need to be considered if evaluating MOFs for applications such as pre- or postcombustion CO₂ capture or natural gas sweetening.

No *a priori* knowledge regarding the expected stability of these structures was considered in assigning these classifications. Instead, only those structures with experimental characterization results that directly support their inclusion in a certain category were considered. As a result, MOFs with structural properties that highly correlate with a certain stability classification but have not yet been appropriately characterized in the literature were omitted from these rankings. This being said, the factors discussed in section 3 will be an invaluable tool for making rational stability predictions for MOFs that have yet to be experimentally characterized on the basis of their structural properties.

Because the specific experimental techniques used to quantify water stability vary greatly among studies, confidence levels were also assigned to each of these classifications. To assign these

Table 3. Metal–Organic Frameworks with Thermodynamic Stability in the Presence of Water According to the Classifications in Table 2

common name	activated formula unit ^a	confidence
Bio-MOF-14 ⁹⁵	Co ₂ (AD) ₂ (C ₄ H ₉ CO ₂) ₂	high
MIL-101(Cr) ^{28,44,49–51,53,62,167}	Cr ₃ F(H ₂ O) ₂ O(BDC) ₃	high
MIL-101-SO ₃ H (Cr) ^{51,301}	Cr ₃ F(H ₂ O) ₂ O(BDC-SO ₃ H) ₃	high
MIL-96(Al) ^{299,302}	Al ₁₂ O(OH) ₁₈ (H ₂ O) ₃ (Al ₂ (OH) ₄) ₆	high
N/A ²⁶¹	Ni ₃ (BTP) ₂	high
PCN-222(Fe) ²⁶⁴		high
PCN-224(M) ²⁶⁶		high
ZIF-8 ^{28,62,63,105,293}	Zn(MEIM) ₂	high
Al-PMOF ³⁰³	TCPP(AIOH) ₂	medium
JUC-110 ⁹³	Cd(HTHIPC) ₂	medium
MIL-100(Cr) ^{38,39,63}	Cr ₃ OX(BTC) ₂ , X = OH, F	medium
MONT1 ³⁰⁴	Cu ₂ (PCP) ₂ BIPY	medium
N/A ³⁰⁵	Pb ₂ (PTPTP) ₂ (H ₂ O) ₂	medium
N/A ³⁰⁵	Pb ₂ (p-PDA)(PTPTP) ₂	medium
N/A ³⁰⁵	Pb ₄ (o-PDA) ₂ (PTPTP) ₂	medium
LaBTB ²⁸¹	La(BTB)H ₂ O	low
N/A ²⁹⁷	H ₃ (Cu ₄ Cl) ₃ (BTTRI) ₈	low
N/A ²⁶⁰	Zn(1,4-BDP)	low
N/A ²⁶⁰	Zn(1,3-BDP)	low
N/A ²⁶¹	Cu ₃ (BTP) ₂	low
N/A ²⁶¹	Zn ₃ (BTP) ₂	low
N/A ²⁹⁸	Cu ₂ (TCMBT)(BPP)(μ ₃ -OH)	low
NOTT-300 ³⁰⁰	Al ₂ (OH) ₂ (H ₄ L)	low
PCMOf-5 ³⁰⁶	La(H ₅ L ₅)(H ₂ O) ₄	low
SNU-80 ⁸²	Cu ₄ (Me ₃ CCOO) ₈ (TEIA)	low

^aSee Abbreviations.

possibility that cannot be ruled out is that because all the structures which are exceptions to this rule are assigned to the thermodynamically stable category with a medium or low confidence level, the porosity of these structures may in fact have been compromised after long-term liquid water exposure though this structural information could not be adequately captured because no postwater porosity measurements were performed. The other possibility is that these structures exhibit only an apparent thermodynamic stability but do not in fact possess a highly inert metal cluster. However, this deficiency is compensated by the fact that other strong kinetic factors (section 3.2) still exist that make the barrier to an irreversible hydrolysis reaction sufficiently high under aqueous conditions.

4.2. High Kinetic Stability

The distinction between thermodynamically stable MOFs and those with high kinetic stability is that the former can withstand exposure to liquid water conditions whereas the latter are stable only after exposure to water in the vapor phase. While some MOFs are stable over long periods in humid air without any loss of crystallinity or surface area, immediate structural breakdown upon exposure to liquid water can still be observed.⁷⁶ This difference in stability may arise from that fact that liquid water exposure can result in equilibrium water loadings in the structure that are greater than what is favored by exposure to water in the vapor phase. All the kinetically stable structures in Table 4 can therefore be considered strong candidates for applications where the adsorbent is exposed to high humidity conditions but does not come into direct contact with water in the liquid phase.

There is a wide array of MOFs included in this high kinetic stability category and around 40 of them fall within this category with a high confidence level. These include well-studied structures such as UiO-66 and several members of the MIL family of materials. These MOFs exhibit high kinetic water stability because they possess somewhat inert metal centers that are also combined with the various kinetic stability factors discussed in section 3.2. For example, the UiO series of MOFs possess Zr centers with high coordination numbers between the metal and ligand which create steric hindrance that make hydrolysis less favorable and provide a greater structural tolerance even if a ligand displacement were to occur via the high number of other ligands that would still remain for structural support. In the case of Zn-DMOF-TM, there are no strong thermodynamic arguments for why the BDC-TM and DABCO ligands coordinated with zinc should not be hydrolyzed in the presence of water (and in the parent Zn-DMOF structure, this hydrolysis readily occurs^{31,71,72}). However, adding four methyl groups on each of these BDC ligands drastically changes the steric factors in the structure and thus prevents structural breakdown from occurring after long-term vapor exposure.⁷⁶ There are some apparent outliers in Table 4 such as MIL-53(Cr) that are classified only as kinetically stable when they possess highly inert centers that make them perfectly fit for the thermodynamically stable category. In these cases it is entirely possible that the stability limit of this structure was simply not tested to its limit, and if such experiments were performed, these structures would also be classified as thermodynamically stable. However, to keep these classifications empirical and remove any *a priori* bias from them, we keep these structures in the high kinetic stability category until the direct experimental evidence needed to justify such classifications is presented.

4.3. Low Kinetic Stability

MOFs classified in Table 5 to have low kinetic stability show some evidence of structural stability after exposure to water in the vapor phase though do not exhibit the stability after high humidity conditions that are present in MOFs with high kinetic stability. These structures can therefore be considered candidates for applications where the adsorbent is exposed to predried gas streams or other low moisture environments where liquid water is not present. The number of MOFs in this category is quite low compared to the number of structures with thermodynamic or high kinetic stability. It would be misleading, however, to believe that these numbers are representative of the overall stability trends in the MOF literature. Instead, the number of stable structures is likely a small fraction of the total number of unstable structures in the literature. In fact, a large number of synthesis procedures for existing MOFs must be performed under controlled environments where exposure of the dried sample to ambient air is avoided to prevent structural breakdown before characterization.

4.4. Unstable

The MOFs in Table 6 show little structural stability after exposure to even small amounts of moisture in the vapor phase. On the basis of their demonstrated stability, applications for these structures should be limited to conditions where almost no moisture is present such as hydrogen and methane storage. However, if use of these structures under higher humidity conditions is desired, the strategies discussed in section 5.2 can be used to modify the structure to improve its water stability. These unstable structures exhibit both labile metal clusters and an absence of any kinetic factors that provide a significant barrier

Table 4. Metal–Organic Frameworks with High Kinetic Stability in the Presence of Water According to the Classifications in Table 2

common name	activated formula unit ^a	confidence
CALF-2S ⁶⁰	BaH ₂ L	high
CAU-10 ¹¹⁰	Al(OH)(ISO)	high
DUT-51(Hf) ⁵⁵	Hf ₆ O ₆ (OH) ₂ (DTTDC) ₄	high
DUT-51(Zr) ⁵⁵	Zr ₆ O ₆ (OH) ₂ (DTTDC) ₄	high
DUT-67(Zr) ^{56,110}	Zr ₆ O ₆ (OH) ₂ (TDC) ₄	high
FMOF-1 ⁹²	Ag(TZ)	high
MIL-100(Al) ^{37,299}	Al ₃ OX(H ₂ O) ₂ (BTC) ₂ , X = F, OH	high
MIL-100(Fe) ^{28,37,41,42,44}	Fe ₃ OX(H ₂ O) ₂ (BTC) ₂ , X = F, OH	high
MIL-101-NH₂(Cr) ^{51,52}	Cr ₃ F(H ₂ O) ₂ O(BDC-NH ₂) ₃	high
MIL-125-NH₂(Ti) ^{46–48}	Ti ₈ O ₈ (OH) ₄ (BDC-NH ₂) ₆	high
MIL-127 ⁴²	Fe ₆ O ₂ (TAZB) ₃ X ₂ , X = Cl, OH	high
MIL-53(Al) ^{62,268,307}	Al(OH)(BDC)	high
MIL-53(Cr) ²⁶⁸	Cr(OH)BDC	high
MOF-52 ²⁶⁵	Zr ₆ O ₄ (OH) ₄ (TCPP-H ₂) ₃	high
MOF-54 ²⁶⁵	Zr ₆ O ₈ (H ₂ O) ₈ (TCPP-H ₂) ₂	high
MOF-801-P ¹¹⁰	Zr ₆ O ₄ (OH) ₄ (FUM) ₆	high
MOF-801-SC ¹¹⁰	Zr ₆ O ₄ (OH) ₄ (FUM) ₆	high
MOF-802 ¹¹⁰	Zr ₆ O ₄ (OH) ₄ (PZDC) ₄ ₅ (HCOO) ₂ (H ₂ O) ₂	high
MOF-804 ¹¹⁰	Zr ₆ O ₄ (OH) ₄ (BDC-(OH) ₂) ₆	high
MOF-841 ¹¹⁰	Zr ₆ O ₄ (OH) ₄ (MTB) ₂ (HCOO) ₄ (H ₂ O) ₄	high
N/A ⁸⁰	Ni ₈ (OH) ₄ (H ₂ O) ₂ (L ₆) ₆	high
N/A ⁸⁰	Ni ₈ (OH) ₄ (H ₂ O) ₂ (L ₈) ₆	high
N/A ⁸⁰	Ni ₈ (OH) ₄ (H ₂ O) ₂ (L ₉) ₆	high
N/A ⁸⁰	Ni ₈ (OH) ₄ (H ₂ O) ₂ (L ₁₀) ₆	high
N/A ⁸⁰	Ni ₈ (OH) ₄ (H ₂ O) ₂ (L ₁₀ -(CH ₃) ₂) ₆	high
N/A ⁸⁰	Ni ₈ (OH) ₄ (H ₂ O) ₂ (L ₁₀ -(CF ₃) ₂) ₆	high
N/A ⁶¹	Zn ₂ (BTC)(OH)-(H ₂ O)	high
N/A ⁸⁹	Zn(L ₁₄)(L ₁₅)	high
Ni-NIC ²⁹²	Ni ₂ (NIC) ₄ (H ₂ O)	high
NU-1000 ²⁸³	Zr ₆ (OH) ₁₆ (TBAPY) ₂	high
PCN-225(M) ¹⁹²	Zr ₆ O ₄ (OH) ₄ (OH) ₄ (H ₂ O) ₄ (MTCPP) ₂	high
SCUTC-18 ^{308,309}	Zn ₂ (BDC) ₂ (2,2'-dimethyl-BPY)	high
UiO-66 ^{31,41,42,58,98,101,110,310}	Zr ₆ O ₆ (BDC) ₁₂	high
UiO-66-MM ⁹⁹	Zr ₆ O ₆ (BDC-CH ₃) ₁₂	high
UiO-66-NH₂ ^{31,42,47,97,98,311}	Zr ₆ O ₆ (BDC-NH ₂) ₁₂	high
Zn-DMOF-A ⁷⁵	Zn ₂ (1,4-ADC) ₂ (DABCO)	high
Zn-DMOF-TM ^{75,76}	Zn ₂ (BDC-(CH ₃) ₄) ₂ (DABCO)	high
Zn-MOF-508 ⁷⁷	Zn ₂ (BDC) ₂ (BPY)	high
ZnPO ₃ ²⁹²	(C ₆ H ₁₄ N) ₂ Zn ₃ (HPO ₃) ₄	high
CAU-10-CH ₃ ⁵⁹	Al(OH)(ISO-CH ₃)	medium
CAU-10-H ⁵⁹	Al(OH)(ISO-H)	medium
CAU-10-NH₂ ⁵⁹	Al(OH)(ISO-NH ₂)	medium
CAU-10-NO ₂ ⁵⁹	Al(OH)(ISO-NO ₂)	medium
CAU-10-OCH ₃ ⁵⁹	Al(OH)(ISO-OCH ₃)	medium
CAU-10-OH ⁵⁹	Al(OH)(ISO-OH)	medium
CdZrSr ²⁹²	CdZrSr(C ₂ O ₄) ₄	medium
Co-NIC ²⁹³	Co ₂ (NIC) ₄ (μ-H ₂ O)	medium
Cu-PCN ²⁹³	Cu ₂ (PCN) ₂ (H ₂ O) ₂	medium
Eu-Cu ²⁹²	EuCu(NIC) ₂ (C ₂ O ₄)	medium
La-Cu ²⁹²	LnCu (NIC) ₂ (C ₂ O ₄)	medium
MIL-53-F(Al) ³¹²	Al(OH)(BDC-F)	medium
N/A ⁵⁴	Al(OH)(1,4-NDC)	medium
Ni-HF ²⁹³	Ni ₂ (HFPDPT)-(BPY) ₂ (H ₂ O) ₂] ₂ (H ₂ O) ₈	medium
UiO-66-Br ^{42,311}	Zr ₆ O ₆ (BDC-Br) ₁₂	medium
UiO-67 ^{98,101,283,310}	Zr ₆ O ₆ (BPDC) ₁₂	medium
UTSA-16 ³¹³	[KC ₀ ₃ (C ₆ H ₄ O ₇) ₂ (C ₆ H ₅ O ₇) ₂ (H ₂ O) ₂ 8H ₂ O] ₈	medium
ZIF-7 ²⁹³	Zn(PhIM) ₂	medium
ZIF-90 ²⁹³	Zn(ICA) ₂	medium
Zn-TTC ²⁹³	Zn ₃ (TTC)(OH) ₂ (H ₂ O)	medium
Zn/Co-BTEC ²⁹³	ZnCo(BTEC)	medium

Table 4. continued

common name	activated formula unit ^a	confidence
Zr-DMBDC ¹⁶²	Zr ₆ O ₆ (DMBDC) ₁₂	medium
AlaZnCl ⁸⁵	Zn(Ala)(Cl)	low
AlaZnOAc ⁸⁵	Zn(Ala)(OAc)	low
Bio-MOF-13 ⁹⁵	Co ₂ (AD) ₂ (C ₃ H ₇ CO ₂) ₂	low
CUK-1 ³¹⁴	Co ₃ (2,4-PDC) ₂ (μ-OH) ₂	low
DUT-67(Hf) ⁵⁶	Hf ₆ O ₆ (OH) ₂ (TDC) ₄	low
DUT-68(Hf) ⁵⁶	Hf ₆ O ₆ (OH) ₂ (TDC) _{4.5}	low
DUT-68(Zr) ⁵⁶	Zr ₆ O ₆ (OH) ₂ (TDC) _{4.5}	low
DUT-69(Zr) ⁵⁶	Zr ₆ O ₄ (OH) ₄ (TDC) ₅	low
MIL-140 A ¹⁰¹	ZrO(BDC)	low
MIL-140 B ¹⁰¹	ZrO(2,6-NDC)	low
MIL-140 C ¹⁰¹	ZrO(BPDC)	low
MIL-140 D ¹⁰¹	ZrO(ABDC-Cl ₂)	low
MOFF-2 ⁸⁴	Cu(L ₁₁)(DABCO) _{0.5}	low
MOOFOUR-1-Ni ³¹⁵	Ni-(BPE) ₂ (MoO ₄)	low
N/A ³¹⁶	Zn ₆ (IDC) ₄ (OH) ₂ (HPRZ) ₂	low
N/A ³¹⁷	Cd(2,6-NDC) _{0.5} (PCA)	low
N/A ³⁰⁹	Zn ₂ (2,6-NDC) ₂ (2,2'-dimethyl-BPY)	low
N/A ⁸³	Cd(L ₁)(Cl)(H ₂ O)	low
N/A ⁸³	Cd(L ₂)(Cl)(H ₂ O)	low
N/A ⁸³	Cd ₂ (L ₂) ₂ (Br) ₂ (H ₂ O) ₃	low
N/A ⁸³	Cd(L ₃)(Cl)(H ₂ O) ₂	low
N/A ⁸¹	Zn ₂ L ₄	low
N/A ³¹⁸	Ni(HPTZ) ₂	low
N/A ³¹⁹	Zn ₄ O(BFBPDC) ₃ (BPY) _{0.5} (H ₂ O)	low
N/A ⁷⁹	Ni(L ₁₃) ₂	low
N/A ⁷⁹	Co(L ₁₃) ₂	low
N/A ³²⁰	Ni ₂ (C ₂ O ₄)(L ₁₆) ₂	low
N/A ²⁷⁶	Zn ₃ (BPDC) ₃ (2,2'-dimethyl-BPY)	low
NU-1000-SALI-1 ¹⁰⁴	Zr ₆ (μ-OH) ₈ (OH) ₈ (TBAPY) ₂ -CF ₃ CO ₂	low
NU-1000-SALI-3 ¹⁰⁴	Zr ₆ (μ ₃ -OH) ₈ (OH) ₈ (TBAPY) ₂ -CF ₃ (CF ₂) ₂ CO ₂	low
NU-1000-SALI-7 ¹⁰⁴	Zr ₆ (μ ₃ -OH) ₈ (OH) ₈ (TBAPY) ₂ -CF ₃ (CF ₂) ₆ CO ₂	low
NU-1000-SALI-9 ¹⁰⁴	Zr ₆ (μ ₃ -OH) ₈ (OH) ₈ (TBAPY) ₂ -CF ₃ (CF ₂) ₈ CO ₂	low
PCN-56 ²⁶³	Zr ₃ O ₂ (OH) ₂ (TPDC-(CH ₃) ₂) ₃	low
PCN-57 ²⁶³	Zr ₃ O ₂ (OH) ₂ (TPDC-(CH ₃) ₄) ₃	low
PCN-58 ²⁶³	Zr ₃ O ₂ (OH) ₂ (TPDC-(CH ₂ N ₃) ₄) ₃	low
SIFSIX-2-Cu-i ¹³⁴	Cu(DPA) ₂ (SiF ₆)	low
Tb-FTZB-MOF ³²¹	((CH ₃) ₂ NH ₂) ₂ Tb ₆ (μ ₃ -OH) ₈ (FTZB) ₆ (H ₂ O) ₆	low
UiO-1,4-NDC ⁹⁷	Zr ₆ O ₆ (1,4-NDC) ₁₂	low
UiO-2,6-NDC ^{101,103}	Zr ₆ O ₆ (2,6-NDC) ₁₂	low
UiO-66-(CO ₂ H) ₂ ³²²	Zr ₆ O ₆ (BDC-(CO ₂ H) ₂) ₁₂	low
UiO-66-(OMe) ₂ ⁹⁷	Zr ₆ O ₆ (BDC-(OMe) ₂) ₁₂	low
UiO-66-Br ₂ ³²²	Zr ₆ O ₆ (BDC-Br ₂) ₁₂	low
UiO-66-CF ₃ ³²²	Zr ₆ O ₆ (BDC-CF ₃) ₁₂	low
UiO-66-Cl ₂ ³²²	Zr ₆ O ₆ (BDC-Cl ₂) ₁₂	low
UiO-66-CO ₂ H ³²³	Zr ₆ O ₆ (BDC-CO ₂ H) ₁₂	low
UiO-66-DM ¹⁰⁰	Zr ₆ O ₆ (BDC-(CH ₃) ₂) ₁₂	low
UiO-66-I ³²³	Zr ₆ O ₆ (BDC-I) ₁₂	low
UiO-66-NO ₂ ^{97,311}	Zr ₆ O ₆ (BDC-NO ₂) ₁₂	low
UiO-66-SO ₃ H ³²³	Zr ₆ O ₆ (BDC-SO ₃ H) ₁₂	low
UMCM-150 ⁶³	Cu ₃ (BHTC)	low
ValZnCl ⁸⁵	Zn(VAL)(Cl)	low
ValZnFor ⁸⁵	Zn(VAL)(FOR)	low
Y-FTZB-MOF ³²¹	(CH ₃) ₂ NH ₂] ₂ [Y ₆ (μ ₃ -OH) ₈ (FTZB) ₆ (H ₂ O) ₆	low
ZIF-11 ¹⁰⁵	Zn(PhIM) ₂	low
Zn-DMOF(NO ₂) ₂ ⁷⁴	Zn ₂ (BDC-(NO ₂) ₂) ₂ (DABCO)	low
Zn(NDI-H) ⁹⁶	Zn(NDI-H)	low
Zr-fum ³²⁴	Zr ₆ O ₆ (FUM) ₁₂	low

^aSee Abbreviations.

Table 5. Metal–Organic Frameworks with Low Kinetic Stability According to the Classifications in Table 2

common name	activated formula unit ^a	confidence
CAU-6 ¹¹⁰	Al ₁₃ (OH) ₂₇ (H ₂ O) ₆ (BDC-NH ₂) ₃ Cl ₆	high
Co-MOF-74/Co-CPO-27/ Co-DOBDC ^{110,132,325}	Co ₂ (DOBDC)	high
Cu-BTC/HKUST-1 ^{28,31,39,41,62,63,326}	Cu ₃ (BTC) ₂	high
Mg-MOF-74/Mg-CPO-27/Mg-DOBDC ^{31,110,132,133,270}	Mg ₂ (DOBDC)	high
MIL-101-NO ₂ (Cr) ^{51,52}	Cr ₃ F(H ₂ O) ₂ O(BDC-NO ₂) ₃	high
MIL-47-F(V) ³¹²	V(O)(BDC-F)	high
MIL-69(Al)/DUT-4 ²⁸	Al(OH)(2,6-NDC)	high
MOF-14 ³²⁷	Cu ₃ (BTB) ₂ (H ₂ O) ₃	high
MOF-805 ¹¹⁰	Zr ₆ O ₄ (OH) ₄ (2,6-NDC-(OH)) ₆	high
MOF-806 ¹¹⁰	Zr ₆ O ₄ (OH) ₄ (BPDC-(OH)) ₆	high
MOF-808 ¹¹⁰	Zr ₆ O ₄ (OH) ₄ (BTC) ₂ (HCOO) ₆	high
N/A ⁸⁰	Ni ₈ (OH) ₄ (H ₂ O) ₂ (L ₇) ₆	high
Ni-DMOF ^{71,72}	Ni ₂ (BDC) ₂ (DABCO)	high
Ni-MOF-74/Ni-CPO-27/ Ni-DOBDC ^{110,132,270}	Ni ₂ (DOBDC)	high
SCUTC-19 ³⁰⁸	Zn ₂ (BDC) ₂ (3,3'-dimethyl-BPY)	high
Zn-DMOF ^{31,71,72}	Zn ₂ (BDC) ₂ (DABCO)	high
Zn-DMOF-N ⁷⁵	Zn ₂ (1,4-NDC) ₂ (DABCO)	high
Zn-DMOF-TM _{0.5} ^{75,76}	Zn ₂ (BDC)(BDC-(CH ₃) ₄)(DABCO)	high
Zn-MOF-74/Zn-CPO-27/ Zn-DOBDC ^{62,132}	Zn ₂ (DOBDC)	high
Zn-NDC ^{292,309}	Zn ₂ (2,6-NDC) ₂ (BPY)	high
Co-DMOF ⁷²	Co ₂ (BDC) ₂ (DABCO)	medium
Cu-DMOF ⁷²	Cu ₂ (BDC) ₂ (DABCO)	medium
IRMOF-1-CF ₃ O/MOF-5-CF ₃ O/Banasorb-22 ⁶⁴	Zn ₄ O(BDC-2-CF ₃ O) ₃	medium
Cu-EBTC ²⁷⁴	Cu ₃ (BTC-(CH ₃) ₂) ₂ (H ₂ O) ₃	low
Cu-HF ²⁹²	Cu(HFIPBB)(H ₂ HFIPBB) _{0.5}	low
Cu-MBTC ²⁷⁴	Cu ₃ (BTC-CH ₃) ₂ (H ₂ O) ₃	low
IRMOF-1-(CH ₃) ₂ /MOF-5-(CH ₃) ₂ ⁶⁶	Zn ₄ O(BDC-(CH ₃) ₂) ₃	low
IRMOF-1-CH ₃ /MOF-5-CH ₃ ⁶⁶	Zn ₄ O(BDC-CH ₃) ₃	low
IRMOF-3-AM15 ⁶⁵	Zn ₄ O(BDC-NH-CO-(CH ₂) ₁₄ CH ₃)	low
IRMOF-3/MOF-5-NH ₂ ⁶⁵	Zn ₄ O(BDC-NH ₂) ₃	low
MIL-110 (Al) ^{62,299}	Al ₈ (OH) ₁₂ (OH) ₃ (H ₂ O) ₃ (BTC) ₃	low
MIL-125 (Ti) ^{46,48}	Ti ₈ O ₈ (OH) ₄ (BDC) ₆	low
MOFF-1 ⁸⁴	Cu(CH ₃ OH)(L ₁₁)	low
MOFF-3 ⁸⁴	CuO(L ₁₂)	low
N/A ²⁷⁵	Cu ₂ (TPTC-O-(ethyl))	low
N/A ²⁷⁵	Cu ₂ (TPTC-O-(n-propyl))	low
N/A ²⁷⁵	Cu ₂ (TPTC-O-(n-hexyl))	low
SIFSIX-3-Zn ¹³⁴	Zn(PYR) ₂ (SiF ₆)	low
UiO-66-F ₃₂₂	Zr ₆ O ₆ (BDC-F ₂) ₁₂	low
UiO-66-F ³²²	Zr ₆ O ₆ (BDC-F) ₁₂	low
Zr ₆ O ₆ (ABDC-Cl ₂) ₁₂ ^{101,310}	Zr ₆ O ₆ (ABDC-Cl ₂) ₁₂	low
Zr ₆ O ₆ (ABDC) ₁₂ ¹⁰²	Zr ₆ O ₆ (ABDC) ₁₂	low

^aSee Abbreviations.

to allowing the hydrolysis reaction to occur. There are some structures that are clear exceptions to this trend that have been placed in this category with a low confidence level. In these cases, while the structures broke down under all the experimental conditions explored in the study, only aqueous phase conditions were investigated, and it is therefore highly possible that these

Table 6. Unstable Metal–Organic Frameworks in the Presence of Water According to the Classifications in Table 2

common name	activated formula unit ^a	confidence
IRMOF-1/MOF-5 ^{62–67}	Zn ₄ O(BDC) ₃	high
MOF-177 ^{63,68,69}	Zn ₄ O(BTB) ₂	high
MOF-508 ^{62,308,309}	Zn ₂ (BDC) ₂ (BPY)	high
MOF-69C ⁶²	Zn ₃ (OH ₂)(BDC) ₂	high
Zn-DMOF-NO ₂ ^{74,75}	Zn ₂ (BDC-NO ₂) ₂ (DABCO)	high
UiO-BPY ⁹⁸	Zr ₆ O ₆ (BPY) ₁₂	medium
UMCM-1 ³¹	Zn ₄ O(BDC) ₃ (BTB) ₄	medium
Zn-DMOF-Br ⁷⁵	Zn ₂ (BDC-Br) ₂ (DABCO)	medium
Zn-DMOF-Cl ₂ ⁷⁵	Zn ₂ (BDC-Cl ₂) ₂ (DABCO)	medium
Zn-DMOF-DM ⁷⁶	Zn ₂ (BDC-(CH ₃) ₂) ₂ (DABCO)	medium
Zn-DMOF-DM _{0.5} ⁷⁶	Zn ₂ (BDC)(BDC-(CH ₃) ₂)(DABCO)	medium
Zn-DMOF-MM ⁷⁶	Zn ₂ (BDC-CH ₃) ₂ (DABCO)	medium
Zn-DMOF-MM _{0.5} ⁷⁶	Zn ₂ (BDC)(BDC-CH ₃)(DABCO)	medium
Zn-DMOF-NH ₂ ³¹	Zn ₂ (BDC-NH ₂) ₂ (DABCO)	medium
Zn-DMOF-OH ⁷⁵	Zn ₂ (BDC-OH) ₂ (DABCO)	medium
Zn-DMOF-TF ⁷⁶	Zn ₂ (BDC-F ₄) ₂ (DABCO)	medium
Zn-MOF-508-TM ⁷⁷	Zn ₂ (BDC-(CH ₃) ₄) ₂ (BPY)	medium
Bio-MOF-11 ⁹⁵	Co ₂ (AD) ₂ (CH ₃ CO ₂)	low
Bio-MOF-12 ⁹⁵	Co ₂ (AD) ₂ (C ₂ H ₅ CO ₂) ₂	low
MIL-47(V) ²⁶⁸	V(O)BDC	low
MOF-505 ⁶³	Cu ₂ (BPTC)	low
N/A ²⁷⁵	Cu ₂ (TPTC-O-ethyl)	low

^aSee Abbreviations.

structures would exhibit a higher level of stability if exposed to water only in the vapor phase.

5. STEPS TO DEVELOP NEXT-GENERATION WATER-STABLE MOFs

5.1. Fundamental Insight into Breakdown Mechanisms

Understanding breakdown mechanisms in existing MOFs is a critical step toward developing design criteria for next generation, water-stable structures. Studies exploring breakdown mechanisms in isostructural MOFs are of particular interest because they allow one to systematically study the impact that specific structural factors have on water stability. In the following sections we discuss emerging experimental and computational techniques that hold great promise for probing the kinetics and mechanisms of MOF decomposition in the presence of water.

5.1.1. Experimental Techniques. While PXRD and N₂ adsorption at 77 K are the most commonly used approaches for characterizing MOF water stability, techniques that provide information that is not structurally averaged are also needed in order to understand exactly how structures change after water exposure. For example, it has been shown that surface cracks and fractures can have an important impact on MOF moisture stability.³²⁸ While these properties may be overlooked when only analyzing a structure's PXRD pattern, through electron microscopy techniques such as SEM and TEM one can obtain high-resolution information about structural defects and other properties local to the crystal surface. DeCoste et al. utilized SEM to illustrate how HKUST-1 exposed to 90% RH for 3 days begins showing modification at the crystal surface that is not captured in the PXRD pattern, suggesting its crystals are first modified from the external surface before affecting the bulk crystal properties.³⁵ While SEM can provide surface-level information, TEM can provide detailed structural information about properties beneath the crystal surface. However, one has to be particularly careful

when using electron microscopy techniques as MOFs can be electrical insulators which creates the problem of sample charging and can also be electron beam sensitive.³²⁹ Confocal fluorescence microscopy is another technique that can provide such information by allowing the three-dimensional imaging of internal defects in carboxylate-based MOFs by using furfuryl alcohol as a probe molecule.³³⁰

In situ characterization techniques are especially valuable as they allow one to derive real-time information about the reaction kinetics present at the exact conditions corresponding to structural breakdown. While vacuum conditions necessary for SEM and TEM operation limit their application to MOF characterization postwater exposure, there are a number of other spectroscopic techniques that do not have this limitation. AFM is one such in situ technique that can collect detailed topographical information that has been used in past work to probe MOF synthesis mechanisms in solution.³³¹ Granick et al. utilized AFM ex situ to confirm that the average crystal size and surface properties in MIL-96(Al) did not change after exposure to aqueous solutions,³⁰² and in structures such as HKUST-1 that may decompose via surface-mediated mechanisms,³⁵ AFM can be a very valuable tool for obtaining in situ insight into its decomposition mechanism. The short-range structural information provided by solid state NMR measurements make it another promising in situ technique for elucidating important structural properties not discernible by structurally averaged techniques. For example, ²H NMR measurements on MOFs synthesized with ligands containing deuterated hydrogen have been used to quantify the flipping rates of benzene rings in various structures^{282,332} whereas NMR utilizing ¹²⁹Xe as a probe molecule has been used to explore MOF structural transitions^{333–335} and ¹³C CPMAS NMR has shown changes in pore environment after heating or ammonia exposure.^{148,336} Provided the MOF contains NMR active metal ions that are conducive to NMR characterization (e.g., ²⁷Al, ⁷¹Ga, ⁴⁵Sc),³³⁷ the local environment of select metal ions can also be explored with high sensitivity using this technique as well. ¹H and ¹³C NMR has already been applied to obtain in situ insight into structural changes present at various water loadings in HKUST-1³⁶ and will continue to be a promising approach for studying further MOF systems. While X-ray absorption spectroscopy techniques such as EXAFS and XANES often require access to synchrotron radiation sources, they also can be used to obtain in situ information into water's interaction with specific binding sites in the MOF pore which can provide insight into very fine changes to the local electronic structure and coordination at binding sites upon adsorption.³³⁸ Positron annihilation lifetime spectroscopy is yet another technique that has demonstrated the ability to provide in situ insight into subtle changes in the pore environment resulting from guest adsorption and structural breakdown in MOFs.³³⁹

IR and Raman spectroscopy are another set of powerful in situ tools for directly observing vibrational modes that correspond to hydrolysis events in MOFs. DeCoste et al. utilized ex situ FTIR to observe that the collapse of HKUST-1 proceeds via a transformation of carboxylate groups from a C=O to a C—OH state after exposure to high humidity.³⁵ Chabal et al. utilized in situ IR spectroscopy in combination with ex situ Raman and PXRD measurements to provide insight into how metal identity affects bond breakage events at various relative humidities in the isostructural M(BDC)₂(DABCO) [M = Cu, Zn, Ni, Co] series of MOFs.⁷² In the future, comprehensive water stability studies should include an array of different characterization techniques

to obtain a full picture of the relevant breakdown phenomena. For instance, Bonino et al. showed that a combination of PXRD, XAS, IR, UV-vis, and EPR were needed to obtain detailed insight into the structural changes of HKUST-1 caused by water in the presence of ammonia.¹⁵⁰ The use of equipment that can simultaneously apply multiple *in situ* techniques on a single sample may provide the most insightful mechanistic insight moving forward. Such approaches have brought great value to the catalysis community, with the technical details of implementing such experimental setups discussed in ref 340.

5.1.2. Computational Techniques. If the underlying physics of the system can be reproduced, simulations can provide critical mechanistic insight into molecular reaction events that occur over length and time scales that are inaccessible to experiment. Allendorf and Greathouse first demonstrated this using classical NPT molecular dynamics (MD) simulations with the CVFF³⁴¹ force field to show drastic decreases in the unit cell size of IRMOF-1 obtained from their simulations occur at roughly the same water loading as the breakdown conditions observed in experiment.³⁴² These simulations indicated that water initially interacts with IRMOF-1 via a mechanism where the oxygen on water either directly replaces one of the oxygen atoms in the ZnO₄ tetrahedron or the hydrogen in water hydrogen bonds with oxygen in the ZnO₄ tetrahedron. In a subsequent work by van Duin et al.³⁴³ the behavior of IRMOF-1, IRMOF-10, and Zn-MOF-74 was explored using REAXFF,³⁴⁴ a reactive classical force field model designed to capture reaction events by calculating bond orders and covalent interactions on the fly. In this work they found that the initial loss of structure in IRMOF-1 and IRMOF-10 was initiated by a water molecule interacting with the ZnO₄ tetrahedron and dissociating into OH⁻ and H⁺ species, with the OH⁻ species then forming a chemical bond with Zn while the H⁺ species protonates the oxygen on the BDC ligand. A similar mechanism involving a water attack on Zn by the dissociated OH⁻ species with a protonation of the DOBDC ligand by H⁺ was also identified at higher water loadings in the MOF-74 structure.

While classical simulations rely on empirical force field functions to describe intermolecular interactions, *ab initio* methods provide a more desirable first-principles approach by relying only on assumptions about the quantum mechanical behavior of the electron to predict reaction events. Plane-wave DFT is a particularly attractive quantum chemistry approach for exploring reaction events in crystalline systems because of the reciprocal space treatment of its wave function basis set. In the past two years, several *ab initio* MD studies investigating water decomposition mechanisms in variations of the IRMOF series have emerged.^{272,279,280} Lopez et al. utilized Born–Oppenheimer MD to identify initial decomposition mechanisms in the presence of liquid water for variations of IRMOF-1 containing different metal centers²⁷² and, in agreement with experiment,²⁷³ found that the Be variation of IRMOF-1 was more hydrothermally stable than the Zn variation. This observation was attributed to differences in the preferred coordination sphere, metal–oxygen bond strength, and rigidity of tetrahedron cores present in the structures. In a subsequent work by Lopez et al.²⁷⁹ the stability of IRMOF-1 was also explored under lower water contents to understand the onset of structural breakdown present under humid conditions. This work utilized a multiscale approach where classical Monte Carlo simulations were used to identify preferential adsorption sites for water that were then used as starting seeds for more detailed Born–Oppenheimer MD calculations. While IRMOF-1 was stable at very low water

contents when individual water molecules remained isolated in the pores, at a water loading of ~6 wt % the molecules formed clusters that increased the basicity of water and therefore caused lattice collapse to occur. The work of Fuchs et al.²⁸⁰ further highlighted the importance of water clustering in the initial structural breakdown of the IRMOF series through their simulations on the hypothetical, noninterpenetrated IRMOF-0 structure containing acetylendicarboxylate as the ligand. Car-Parrinello MD simulations were performed to show that isolated water molecules reversibly react with the zinc tetrahedron and only after water clusters are able to form in the pore are irreversible hydrolysis reactions thermodynamically favored.

While these past DFT MD studies have provided valuable insight into initial breakdown mechanisms in the IRMOF series, further studies exploring breakdown mechanisms in a wider array of MOFs will be a rich area for future research. The primary challenges that complicate the use of *ab initio* MD in further systems arise from system size and time scale considerations. With regards to system size, the computational demands of *ab initio* MD limit its applicability to unit cells on the order of hundreds of atoms. When the primitive cell of the structures exceeds this limit, various simplifications should be considered to make the calculations more tractable. One simplification that should be made with great caution is that of using a truncated MOF cluster as a representative model for the full periodic system. This assumption has been made in past work,⁶² but it has since been suggested that such simplifications may not accurately capture the dynamic behavior of the full periodic structure in some MOFs.^{280,76} This is likely due to the unphysical dynamics that are introduced when treating periodic structures as isolated clusters; without the lattice stiffness arising from the interconnected building units in the periodic system, clusters can achieve bending and torsion angles that would be highly unfavorable in the full crystalline system. Another solution is to convert the unit cell into a polymorph with reduced lattice constants. Such an approach was used in the work of Lopez et al. to reduce the 424 atom unit cell of IRMOF-1 ($Zn_4(\mu-O_4)(\mu-BDC)_3$) into a 53 atom system ($Zn_4(\mu-O_4)(\mu-BDC)_3$) by introducing slight torsions to the BDC linkers.²⁷⁹ Calculations were then run in this work to ensure the energy of formation and geometric properties were similar between the two polymorphs. In hybrid QM/MM approaches the accuracy and speed of quantum mechanics and molecular mechanics approaches are combined by treating the reactive part of the system quantum mechanically and the nonreactive part classically. This approach has been successfully applied to model reactivity in other periodic systems³⁴⁵ and provides an alternative avenue for reducing the computational costs associated with modeling large reactive systems.

The second major hurdle of applying *ab initio* methods toward further MOF systems is related to the simulation time scale. Ideally, a reaction event would occur on the picoseconds time scale accessible to *ab initio* MD calculations. However, in cases where the thermal energy of the system is small compared to the reaction barrier needed to reach the transition state, the reaction becomes a rare event on the time scale of simulation. This will likely arise when investigating decomposition mechanisms in MOFs more stable than the IRMOF series. In such cases, rare event methods that impose umbrella potentials³⁴⁶ or geometric constraints³⁴⁷ will be needed to directly explore the kinetics of important reaction pathways. These methods require prior chemical intuition of reaction mechanisms and clearly alter the natural dynamics of the system. Thus, to ensure identified

pathways contain representative transition states along the complex reaction pathway, transition path sampling methods³⁴⁸ should also be employed to generate and explore the relative importance of alternative trajectories. As a final consideration in running such calculations, it should also be noted that any standard periodic model will neglect the potentially important role that the external surface area and internal defect heterogeneity may have as hydrolysis sites in the MOF. Three-dimensional maps of experimental defects in various carboxylate-based MOFs have recently been obtained,³³⁰ and given the significant impact such heterogeneity can have on MOF adsorption and catalytic properties,^{108,202,349,350} these effects represent another area that merits careful consideration.

5.2. Approaches to Impart Water Stability

Techniques that allow one to tune the properties of existing MOFs without compromising their isostructural nature are particularly attractive ways to tailor structures for target applications. This is because such strategies allow the highly specific tuning of attributes in select MOFs that have been already identified as strong candidates for target applications. Such strategies are advantageous over synthesis efforts directed toward the discovery of novel MOFs because, even if the ideal adsorbent can be envisioned, the frustrating unpredictability of MOF coordination chemistry³⁵¹ can make the *a priori* identification of appropriate synthesis conditions for the target structure a difficult or impossible task. The approaches reviewed in this section are therefore particularly useful because they allow the water stability of already synthesized MOFs to be adjusted. The stability mechanisms for each of these experimental approaches are summarized in Figure 29 and are directly related to the structural factors discussed in section 3.

The first class of approaches involves increasing the external crystal surface's hydrophobicity in order to exclude water from entering the pore. Experimentally, the introduction of such

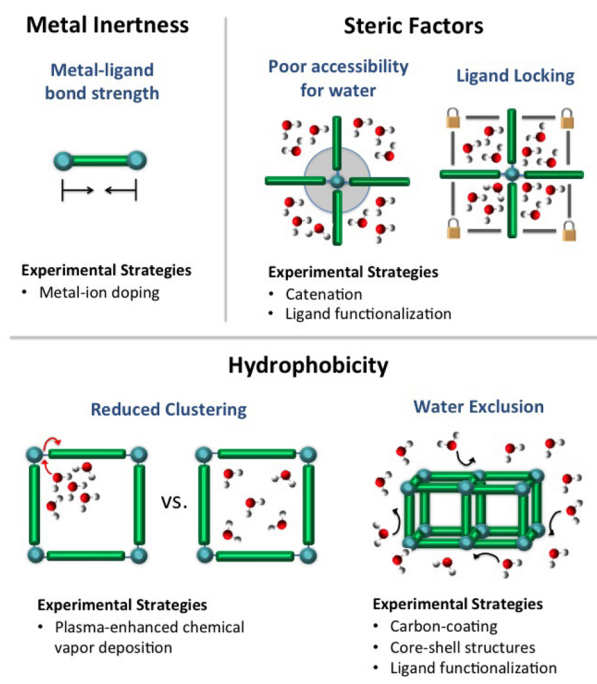


Figure 29. Mechanisms and experimental approaches for improving the water stability in existing MOFs. All mechanisms are directly related to the structural factors discussed in Figure 27.

external hydrophobicity can be directly quantified via a measurement of the contact angle for water on the surface-modified material.⁶⁵ Park et al. utilized this approach to improve the water stability of IRMOF-1 by turning the organic ligands on the surface of the crystal into an amorphous carbon layer via heating under nitrogen (Figure 30).³⁵² While the crystal

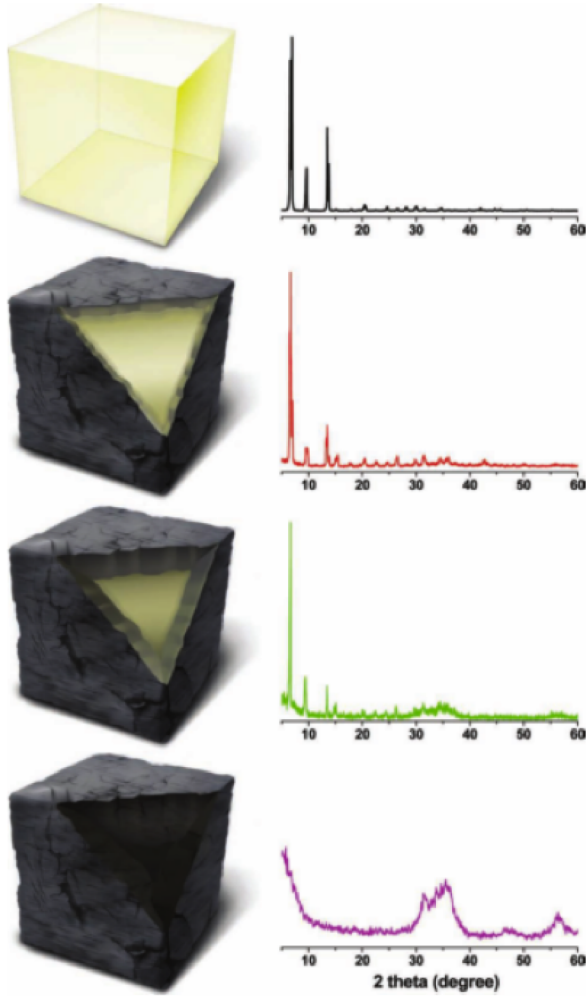


Figure 30. Schematic representations and PXRD patterns of IRMOF-1 (top) and carbon-coated IRMOF-1 after thermal modification at increasing temperatures (middle). At a temperature of 550 °C the structure transforms into ZnO nanoparticles@amorphous carbon (bottom). Reprinted with permission from ref 352. Copyright 2012 Wiley Online Library.

structure and pore size distribution of IRMOF-1 were maintained in the carbon-coated samples, the textural properties were changed and BET surface areas reduced by 10%, 20%, and 50% at the 480, 510, and 530 °C heating temperatures, respectively. At a temperature of 550 °C the internal structure completely transformed into a ZnO nanocrystals@amorphous carbon form. After exposure to 34% RH air for 14 days the carbon-coated samples maintained their crystallinity and exhibited little loss of BET surface area relative to the uncoated IRMOF-1 sample. In a further test, the carbon-coated sample treated at 510 °C also maintained its crystallinity after immersion in liquid water for 2 h. In a separate work, Jeong et al. increased the moisture stability of IRMOF-3 crystals by incorporating surfactants during the solvent drying process.³²⁸ Because surfactants reduce the interfacial tension at the crystal surface,

fewer surface cracks and fractures were formed, and the resulting crystal surface became more hydrophobic. After one month in ambient air the surfactant-dried IRMOF-3 crystals also showed little change in their PXRD pattern whereas the untreated IRMOF-3 showed a significant transformation after only 6 h.

Another way to increase crystal surface hydrophobicity is via core–shell structures where a more hydrolytically stable, hydrophobic MOF serves as a shell to protect a more moisture-sensitive MOF encapsulated at the core. Rosi et al. used this approach to encapsulate the water-sensitive Bio-MOF-11 structure with the more water-stable Bio-MOF-14 (Figure 31).¹⁴⁶ The resulting material exploited the desirable properties

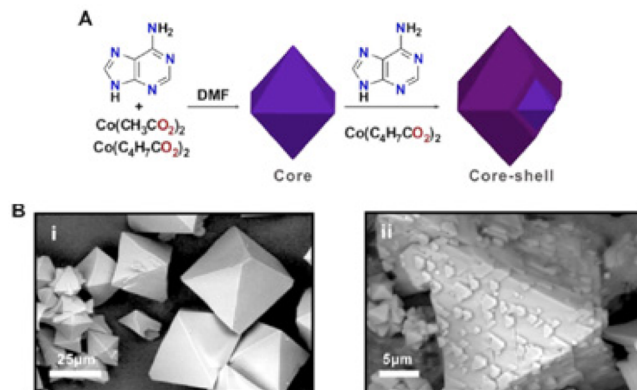


Figure 31. Schematic of the synthetic procedure for preparing a core–shell structure with a water-sensitive Bio-MOF-11 core encapsulated by a more stable Bio-MOF-14 shell (A), SEM images of the core-crystal (B-i), and core–shell crystal (B-ii). Adapted with permission from ref 146. Copyright 2013 American Chemical Society.

of both the individual structures by combining the attractive N₂ sieving and water stability properties of the Bio-MOF-14 shell with the higher CO₂ capacity of the Bio-MOF-11 core. While this core–shell material maintained its crystallinity after 1 day in aqueous conditions, the exposed Bio-MOF-11 structure alone exhibited significant loss of crystallinity after exposure to aqueous conditions. Using a similar approach, Yang et al. improved the hydrothermal stability of various ZIF materials by utilizing a shell–ligand-exchange-reaction procedure where the existing ligands in ZIF-8, ZIF-7, and ZIF-93 were exchanged with the 5,6-dimethylbenzimidazole ligand at the surface of the crystal.¹⁴⁷

Instead of utilizing hydrophobicity on the external crystal surface as a means of excluding water from entering the pore, introducing hydrophobicity on the internal surface of the structure can be used to increase the structure's water stability. Water clustering has been identified as an important prerequisite for some hydrolysis reactions to occur,^{279,280} and introducing internal hydrophobicity can prevent this phenomenon from occurring. In the work of Decoste et al. they used this strategy to increase HKUST-1 stability by using a plasma-enhanced chemical vapor deposition approach to coat the internal pores of the structure with perfluorohexane.²⁷⁷ This perfluorohexane coating reduced the BET surface area and porosity of HKUST-1 by roughly 30% but improved the structure's ammonia breakthrough capacity and ability to maintain crystallinity after high humidity and liquid water exposure. A past study identified multiple sorption sites for water in HKUST-1, with the most favorable site corresponding to water coordinated to the Cu atom and the second most favorable site corresponding to water hydrogen-bonded to the water molecule in the most favorable

site.³⁵³ Monte Carlo simulations and TGA experiments were used to suggest that coated HKUST-1's increased stability arises from the perfluorohexane molecules preferentially adsorbing at the second most favorable site and therefore preventing water molecules from clustering with the water molecules adsorbed at the most favorable site.

Ligand functionalization is the most widely used approach for tuning MOF water stability and can be achieved through one of two approaches. In the first approach, the functionalized ligand is directly incorporated as a reagent in the synthesis procedure. Alternatively, in cases where ligand stability or functional group interactions prevent a particular topology from being self-assembled in solution, postsynthetic ligand modification can be used to modify the functional groups present on the already assembled structure.³⁵⁴ Nonpolar ligand functionalization is a particularly promising approach for improving the water stability of MOFs,^{60,64–66,75,76,84,91,92,95,274–276,308} though the exact mechanism by which this stability improvement occurs is likely to be system-specific. As shown in Figure 29, ligand functionalization can increase the stability by mechanisms related to the functional groups altering the external hydrophobicity of the framework or the sterics around the ligand and metal. However, in order to decouple hydrophobicity from steric effects, it is necessary to obtain water adsorption isotherms on the structures of interest in order to understand whether ligand functionalization is increasing the inherent stability of the structure or if it simply excludes water from entering the pore.⁷⁶ Another approach that can be used to alter the steric factors of the framework is catenation, a structural phenomena that has been successfully controlled in a number of structures³⁵⁵ and has been shown to improve the water stability of several pillared MOFs.⁷⁷

The last category of approaches deals with altering the thermodynamic stability factors of the framework. Postsynthetic cation exchange is one such example and can be used to increase the stability of the MOF's metal cluster by replacing the existing metal with a more inert species. This was demonstrated by Cheng et al. by doping IRMOF-1 framework with Ni ions during the crystallization process.³⁵⁶ They found the Ni-doped structure maintained its crystallinity after a week exposure to ~30% RH whereas the undoped structure showed significant structural changes over this same time period. This increase in stability was attributed to the improved hydrostability of the $\text{Ni}_x\text{Zn}_{4-x}\text{O}^{6+}$ versus Zn_4O^{6+} secondary building units. As a general rule, utilizing ligands possessing coordinating atoms with high pK_a values is another useful strategy for targeting novel structures with higher water tolerances as well.

To summarize, a wide array of modification approaches can be used to tune both the kinetic and thermodynamic factors governing water stability in existing MOFs. Ligand functionalization is the most well-studied approach though is restricted to structures where nonpolar entities can be incorporated without compromising the framework's isostructural nature. Surface modification approaches based on core–shell models hold promise for a number of further systems provided there is compatibility in the binding domain for the core and shell entities. Imparting crystal surface hydrophobicity via carbon-coating approaches is perhaps one of the most simple and generalizable approaches for improving MOF water stability, though significant changes to the specific surface area and crystal textural properties can result depending on the heat treatment conditions. Plasma-enhanced chemical vapor deposition may also hold promise as an approach for altering the internal

hydrophobicity of systems other than HKUST-1, though the need for a plasma reactor in the treatment step is one significant disadvantage of this approach. While postsynthetic metal and ligand exchange have been demonstrated in a variety of different MOF systems in the literature,^{357–361} it is still relatively unexplored as an approach for improving water stability and therefore represents a particularly promising avenue for future studies. Regardless of the approach, further insight into how the modification strategy affects the MOF adsorption and mechanical properties in the target application must first be explored.

6. CONCLUDING REMARKS AND OUTLOOK

Despite the presence of metal–ligand coordination bonds that make MOFs more susceptible to hydrolysis than zeolites or activated carbons, a growing number of highly stable structures are being reported in the literature. A limited number of structures with the stability properties needed for use under aqueous conditions already exist; however, for many applications this high level of stability will not be necessary, and there likely exists a much wider array of candidate materials with the needed stability characteristics (see Tables 2–6). However, a fully informed decision regarding the suitability of an adsorbent for some target application will depend not only on the amount of moisture that the adsorbent is exposed to but also on the duration and number of cycles over which the adsorbent will face these conditions. As a result, any candidate material will likely require stability testing beyond what has already been reported in the literature.

Moving forward, more systematic experimental characterization procedures are needed to obtain a higher confidence about the true water stability of MOFs reported in the literature. While there are certain telltale signs that a structure is unstable, determining whether or not a MOF is fully stable after water exposure requires an array of complementary techniques. At the very minimum, PXRD measurements and BET surface area analysis should be performed before and after water exposure to obtain a general sense of the structure's stability. Depending on the application of interest, we also refer researchers to the minimum characterization guidelines presented in Table 1 before seeking to make claims as to the suitability of their material for the target application. However, these techniques provide no information regarding the how or why of the process, and in order to fully understand why a structure is unstable, further characterization techniques are needed. In this regard, the spectroscopic and microscopic techniques discussed in section 5.1.1 will be particularly useful for obtaining insight into breakdown mechanisms in MOFs. Such mechanistic insight will then pave the way for the development of further experimental strategies, beyond those discussed in Figure 29, that can impart greater water stability on existing structures and facilitate the identification of new synthesis targets. Furthermore, experimental techniques that can accurately quantify properties such as defect presence and crystal size distributions within a sample are also needed to obtain a better understanding of the potentially important role these factors may play in dictating the stability of some structures.

Computational studies will continue to play an increasingly important role in this field as well. As the number of newly reported structures continues to grow it will become exceedingly difficult to experimentally characterize the performance of all new materials in the lab. Past computational studies have successfully screened candidate structures to identify materials

that merit experimental characterization based on their adsorptive performance; understanding the kinetic and thermodynamic stability factors presented in section 3 of this review now opens the door for the very first screening studies based on the structural properties necessary for chemical stability. Furthermore, classical and quantum chemistry calculations on target structures will continue to provide mechanistic insight into water diffusion and reaction events that occur over time and length scales inaccessible to experiment.

The outlook for MOFs is bright. The over 20 000 MOFs that have been reported in the Cambridge Structural Database over the past decade represent orders of magnitude more than the number of natural and synthetic zeolite frameworks (218) that have been discovered in less than a quarter of the time. Among this limited number of zeolite structures, multiple materials have already achieved widespread commercial success. It is therefore reasonable to assume that among the much greater diversity of MOFs there will be multiple structures that find similar success. An understanding of the water stability and adsorption concepts presented in this review lays important groundwork that will help accelerate the attainment of this goal.

ASSOCIATED CONTENT

Supporting Information

Comprehensive list of experimental MOF water stability rankings along with the characterization results for each study. This material is available free of charge via the Internet at <http://pubs.acs.org/>.

AUTHOR INFORMATION

Corresponding Author

*E-mail: krista.walton@chbe.gatech.edu.

Notes

Any opinion, findings, and conclusions or recommendations expressed in this material are those of the authors and do not necessarily reflect the views of the National Science Foundation. The authors declare no competing financial interest.

Biographies



Nicholas Burtch was born in Canada but also spent time living in the United States and Dubai before receiving his B.S.E. in chemical engineering from the University of Michigan. He is currently an NSF fellow in Professor Krista Walton's research laboratory at the Georgia Institute of Technology. His research interests include the experimental synthesis and computational design of nanoporous materials for adsorption applications.



Himanshu Jasuja was born and raised in Rajasthan, India. In 2010, he received his B.Tech. in Chemical Engineering from the Indian Institute of Technology (IIT) Madras in Chennai, India. His fondness for research developed through courses and interactions with faculty at the undergraduate level led him to join the Walton Research Group at the Georgia Institute of Technology for his Ph.D. studies. His current research focus is developing design criteria and scale-up methods for water-stable metal–organic frameworks for adsorption applications.



Krista Walton was born in Florence, Alabama, and grew up in nearby Elgin. She received a B.S.E. degree from the University of Alabama—Huntsville and Ph.D. from Vanderbilt University, both in chemical engineering. She joined the faculty of the Georgia Institute of Technology in the School of Chemical & Biomolecular Engineering in August 2009 and is now Associate Professor and Marvin R. McClatchey and Ruth McClatchey Cline Faculty Fellow. Her research involves the design and synthesis of next-generation multifunctional, porous materials for adsorption applications.

ACKNOWLEDGMENTS

We gratefully acknowledge support from Army Research Office PECASE Award W911NF-10-1-0079 and Contract W911NF-10-1-0076, the National Science Foundation CAREER Award 0969261, and the National Science Foundation Graduate Research Fellowship under Grant 0946809.

ABBREVIATIONS

ALA	alanine
ABDC	4,4'-azobenzenedicarboxylate
AC	acetate
AD	adenine
ADC	anthracenedicarboxylate
BDC	1,4-benzenedicarboxylate
BDP	benzenedi(4-pyrazolyl)

BFBPDC	2,2'-bis-trifluoromethyl-biphenyl-4,4'-dicarboxylate
BHTC	biphenyl-3,4',5-tricarboxylate
BPDC	4,4'-biphenyldicarboxylate
BPE	1,2-bis(4-pyridyl)ethane
BPP	1,3-bis(4-pyridyl)propane
BPTC	biphenyl-3,3',5'-tetracarboxylate
BPY	4,4'-bipyridine
BPZ	3,3',5,5'-tetramethyl-4,4'-bipyrazolate
BTC	1,3,5-benzenetricarboxylate
BTP	1,3,5-tris(1 <i>H</i> -pyrazol-4-yl)benzene
BTTRI	1,3,5-tris(1 <i>H</i> -1,2,3-triazol-5-yl)benzene
C ₆ H ₅ O ₇	2-hydroxypropane-1,2,3-tricarboxylate
C ₆ H ₄ O ₇	2-oxidopropane-1,2,3-tricarboxylate
DABCO	4-diazabicyclo[2.2.2]-octane
DMBDC	2,5-dimercapto-1,4-benzenedicarboxylate
DOBDC	2,5-dihydroxyterephthalate
DPA	4,4'-dipyridylacetylene
DTTDC	dithieno[3,2- <i>b</i> ;2',3'- <i>d</i>]-thiophene-2,6-dicarboxylate
FOR	formate
FTZB	3-fluoro-4'-(2 <i>H</i> -tetrazol-5-yl)biphenyl-4-carboxylate
FUM	fumarate
H ₂ L	tetraethyl-1,3,6,8-pyrenetetraphosphonate
H ₂ PDA	phenylenediacetate
H ₂ PTPTP	2-(5-6-[5-(pyrazin-2-yl)-1 <i>H</i> -1,2,4-triazol-3-yl]-pyridin-2-yl-1 <i>H</i> -1,2,4-triazol-3-yl)pyrazine
H ₄ L	biphenyl-3,3',5,5'-tetracarboxylate
HPTZ	4-(1,2,4-triazol-4-yl)phenylphosphonate
IDC	imidazole-4,5-dicarboxylate
ISO	isophthalate
L ₁	2-((pyridin-4-yl)methylamino)-4-methylpentanoate
L ₂	2-(pyridin-4-yl)methylamino)-3-hydroxypropanoate
L ₃	2-((pyridin-4-yl)methylamino)-3-hydroxybutanoate
L ₄	4,4'-bipyridine-2,6,2',6'-tetracarboxylate
L ₅	1,2,4,5-tetrakisphosphonomethylbenzene
L ₆	1 <i>H</i> -pyrazole-4-carboxylate
L ₇	4-(1 <i>H</i> -pyrazole-4-yl)benzoate
L ₈	4,4'-benzene-1,4-diylbis(1 <i>H</i> -pyrazole)
L ₉	4,4'-buta-1,3-diene-1,4-diylbis(1 <i>H</i> -pyrazole)
L ₁₀	4,4'-(benzene-1,4-diylidethyne-2,1-diyl)bis(1 <i>H</i> -pyrazole)
L ₁₁	perfluorinated biphenyl carboxylate
L ₁₂	perfluorinated biphenyl bistetrazole
L ₁₃	3,5-di(pyridine-4-yl) benzoate
L ₁₄	4,4'-(2,3,5,6-tetramethoxy-1,4-phenylene)-dipyridine
L ₁₅	4,4',4'',4'''-dibromo-benzene-1,2,4,5-tetrayl-tetra-benzoate
L ₁₆	4,2',4'',2''-terpyridine-4'-carboxylate
L ₁₇	2-methylimidazolate-4-amide-5-imidate
MEIM	2-methylimidazole
MTB	4,4',4'',4'''-methanetetrayltetrabenzoic acid
NDC	naphthalenedicarboxylate
PCP	<i>P,P'</i> -diphenylmethylenediphosphinate
PDC	pyridine-2,4-dicarboxylate
PHIM	phenyl benzimidazolate
PRZ	piperazine
PYR	pyrazine
PZDC	1 <i>H</i> -pyrazole-3,5-dicarboxylic acid
TAZB	3,3',5,5'-azobzenzenetetracarboxylate

TBAPY	1,3,6,8-tetrakis(p-benzoate)pyrene
TCMBT	<i>N,N',N''</i> -tris(carboxymethyl)-1,3,5-benzenetricarboxamide
TCPP	<i>meso</i> -tetra(4-carboxyl-phenyl)porphyrin
TCPP(M)	tetrakis(4-carboxyphenyl)porphyrin(M); M = Ni, Co, or Fe
TDC	2,5-thiophenedicarboxylate
TEIA	1,3,5,7-tetrakis(4-(2-ethyl-1 <i>H</i> -imidazol-1-yl)-phenyl)-ane
THIPC	(<i>S</i>)-4,5,6,7-tetrahydro-1 <i>H</i> -imidazo[4,5- <i>c</i>]pyridine-6-carboxylate
TPTC-O	2',5'-dialkyloxy-[1,1':4',1"-terphenyl]-3,3",5,5"-tetracarboxylate
TZ	3,5-bis(trifluoromethyl)-1,2,4-triazolate
VAL	valine

REFERENCES

- (1) Foo, M. L.; Matsuda, R.; Kitagawa, S. *Chem. Mater.* **2014**, *26*, 310.
- (2) Ferey, G. *Dalton Trans.* **2009**, 4400.
- (3) Farha, O. K.; Hupp, J. T. *Acc. Chem. Res.* **2010**, *43*, 1166.
- (4) Tanabe, K. K.; Cohen, S. M. *Chem. Soc. Rev.* **2011**, *40*, 498.
- (5) Furukawa, H.; Cordova, K. E.; O'Keeffe, M.; Yaghi, O. M. *Science* **2013**, *341*, 974.
- (6) Zhao, D.; Timmons, D. J.; Yuan, D. Q.; Zhou, H. C. *Acc. Chem. Res.* **2011**, *44*, 123.
- (7) Li, S. L.; Xu, Q. *Energy Environ. Sci.* **2013**, *6*, 1656.
- (8) Liu, J.; Thallapally, P. K.; McGrail, B. P.; Brown, D. R.; Liu, J. *Chem. Soc. Rev.* **2012**, *41*, 2308.
- (9) Makal, T. A.; Li, J. R.; Lu, W. G.; Zhou, H. C. *Chem. Soc. Rev.* **2012**, *41*, 7761.
- (10) Ma, S.; Zhou, H.-C. *Chem. Commun.* **2010**, *46*, 44.
- (11) Ribeiro, A. M.; Sauer, T. P.; Grande, C. A.; Moreira, R. F. P. M.; Loureiro, J. M.; Rodrigues, A. E. *Ind. Eng. Chem. Res.* **2008**, *47*, 7019.
- (12) Tao, W. H.; Yang, T. C. K.; Chang, Y. N.; Chang, L. K.; Chung, T. W. *J. Environ. Eng.* **2004**, *130*, 1210.
- (13) Rodriguez-Mirasol, J.; Bedia, J.; Cordero, T.; Rodriguez, J. J. *Sep. Sci. Technol.* **2005**, *40*, 3113.
- (14) Ferreira, D.; Magalhaes, R.; Taveira, P.; Mendes, A. *Ind. Eng. Chem. Res.* **2011**, *50*, 10201.
- (15) Kanchanalai, P.; Lively, R. P.; Realff, M. J.; Kawajiri, Y. *Ind. Eng. Chem. Res.* **2013**, *52*, 11132.
- (16) Sing, K.; Everett, D.; Haul, R.; Moscou, L.; Pierotti, R.; Rouquerol, J.; Siemieniewska, T. *Pure Appl. Chem.* **1985**, *57*, 603.
- (17) For more information see <http://www.iupac.org/web/ins/2010-009-1-100>.
- (18) Coudert, F.; Boutin, A.; Fuchs, A. H.; Neimark, A. *J. Phys. Chem. Lett.* **2013**, *4*, 3198.
- (19) Ng, E.-P.; Mintova, S. *Microporous Mesoporous Mater.* **2008**, *114*, 1.
- (20) Chua, H. T.; Ng, K. C.; Chakraborty, A.; Oo, N. M.; Othman, M. A. *J. Chem. Eng. Data* **2002**, *47*, 1177.
- (21) Stach, H.; Mugele, J.; Janchen, J.; Weiler, E. *Adsorption* **2005**, *11*, 393.
- (22) Oh, J. S.; Shim, W. G.; Lee, J. W.; Kim, J. H.; Moon, H.; Seo, G. J. *Chem. Eng. Data* **2003**, *48*, 1458.
- (23) Qi, N.; LeVan, M. D. *Carbon* **2005**, *43*, 2258.
- (24) Fan, Y.; Bao, X.; Lin, X.; Shi, G.; Liu, H. *J. Phys. Chem. B* **2006**, *110*, 15411.
- (25) Li, Q.; Wu, Z.; Tu, B.; Park, S. S.; Ha, C.-S.; Zhao, D. *Microporous Mesoporous Mater.* **2010**, *135*, 95.
- (26) Wang, Q. M.; Shen, D. M.; Bulow, M.; Lau, M. L.; Deng, S. G.; Fitch, F. R.; Lemcoff, N. O.; Semancin, J. *Microporous Mesoporous Mater.* **2002**, *55*, 217.
- (27) Chui, S. S.-Y.; Lo, S. M.-F.; Charmant, J. P. H.; Orpen, A. G.; Williams, I. D. *Science* **1999**, *283*, 1148.
- (28) Kusgens, P.; Rose, M.; Senkovska, I.; Froede, H.; Henschel, A.; Siegle, S.; Kaskel, S. *Microporous Mesoporous Mater.* **2009**, *120*, 325.

- (29) Wang, Y.; LeVan, M. D. *J. Chem. Eng. Data* **2009**, *54*, 2839.
- (30) Liang, Z.; Marshall, M.; Chaffee, A. L. *Energy Fuels* **2009**, *23*, 2785.
- (31) Schoenecker, P. M.; Carson, C. G.; Jasuja, H.; Flemming, C. J. J.; Walton, K. S. *Ind. Eng. Chem. Res.* **2012**, *51*, 6513.
- (32) Henninger, S. K.; Schmidt, F. P.; Henning, H. M. *Adsorption* **2011**, *17*, 833.
- (33) Henninger, S. K.; Jeremias, F.; Kummer, H.; Janiak, C. *Eur. J. Inorg. Chem.* **2012**, 2625.
- (34) Li, Y.; Yang, R. T. *AIChE J.* **2008**, *54*, 269.
- (35) DeCoste, J. B.; Peterson, G. W.; Schindler, B. J.; Killops, K. L.; Browe, M. A.; Mahle, J. J. *J. Mater. Chem. A* **2013**, *1*, 11922.
- (36) Gul-E-Noor, F.; Jee, B.; Poppl, A.; Hartmann, M.; Himsl, D.; Bertner, M. *Phys. Chem. Chem. Phys.* **2011**, *13*, 7783.
- (37) Jeremias, F.; Khutia, A.; Henninger, S. K.; Janiak, C. *J. Mater. Chem.* **2012**, *22*, 10148.
- (38) Akiyama, G.; Matsuda, R.; Kitagawa, S. *Chem. Lett.* **2010**, *39*, 360.
- (39) Pirngruber, G. D.; Hamon, L.; Bourrelly, S.; Llewellyn, P. L.; Lenoir, E.; Guillerm, V.; Serre, C.; Devic, T. *ChemSusChem* **2012**, *5*, 762.
- (40) Wickenheisser, M.; Jeremias, F.; Henninger, S. K.; Janiak, C. *Inorg. Chim. Acta* **2013**, *407*, 145.
- (41) Soubeyrand-Lenoir, E.; Vagner, C.; Yoon, J. W.; Bazin, P.; Ragon, F.; Hwang, Y. K.; Serre, C.; Chang, J.-S.; Llewellyn, P. L. *J. Am. Chem. Soc.* **2012**, *134*, 10174.
- (42) Cunha, D.; Ben Yahia, M.; Hall, S.; Miller, S. R.; Chevreau, H.; Elkaim, E.; Maurin, G.; Horcajada, P.; Serre, C. *Chem. Mater.* **2013**, *25*, 2767.
- (43) Demir, H.; Mobedi, M.; Ulku, S. *J. Therm. Anal. Calorim.* **2011**, *105*, 375.
- (44) Seo, Y.-K.; Yoon, J. W.; Lee, J. S.; Hwang, Y. K.; Jun, C.-H.; Chang, J.-S.; Wuttke, S.; Bazin, P.; Vimont, A.; Daturi, M.; Bourrelly, S.; Llewellyn, P. L.; Horcajada, P.; Serre, C.; Ferey, G. *Adv. Mater.* **2012**, *24*, 806.
- (45) De Lange, M. F.; Gutierrez-Sevillano, J.-J.; Hamad, S.; Vlugt, T. J. H.; Calero, S.; Gascon, J.; Kapteijn, F. *J. Phys. Chem. C* **2013**, *117*, 7613.
- (46) Kim, S.-N.; Kim, J.; Kim, H.-Y.; Cho, H.-Y.; Ahn, W.-S. *Catal. Today* **2013**, *204*, 85.
- (47) Jeremias, F.; Lozan, V.; Henninger, S. K.; Janiak, C. *Dalton Trans.* **2013**, *42*, 15967.
- (48) Vaesen, S.; Guillerm, V.; Yang, Q. Y.; Wiersum, A. D.; Marszalek, B.; Gil, B.; Vimont, A.; Daturi, M.; Devic, T.; Llewellyn, P. L.; Serre, C.; Maurin, G.; De Weireld, G. *Chem. Commun.* **2013**, *49*, 10082.
- (49) Ferey, G.; Mellot-Draznieks, C.; Serre, C.; Millange, F.; Dutour, J.; Surble, S.; Margiolaki, I. *Science* **2005**, *309*, 2040.
- (50) Ehrenmann, J.; Henninger, S. K.; Janiak, C. *Eur. J. Inorg. Chem.* **2011**, *471*.
- (51) Akiyama, G.; Matsuda, R.; Sato, H.; Hori, A.; Takata, M.; Kitagawa, S. *Microporous Mesoporous Mater.* **2012**, *157*, 89.
- (52) Khutia, A.; Rammelberg, H. U.; Schmidt, T.; Henninger, S.; Janiak, C. *Chem. Mater.* **2013**, *25*, 790.
- (53) Hong, D.-Y.; Hwang, Y. K.; Serre, C.; Feàrey, G.; Chang, J.-S. *Adv. Funct. Mater.* **2009**, *19*, 1537.
- (54) Comotti, A.; Bracco, S.; Sozzani, P.; Horike, S.; Matsuda, R.; Chen, J.; Takata, M.; Kubota, Y.; Kitagawa, S. *J. Am. Chem. Soc.* **2008**, *130*, 13664.
- (55) Bon, V.; Senkovskyy, V.; Senkovska, I.; Kaskel, S. *Chem. Commun.* **2012**, *48*, 8407.
- (56) Bon, V.; Senkovska, I.; Baburin, I. A.; Kaskel, S. *Cryst. Growth Des.* **2013**, *13*, 1231.
- (57) Bon, V.; Senkovska, I.; Weiss, M. S.; Kaskel, S. *CrystEngComm* **2013**, *15*, 9572.
- (58) Cavka, J. H.; Jakobsen, S.; Olsbye, U.; Guillou, N.; Lamberti, C.; Bordiga, S.; Lillerud, K. P. *J. Am. Chem. Soc.* **2008**, *130*, 13850.
- (59) Reinsch, H.; van der Veen, M. A.; Gil, B.; Marszalek, B.; Verbiest, T.; de Vos, D.; Stock, N. *Chem. Mater.* **2012**, *25*, 17.
- (60) Taylor, J. M.; Vaidyanathan, R.; Iremonger, S. S.; Shimizu, G. K. *H. J. Am. Chem. Soc.* **2012**, *134*, 14338.
- (61) Celic, T. B.; Mazaj, M.; Guillou, N.; Elkaaim, E.; El Roz, M.; Thibault-Starzyk, F.; Mali, G.; Rangus, M.; Cendak, T.; Kaucic, V.; Zubukovec Logar, N. *J. Phys. Chem. C* **2013**, *117*, 14608.
- (62) Low, J. J.; Benin, A. I.; Jakubczak, P.; Abrahamian, J. F.; Faheem, S. A.; Willis, R. R. *J. Am. Chem. Soc.* **2009**, *131*, 15834.
- (63) Cybosz, K. A.; Matzger, A. J. *Langmuir* **2010**, *26*, 17198.
- (64) Wu, T.; Shen, L.; Luebbers, M.; Hu, C.; Chen, Q.; Ni, Z.; Masel, R. I. *Chem. Commun.* **2010**, *46*, 6120.
- (65) Nguyen, J. G.; Cohen, S. M. *J. Am. Chem. Soc.* **2010**, *132*, 4560.
- (66) Yang, J.; Grzech, A.; Mulder, F. M.; Dingemans, T. *J. Chem. Commun.* **2011**, *47*, 5244.
- (67) Yang, S.; Chen, C.; Yan, Z.; Cai, Q.; Yao, S. *J. Sep. Sci.* **2013**, *36*, 1283.
- (68) Li, Y.; Yang, R. T. *Langmuir* **2007**, *23*, 12937.
- (69) Saha, D.; Deng, S. *J. Phys. Chem. Lett.* **2010**, *1*, 73.
- (70) Lee, J. Y.; Olson, D. H.; Pan, L.; Emge, T. J.; Li, J. *Adv. Funct. Mater.* **2007**, *17*, 1255.
- (71) Liang, Z.; Marshall, M.; Chaffee, A. L. *Microporous Mesoporous Mater.* **2010**, *132*, 305.
- (72) Tan, K.; Nijem, N.; Canepa, P.; Gong, Q.; Li, J.; Thonhauser, T.; Chabal, Y. *J. Chem. Mater.* **2012**, *24*, 3153.
- (73) Chen, Z.; Xiang, S.; Zhao, D.; Chen, B. *Cryst. Growth Des.* **2009**, *9*, S293.
- (74) Uemura, K.; Onishi, F.; Yamasaki, Y.; Kita, H. *J. Solid State Chem.* **2009**, *182*, 2852.
- (75) Jasuja, H.; Huang, Y.-g.; Walton, K. S. *Langmuir* **2012**, *28*, 16874.
- (76) Jasuja, H.; Burtch, N. C.; Huang, Y.-G.; Cai, Y.; Walton, K. S. *Langmuir* **2013**, *29*, 633.
- (77) Jasuja, H.; Walton, K. S. *Dalton Trans.* **2013**, *42*, 15421.
- (78) Kondo, A.; Daimaru, T.; Noguchi, H.; Ohba, T.; Kaneko, K.; Kanob, H. *J. Colloid Interface Sci.* **2007**, *314*, 422.
- (79) Hou, C.; Liu, Q.; Wang, P.; Sun, W.-Y. *Microporous Mesoporous Mater.* **2013**, *172*, 61.
- (80) Padial, N. M.; Quartapelle Procopio, E.; Montoro, C.; Lopez, E.; Enrique Oltra, J.; Colombo, V.; Maspero, A.; Masciocchi, N.; Galli, S.; Senkovska, I.; Kaskel, S.; Barea, E.; Navarro, J. A. R. *Angew. Chem., Int. Ed.* **2013**, *52*, 8290.
- (81) Lin, X.; Blake, A. J.; Wilson, C.; Sun, X. Z.; Champness, N. R.; George, M. W.; Hubberstey, P.; Mokaya, R.; Schroder, M. *J. Am. Chem. Soc.* **2006**, *128*, 10745.
- (82) Xie, L.-H.; Suh, M. P. *Chem.—Eur. J.* **2011**, *17*, 13653.
- (83) Kundu, T.; Sahoo, S. C.; Banerjee, R. *Cryst. Growth Des.* **2012**, *12*, 4633.
- (84) Chen, T. H.; Popov, I.; Zenasni, O.; Daugulis, O.; Miljanic, O. S. *Chem. Commun.* **2013**, *49*, 6846.
- (85) Kundu, T.; Sahoo, S. C.; Saha, S.; Banerjee, R. *Chem. Commun.* **2013**, *49*, 5262.
- (86) Kundu, T.; Sahoo, S. C.; Banerjee, R. *CrystEngComm* **2013**, *15*, 9634.
- (87) Racles, C.; Shova, S.; Cazacu, M.; Timpu, D. *Polymer* **2013**, *54*, 6096.
- (88) Tsymbal, L. V.; Andriichuk, I. L.; Yaremov, P. S.; Ilyin, V. G.; Lampeka, Y. D. *Theor. Exp. Chem.* **2013**, *49*, 270.
- (89) Weston, M. H.; Delaquil, A. A.; Sarjeant, A. A.; Farha, O. K.; Edu, J. H. N.; Nguyen, S. T. *Cryst. Growth Des.* **2013**, *13*, 2938.
- (90) Zhang, J.-P.; Chen, X.-M. *J. Am. Chem. Soc.* **2008**, *130*, 6010.
- (91) Serre, C. *Angew. Chem., Int. Ed.* **2012**, *51*, 6048.
- (92) Yang, C.; Kaipa, U.; Mather, Q. Z.; Wang, X.; Nesterov, V.; Venero, A. F.; Omary, M. A. *J. Am. Chem. Soc.* **2011**, *133*, 18094.
- (93) Borjigin, T.; Sun, F.; Zhang, J.; Cai, K.; Ren, H.; Zhu, G. *Chem. Commun.* **2012**, *48*, 7613.
- (94) Burd, S. D.; Ma, S.; Perman, J. A.; Sikora, B. J.; Snurr, R. Q.; Thallapally, P. K.; Tian, J.; Wojtas, L.; Zaworotko, M. J. *J. Am. Chem. Soc.* **2012**, *134*, 3663.
- (95) Li, T.; Chen, D.-L.; Sullivan, J. E.; Kozlowski, M. T.; Johnson, J. K.; Rosi, N. L. *Chem. Sci.* **2013**, *4*, 1746.
- (96) Wade, C. R.; Corrales-Sanchez, T.; Narayan, T. C.; Dinca, M. *Energy Environ. Sci.* **2013**, *6*, 2172.
- (97) Cmarik, G. E.; Kim, M.; Cohen, S. M.; Walton, K. S. *Langmuir* **2012**, *28*, 15606.
- (98) DeCoste, J. B.; Peterson, G. W.; Jasuja, H.; Glover, T. G.; Huang, Y.-g.; Walton, K. S. *J. Mater. Chem. A* **2013**, *1*, 5642.

- (99) Jasuja, H.; Zang, J.; Sholl, D. S.; Walton, K. S. *J. Phys. Chem. C* **2012**, *116*, 23526.
- (100) Jasuja, H.; Walton, K. S. *J. Phys. Chem. C* **2013**, *117*, 7062.
- (101) Guillerm, V.; Ragon, F.; Dan-Hardi, M.; Devic, T.; Vishnuvarthan, M.; Campo, B.; Vimont, A.; Clet, G.; Yang, Q.; Maurin, G.; Ferey, G.; Vittadini, A.; Gross, S.; Serre, C. *Angew. Chem., Int. Ed.* **2012**, *51*, 9267.
- (102) Schaate, A.; Duehnens, S.; Platz, G.; Lilenthal, S.; Schneider, A. M.; Behrens, P. *Eur. J. Inorg. Chem.* **2012**, *790*.
- (103) Zhang, W.; Huang, H.; Liu, D.; Yang, Q.; Xiao, Y.; Ma, Q.; Zhong, C. *Microporous Mesoporous Mater.* **2013**, *171*, 118.
- (104) Deria, P.; Mondloch, J. E.; Tylianakis, E.; Ghosh, P.; Bury, W.; Snurr, R. Q.; Hupp, J. T.; Farha, O. K. *J. Am. Chem. Soc.* **2013**, *135*, 16801.
- (105) Park, K. S.; Ni, Z.; Cote, A. P.; Choi, J. Y.; Huang, R.; Uribe-Romo, F. J.; Chae, H. K.; O'Keeffe, M.; Yaghi, O. M. *Proc. Natl. Acad. Sci. U.S.A.* **2006**, *103*, 10186.
- (106) Zhang, K.; Lively, R. P.; Dose, M. E.; Brown, A. J.; Zhang, C.; Chung, J.; Nair, S.; Koros, W. J.; Chance, R. R. *Chem. Commun.* **2013**, *49*, 3245.
- (107) Zhang, K.; Lively, R. P.; Zhang, C.; Chance, R. R.; Koros, W. J.; Sholl, D. S.; Nair, S. *J. Phys. Chem. Lett.* **2013**, *4*, 3618.
- (108) Zhang, K.; Lively, R. P.; Zhang, C.; Koros, W. J.; Chance, R. R. *J. Phys. Chem. C* **2013**, *117*, 7214.
- (109) Zhang, Z.; Xian, S.; Xia, Q.; Wang, H.; Li, Z.; Li, J. *AIChE J.* **2013**, *59*, 2195.
- (110) Furukawa, H.; Gandara, F.; Zhang, Y.-B.; Jiang, J.; Queen, W. L.; Hudson, M. R.; Yaghi, O. M. *J. Am. Chem. Soc.* **2014**, *136*, 4369.
- (111) Ferey, G.; Serre, C. *Chem. Soc. Rev.* **2009**, *38*, 1380.
- (112) Uemura, K.; Matsuda, R.; Kitagawa, S. *J. Solid State Chem.* **2005**, *178*, 2420.
- (113) Serre, C.; Millange, F.; Thouvenot, C.; Nogues, M.; Marsolier, G.; Louer, D.; Ferey, G. *J. Am. Chem. Soc.* **2002**, *124*, 13519.
- (114) Bourrelly, S.; et al. *J. Am. Chem. Soc.* **2010**, *132*, 9488.
- (115) Loiseau, T.; Serre, C.; Huguenard, C.; Fink, G.; Taulelle, F.; Henry, M.; Bataille, T.; Ferey, G. *Chem.—Eur. J.* **2004**, *10*, 1373.
- (116) Biswas, S.; Ahnfeldt, T.; Stock, N. *Inorg. Chem.* **2011**, *50*, 9518.
- (117) Reimer, N.; Gil, B.; Marszalek, B.; Stock, N. *CrystEngComm* **2012**, *14*, 4119.
- (118) Devautour-Vinot, S.; Maurin, G.; Henn, F.; Serre, C.; Ferey, G. *Phys. Chem. Chem. Phys.* **2010**, *12*, 12478.
- (119) Couder, F.-X.; Ortiz, A. U.; Haigis, V.; Bousquet, D.; Fuchs, A. H.; Ballandras, A.; Weber, G.; Bezverkhyy, I.; Geoffroy, N.; Bellat, J.-P.; Ortiz, G.; Chaplain, G.; Patarin, J.; Boutin, A. *J. Phys. Chem. C* **2014**, *118*, 5397.
- (120) Scherb, C.; Koehn, R.; Bein, T. *J. Mater. Chem.* **2010**, *20*, 3046.
- (121) Fukushima, T.; Horike, S.; Inubushi, Y.; Nakagawa, K.; Kubota, Y.; Takata, M.; Kitagawa, S. *Angew. Chem., Int. Ed.* **2010**, *49*, 4820.
- (122) Yamada, T.; Shirai, Y.; Kitagawa, H. *Chem.—Asian. J.* **2014**, *9*, 1316.
- (123) Sumida, K.; Rogow, D. L.; Mason, J. A.; McDonald, T. M.; Bloch, E. D.; Herm, Z. R.; Bae, T.-H.; Long, J. R. *Chem. Rev.* **2012**, *112*, 724.
- (124) D'Alessandro, D. M.; Smit, B.; Long, J. R. *Angew. Chem., Int. Ed.* **2010**, *49*, 6058.
- (125) Bae, Y.-S.; Snurr, R. Q. *Angew. Chem., Int. Ed.* **2011**, *50*, 11586.
- (126) Choi, S.; Drese, J. H.; Jones, C. W. *ChemSusChem* **2009**, *2*, 796.
- (127) Keskin, S.; van Heest, T. M.; Sholl, D. S. *ChemSusChem* **2010**, *3*, 879.
- (128) Yazaydin, A. O.; Benin, A. I.; Faheem, S. A.; Jakubczak, P.; Low, J.; Willis, R. R.; Snurr, R. Q. *Chem. Mater.* **2009**, *21*, 1425.
- (129) Yu, J.; Ma, Y.; Balbuena, P. B. *Langmuir* **2012**, *28*, 8064.
- (130) Liu, J.; Wang, Y.; Benin, A. I.; Jakubczak, P.; Willis, R. R.; LeVan, M. D. *Langmuir* **2010**, *26*, 14301.
- (131) Caskey, S. R.; Wong-Foy, A. G.; Matzger, A. J. *J. Am. Chem. Soc.* **2008**, *130*, 10870.
- (132) Kizzie, A. C.; Wong-Foy, A. G.; Matzger, A. J. *Langmuir* **2011**, *27*, 6368.
- (133) Remy, T.; Peter, S. A.; Van der Perre, S.; Valvekens, P.; De Vos, D. E.; Baron, G. V.; Denayer, J. F. M. *J. Phys. Chem. C* **2013**, *117*, 9301.
- (134) Nugent, P.; Belmabkhout, Y.; Burd, S. D.; Cairns, A. J.; Luebke, R.; Forrest, K.; Pham, T.; Ma, S.; Space, B.; Wojtas, L.; Eddaoudi, M.; Zaworotko, M. *J. Nature* **2013**, *495*, 80.
- (135) Zhang, Z.; Li, Z.; Li, J. *Langmuir* **2012**, *28*, 12122.
- (136) Babarao, R.; Jiang, J. *Energy Environ. Sci.* **2009**, *2*, 1088.
- (137) Babarao, R.; Eddaoudi, M.; Jiang, J. W. *Langmuir* **2010**, *26*, 11196.
- (138) Babarao, R.; Dai, S.; Jiang, D.-e. *Langmuir* **2011**, *27*, 3451.
- (139) Huang, H.; Zhang, W.; Liu, D.; Zhong, C. *Ind. Eng. Chem. Res.* **2012**, *51*, 10031.
- (140) Stavitski, E.; Pidko, E. A.; Couck, S.; Remy, T.; Hensen, E. J. M.; Weckhuysen, B. M.; Denayer, J.; Gascon, J.; Kapteijn, F. *Langmuir* **2011**, *27*, 3970.
- (141) Liu, Q.; Ning, L. Q.; Zheng, S. D.; Tao, M. N.; Shi, Y.; He, Y. *Sci. Rep.* **2013**, *3*, 6.
- (142) Chen, Y. F.; Babarao, R.; Sandler, S. I.; Jiang, J. W. *Langmuir* **2010**, *26*, 8743.
- (143) Chen, Y.; Jiang, J. *ChemSusChem* **2010**, *3*, 982.
- (144) Liu, B.; Smit, B. *J. Phys. Chem. C* **2010**, *114*, 8515.
- (145) Burtch, N. C.; Jasuja, H.; Dubbeldam, D.; Walton, K. S. *J. Am. Chem. Soc.* **2013**, *135*, 7172.
- (146) Li, T.; Sullivan, J. E.; Rosi, N. L. *J. Am. Chem. Soc.* **2013**, *135*, 9984.
- (147) Liu, X.; Li, Y.; Ban, Y.; Peng, Y.; Jin, H.; Bux, H.; Xu, L.; Caro, J.; Yang, W. *Chem. Commun.* **2013**, *49*, 9140.
- (148) Peterson, G. W.; Wagner, G. W.; Balboa, A.; Mahle, J.; Sewell, T.; Karwacki, C. *J. J. Phys. Chem. C* **2009**, *113*, 13906.
- (149) Glover, T. G.; Peterson, G. W.; Schindler, B. J.; Britt, D.; Yaghi, O. *Chem. Eng. Sci.* **2011**, *66*, 163.
- (150) Borfecchia, E.; Maurelli, S.; Gianolio, D.; Groppo, E.; Chiesa, M.; Bonino, F.; Lamberti, C. *J. Phys. Chem. C* **2012**, *116*, 19839.
- (151) Zou, X.; Goupil, J.-M.; Thomas, S.; Zhang, F.; Zhu, G.; Valtchev, V.; Mintova, S. *J. Phys. Chem. C* **2012**, *116*, 16593.
- (152) Ebrahim, A. M.; Levasseur, B.; Bandosz, T. *J. Langmuir* **2013**, *29*, 168.
- (153) Ebrahim, A. M.; Bandosz, T. *J. ACS Appl. Mater. Interfaces* **2013**, *5*, 10565.
- (154) Ebrahim, A. M.; Bandosz, T. *J. Microporous Mesoporous Mater.* **2014**, *188*, 149.
- (155) Ghosh, P.; Kim, K. C.; Snurr, R. Q. *J. Phys. Chem. C* **2014**, *118*, 1102.
- (156) Sava, D. F.; Chapman, K. W.; Rodriguez, M. A.; Greathouse, J. A.; Crozier, P. S.; Zhao, H.; Chupas, P. J.; Nenoff, T. M. *Chem. Mater.* **2013**, *25*, 2591.
- (157) Gutierrez-Sevillano, J. J.; Dubbeldam, D.; Bellarosa, L.; Lopez, N.; Liu, X.; Vlugt, T. J. H.; Calero, S. *J. Phys. Chem. C* **2013**, *117*, 20706.
- (158) Mito-oka, Y.; Horike, S.; Nishitani, Y.; Masumori, T.; Inukai, M.; Hijikata, Y.; Kitagawa, S. *J. Mater. Chem. A* **2013**, *1*, 7885.
- (159) McKinlay, A. C.; Eubank, J. F.; Wuttke, S.; Xiao, B.; Wheadey, P. S.; Bazin, P.; Lavallee, J. C.; Daturi, M.; Vimont, A.; De Weireld, G.; Horcajada, P.; Serre, C.; Morris, R. E. *Chem. Mater.* **2013**, *25*, 1592.
- (160) Feng, Y. F.; Jiang, H.; Li, S. N.; Wang, J.; Jing, X. Y.; Wang, Y. R.; Chen, M. *Colloids Surf., A* **2013**, *431*, 87.
- (161) Xu, F.; Kou, L.; Jia, J.; Hou, X.; Long, Z.; Wang, S. *Anal. Chim. Acta* **2013**, *804*, 240.
- (162) Yee, K. K.; Reimer, N.; Liu, J.; Cheng, S. Y.; Yiu, S. M.; Weber, J.; Stock, N.; Xu, Z. T. *J. Am. Chem. Soc.* **2013**, *135*, 7795.
- (163) Shahat, A.; Hassan, H. M. A.; Azzazy, H. M. E. *Anal. Chim. Acta* **2013**, *793*, 90.
- (164) Zou, F.; Yu, R.; Li, R.; Li, W. *ChemPhysChem* **2013**, *14*, 2825.
- (165) Meng, X.; Zhong, R.-L.; Song, X.-Z.; Song, S.-Y.; Hao, Z.-M.; Zhu, M.; Zhao, S.-N.; Zhang, H.-J. *Chem. Commun.* **2014**, *50*, 6406.
- (166) Devautour-Vinot, S.; Martineau, C.; Diaby, S.; Ben-Yahia, M.; Miller, S.; Serre, C.; Horcajada, P.; Cunha, D.; Taulelle, F.; Maurin, G. *J. Phys. Chem. C* **2013**, *117*, 11694.
- (167) Hu, Y. L.; Song, C. Y.; Liao, J.; Huang, Z. L.; Li, G. K. *J. Chromatogr. A* **2013**, *1294*, 17.
- (168) Hasan, Z.; Jeon, J.; Jhung, S. H. *J. Hazard. Mater.* **2012**, *209*, 151.

- (169) Zhao, X.; Liu, D.; Huang, H.; Zhang, W.; Yang, Q.; Zhong, C. *Microporous Mesoporous Mater.* **2014**, *185*, 72.
- (170) Xie, L.; Liu, D.; Huang, H.; Yang, Q.; Zhong, C. *Chem. Eng. J.* **2014**, *246*, 142.
- (171) Jhung, S.; Lee, J.-H.; Yoon, J.; Serre, C.; Ferey, G.; Chang, J.-S. *Adv. Mater.* **2007**, *19*, 121.
- (172) Jiang, J.-Q.; Yang, C.-X.; Yan, X.-P. *ACS Appl. Mater. Interfaces* **2013**, *5*, 9837.
- (173) Kim, H.-Y.; Kim, S.-N.; Kim, J.; Ahn, W.-S. *Mater. Res. Bull.* **2013**, *48*, 4499.
- (174) Yang, X. Q.; Yang, C. X.; Yan, X. P. *J. Chromatogr. A* **2013**, *1304*, 28.
- (175) Kang, X. Z.; Song, Z. W.; Shi, Q.; Dong, J. X. *Asian J. Chem.* **2013**, *25*, 8324.
- (176) Li, X. J.; Zheng, L. Y.; Huang, L. Z.; Zheng, O.; Lin, Z. Y.; Guo, L. H.; Qiu, B.; Chen, G. N. *J. Appl. Polym. Sci.* **2013**, *129*, 2857.
- (177) Tong, M. M.; Liu, D. H.; Yang, Q. Y.; Devautour-Vinot, S.; Maurin, G.; Zhong, C. L. *J. Mater. Chem. A* **2013**, *1*, 8534.
- (178) Wong, K. L.; Law, G. L.; Yang, Y. Y.; Wong, W. T. *Adv. Mater.* **2006**, *18*, 1051.
- (179) Huang, X.-X.; Qiu, L.-G.; Zhang, W.; Yuan, Y.-P.; Jiang, X.; Xie, A.-J.; Shen, Y.-H.; Zhu, J.-F. *CrystEngComm* **2012**, *14*, 1613.
- (180) Huo, S.-H.; Yan, X.-P. *J. Mater. Chem.* **2012**, *22*, 7449.
- (181) Haque, E.; Lee, J. E.; Jang, I. T.; Hwang, Y. K.; Chang, J.-S.; Jegal, J.; Jhung, S. H. *J. Hazard. Mater.* **2010**, *181*, 535.
- (182) Maes, M.; Schouteden, S.; Alaerts, L.; Depla, D.; De Vos, D. E. *Phys. Chem. Chem. Phys.* **2011**, *13*, 5587.
- (183) Tan, Y.-X.; He, Y.-P.; Wang, M.; Zhang, J. *RSC Adv.* **2014**, *4*, 1480.
- (184) Leng, F.; Wang, W.; Zhao, X. J.; Hu, X. L.; Li, Y. F. *Colloid Surf., A* **2014**, *441*, 164.
- (185) Lin, S.; Song, Z.; Che, G.; Ren, A.; Li, P.; Liu, C.; Zhang, J. *Microporous Mesoporous Mater.* **2014**, *193*, 27.
- (186) Jung, B. K.; Hasan, Z.; Jhung, S. H. *Chem. Eng. J.* **2013**, *234*, 99.
- (187) Saint Remi, J. C.; Baron, G.; Denayer, J. *Adsorption* **2012**, *18*, 367.
- (188) Chen, B.; Ji, Y.; Xue, M.; Fronczek, F. R.; Hurtado, E. J.; Mondal, J. U.; Liang, C.; Dai, S. *Inorg. Chem.* **2008**, *47*, 5543.
- (189) Kosal, M. E.; Chou, J. H.; Wilson, S. R.; Suslick, K. S. *Nat. Mater.* **2002**, *1*, 118.
- (190) Yang, C. X.; Ren, H. B.; Yan, X. P. *Anal. Chem.* **2013**, *85*, 7441.
- (191) Hinterholzinger, F. M.; Ruhle, B.; Wuttke, S.; Karaghiosoff, K.; Bein, T. *Sci. Rep.* **2013**, *3*, 2562.
- (192) Jiang, H.-L.; Feng, D.; Wang, K.; Gu, Z.-Y.; Wei, Z.; Chen, Y.-P.; Zhou, H.-C. *J. Am. Chem. Soc.* **2013**, *135*, 13934.
- (193) Aguilera-Sigalat, J.; Bradshaw, D. *Chem. Commun.* **2014**, *50*, 4711.
- (194) Bai, Y.; He, G. J.; Zhao, Y. G.; Duan, C. Y.; Dang, D. B.; Meng, Q. *J. Chem. Commun.* **2006**, 1530.
- (195) Yang, Q.; Liu, D.; Zhong, C.; Li, J.-R. *Chem. Rev.* **2013**, *113*, 8261.
- (196) Dueren, T.; Bae, Y.-S.; Snurr, R. Q. *Chem. Soc. Rev.* **2009**, *38*, 1237.
- (197) Dubbeldam, D.; Snurr, R. Q. *Mol. Simul.* **2007**, *33*, 305.
- (198) Dubbeldam, D.; Torres-Knoop, A.; Walton, K. S. *Mol. Simul.* **2013**, *39*, 1253.
- (199) Keskin, S.; Liu, J.; Rankin, R. B.; Johnson, J. K.; Sholl, D. S. *Ind. Eng. Chem. Res.* **2009**, *48*, 2355.
- (200) Fang, H.; Demir, H.; Kamakoti, P.; Sholl, D. S. *J. Mater. Chem. A* **2014**, *2*, 274.
- (201) Frenkel, D.; Smit, B. *Understanding Molecular Simulation: From Algorithms to Applications*; Elsevier Science: New York, 2001.
- (202) Wu, H.; Chua, Y.; Krungleviciute, V. *J. Am. Chem. Soc.* **2013**, *135*, 10525.
- (203) Grosch, J. S.; Paesani, F. *J. Am. Chem. Soc.* **2012**, *134*, 4207.
- (204) Tafipolsky, M.; Amirjalayer, S.; Schmid, R. *J. Comput. Chem.* **2007**, *28*, 1169.
- (205) Zheng, B.; Sant, M.; Demontis, P.; Suffritti, G. B. *J. Phys. Chem. C* **2012**, *116*, 933.
- (206) Zhao, L.; Yang, Q.; Ma, Q.; Zhong, C.; Mi, J.; Liu, D. *J. Mol. Model.* **2011**, *17*, 227.
- (207) Dubbeldam, D.; Walton, K. S.; Ellis, D. E.; Snurr, R. Q. *Angew. Chem., Int. Ed.* **2007**, *46*, 4496.
- (208) Salles, F.; Ghoufi, A.; Maurin, G.; Bell, R. G.; Mellot-Draznieks, C.; Ferey, G. *Angew. Chem., Int. Ed.* **2008**, *47*, 8487.
- (209) Watanabe, T.; Sholl, D. S. *Langmuir* **2012**, *28*, 14114.
- (210) Wilmer, C. E.; Leaf, M.; Lee, C. Y.; Farha, O. K.; Hauser, B. G.; Hupp, J. T.; Snurr, R. Q. *Nat. Chem.* **2012**, *4*, 83.
- (211) Wu, H.; Gong, Q.; Olson, D. H.; Li, J. *Chem. Rev.* **2012**, *112*, 836.
- (212) Ball, P. *Nature* **2008**, *452*, 291.
- (213) Guillot, B. *J. Mol. Liq.* **2002**, *101*, 219.
- (214) Cicu, P.; Demontis, P.; Spanu, S.; Suffritti, G. B.; Tilocca, A. J. *Chem. Phys.* **2000**, *112*, 8267.
- (215) Paranthaman, S.; Coudert, F. X.; Fuchs, A. H. *Phys. Chem. Chem. Phys.* **2010**, *12*, 8123.
- (216) Castillo, J. M.; Dubbeldam, D.; Vlugt, T. J. H.; Smit, B.; Calero, S. *Mol. Simul.* **2009**, *35*, 1067.
- (217) Trzpit, M.; Soulard, M.; Patarin, J.; Desbiens, N.; Cailliez, F.; Boutin, A.; Demachy, I.; Fuchs, A. H. *Langmuir* **2007**, *23*, 10131.
- (218) Ramachandran, C. E.; Chempath, S.; Broadbelt, L. J.; Snurr, R. Q. *Microporous Mesoporous Mater.* **2006**, *90*, 293.
- (219) Halasz, I.; Kim, S.; Marcus, B. *Mol. Phys.* **2002**, *100*, 3123.
- (220) Di Lella, A.; Desbiens, N.; Boutin, A.; Demachy, I.; Ungerer, P.; Bellat, J.-P.; Fuchs, A. H. *Phys. Chem. Chem. Phys.* **2006**, *8*, 5396.
- (221) Cailliez, F.; Trzpit, M.; Soulard, M.; Demachy, I.; Boutin, A.; Patarin, J.; Fuchs, A. H. *Phys. Chem. Chem. Phys.* **2008**, *10*, 4817.
- (222) Desbiens, N.; Boutin, A.; Demachy, I. *J. Phys. Chem. B* **2005**, *109*, 24071.
- (223) Puibasset, J.; Pellenq, R. J. M. *J. Phys. Chem. B* **2008**, *112*, 6390.
- (224) Pellenq, R. J. M.; Roussel, T.; Puibasset, J. *Adsorption* **2008**, *14*, 733.
- (225) Desbiens, N.; Demachy, I.; Fuchs, A. H.; Kirsch-Rodeschini, H.; Soulard, M.; Patarin, J. *Angew. Chem., Int. Ed.* **2005**, *44*, 5310.
- (226) Mayo, S. L.; Olafson, B. D.; Goddard, W. A. *J. Phys. Chem.* **1990**, *94*, 8897.
- (227) Rappe, A. K.; Casewit, C. J.; Colwell, K. S.; Goddard, W. A.; Skiff, W. M. *J. Am. Chem. Soc.* **1992**, *114*, 10024.
- (228) Salles, F.; Bourrelly, S.; Jobic, H.; Devic, T.; Guillerm, V.; Llewellyn, P.; Serre, C.; Maurin, G. *J. Phys. Chem. C* **2011**, *115*, 10764.
- (229) Coudert, F.-X.; Cailliez, F.; Vuilleumier, R.; Fuchs, A. H.; Boutin, A. *Faraday Discuss.* **2009**, *141*, 377.
- (230) Bordat, P.; Cazade, P.-A.; Baraille, I.; Brown, R. *J. Chem. Phys.* **2010**, *132*, 094501.
- (231) Ortiz, A. U.; Freitas, A. P.; Boutin, A.; Fuchs, A. H.; Coudert, F.-X. *Phys. Chem. Chem. Phys.* **2014**, *16*, 9940.
- (232) Abascal, J. L. F.; Vega, C. *J. Chem. Phys.* **2005**, *123*, 1574.
- (233) Dubbeldam, D.; Krishna, R.; Snurr, R. Q. *J. Phys. Chem. C* **2009**, *113*, 19317.
- (234) Cirera, J.; Sung, J. C.; Howland, P. B.; Paesani, F. *J. Chem. Phys.* **2012**, *137*, 054704.
- (235) Fanourgakis, G. S.; Xantheas, S. S. *J. Chem. Phys.* **2008**, *128*, 074506.
- (236) Zang, J.; Nair, S.; Sholl, D. S. *J. Phys. Chem. C* **2013**, *117*, 7519.
- (237) Paesani, F. *Mol. Simul.* **2012**, *38*, 631.
- (238) Sadakiyo, M.; Okawa, H.; Shigematsu, A.; Ohba, M.; Yamada, T.; Kitagawa, H. *J. Am. Chem. Soc.* **2012**, *134*, 5472.
- (239) Hurd, J. A.; Vaidhyanathan, R.; Thangadurai, V.; Ratcliffe, C. I.; Moudrakovski, I. L.; Shimizu, G. K. H. *Nat. Chem.* **2009**, *1*, 705.
- (240) Ramaswamy, P.; Matsuda, R.; Kosaka, W.; Akiyama, G.; Jeon, H. J.; Kitagawa, S. *Chem. Commun.* **2014**, *50*, 1144.
- (241) Nagarkar, S. S.; Unni, S. M.; Sharma, A.; Kurungot, S.; Ghosh, S. K. *Angew. Chem., Int. Ed.* **2014**, *53*, 2638.
- (242) Shigematsu, A.; Yamada, T.; Kitagawa, H. *J. Am. Chem. Soc.* **2011**, *133*, 2034.
- (243) Mallick, A.; Kundu, T.; Banerjee, R. *Chem. Commun.* **2012**, *48*, 8829.

- (244) Sahoo, S. C.; Kundu, T.; Banerjee, R. *J. Am. Chem. Soc.* **2011**, *133*, 17950.
- (245) Taylor, J. M.; Mah, R. K.; Moudrakovski, I. L.; Ratcliffe, C. I.; Vaidyanathan, R.; Shimizu, G. K. H. *J. Am. Chem. Soc.* **2010**, *132*, 14055.
- (246) Kim, S.; Dawson, K. W.; Gelfand, B. S.; Taylor, J. M.; Shimizu, G. K. H. *J. Am. Chem. Soc.* **2013**, *135*, 963.
- (247) Colodrero, R. M. P.; Olivera-Pastor, P.; Losilla, E. R.; Aranda, M. A. G.; Leon-Reina, L.; Papadaki, M.; McKinlay, A. C.; Morris, R. E.; Demadis, K. D.; Cabeza, A. *Dalton Trans.* **2012**, *41*, 4045.
- (248) Colodrero, R. M. P.; Olivera-Pastor, P.; Losilla, E. R.; Hernandez-Alonso, D.; Aranda, M. A. G.; Leon-Reina, L.; Rius, J.; Demadis, K. D.; Moreau, B.; Villemin, D.; Palomino, M.; Rey, F.; Cabeza, A. *Inorg. Chem.* **2012**, *51*, 7689.
- (249) Pardo, E.; Train, C.; Gontard, G.; Boubekeur, K.; Fabelo, O.; Liu, H.; Dkhil, B.; Lloret, F.; Nakagawa, K.; Tokoro, H.; Ohkoshi, S.-i.; Verdaguera, M. *J. Am. Chem. Soc.* **2011**, *133*, 15328.
- (250) Sadakiyo, M.; Yamada, T.; Kitagawa, H. *J. Am. Chem. Soc.* **2009**, *131*, 9906.
- (251) Sen, S.; Nair, N. N.; Yamada, T.; Kitagawa, H.; Bharadwaj, P. K. *J. Am. Chem. Soc.* **2012**, *134*, 19432.
- (252) Horike, S.; Kamitsubo, Y.; Inukai, M.; Fukushima, T.; Umeyama, D.; Itakura, T.; Kitagawa, S. *J. Am. Chem. Soc.* **2013**, *135*, 4612.
- (253) Wu, B.; Lin, X.; Ge, L.; Wu, L.; Xu, T. *Chem. Commun.* **2013**, *49*, 143.
- (254) Paesani, F. *J. Phys. Chem. C* **2013**, *117*, 19508.
- (255) Nijem, N.; Canepa, P.; Kaipa, U.; Tan, K.; Roodenko, K.; Tekarli, S.; Halbert, J.; Oswald, I. W. H.; Arvapally, R. K.; Yang, C.; Thonhauser, T.; Omary, M. a.; Chabal, Y. *J. Am. Chem. Soc.* **2013**, *135*, 12615.
- (256) Rasaiah, J. C.; Garde, S.; Hummer, G. *Annu. Rev. Phys. Chem.* **2008**, *59*, 713.
- (257) Hughes, J. T.; Navrotsky, A. *J. Am. Chem. Soc.* **2011**, *133*, 9184.
- (258) Hughes, J. T.; Bennett, T. D.; Cheetham, A. K.; Nayrotsky, A. *J. Am. Chem. Soc.* **2013**, *135*, 598.
- (259) Gee, J. A.; Sholl, D. S. *J. Phys. Chem. C* **2013**, *117*, 20636.
- (260) Choi, H. J.; Dinca, M.; Dailly, A.; Long, J. R. *Energy Environ. Sci.* **2010**, *3*, 117.
- (261) Colombo, V.; Galli, S.; Choi, H. J.; Han, G. D.; Maspero, A.; Palmisano, G.; Masciocchi, N.; Long, J. R. *Chem. Sci.* **2011**, *2*, 1311.
- (262) Hilal, S. H.; Karickhoff, S. W.; Carreira, L. A. *Quant. Struct.-Act. Relat.* **1995**, *14*, 348 DOI: 10.1002/qsar.19950140405.
- (263) Jiang, H.-L.; Feng, D.; Liu, T.-F.; Li, J.-R.; Zhou, H.-C. *J. Am. Chem. Soc.* **2012**, *134*, 14690.
- (264) Feng, D.; Gu, Z.-Y.; Li, J.-R.; Jiang, H.-L.; Wei, Z.; Zhou, H.-C. *Angew. Chem., Int. Ed.* **2012**, *51*, 10307.
- (265) Morris, W.; Voloskiy, B.; Demir, S.; Gandara, F.; McGrier, P. L.; Furukawa, H.; Cascio, D.; Stoddart, J. F.; Yaghi, O. M. *Inorg. Chem.* **2012**, *51*, 6443.
- (266) Feng, D.; Chung, W.-C.; Wei, Z.; Gu, Z.-Y.; Jiang, H.-L.; Chen, Y.-P.; Darenbourg, D. J.; Zhou, H.-C. *J. Am. Chem. Soc.* **2013**, *135*, 17105.
- (267) Pearson, R. G. *J. Am. Chem. Soc.* **1963**, *85*, 3533.
- (268) Kang, I. J.; Khan, N. A.; Haque, E.; Jhung, S. H. *Chem.—Eur. J.* **2011**, *17*, 6437.
- (269) Irving, H.; Williams, R. J. P. *J. Chem. Soc.* **1953**, 3192.
- (270) Liu, J.; Benin, A. I.; Furtado, A. M. B.; Jakubczak, P.; Willis, R. R.; LeVan, M. D. *Langmuir* **2011**, *27*, 11451.
- (271) Pauling, L. *J. Am. Chem. Soc.* **1929**, *51*, 1010.
- (272) Bellarosa, L.; Calero, S.; Lopez, N. *Phys. Chem. Chem. Phys.* **2012**, *14*, 7240.
- (273) Hausdorf, S.; Baitalow, F.; Bohle, T.; Rafaja, D.; Mertens, F. J. *Am. Chem. Soc.* **2010**, *132*, 10978.
- (274) Cai, Y.; Zhang, Y.; Huang, Y.; Marder, S. R.; Walton, K. S. *Cryst. Growth Des.* **2012**, *12*, 3709.
- (275) Makal, T. A.; Wang, X.; Zhou, H.-C. *Cryst. Growth Des.* **2013**, *13*, 4760.
- (276) Liu, H.; Zhao, Y.; Zhang, Z.; Nijem, N.; Chabal, Y. J.; Peng, X.; Zeng, H.; Li, J. *Chem.—Asian J.* **2013**, *8*, 674.
- (277) DeCoste, J. B.; Peterson, G. W.; Smith, M. W.; Stone, C. A.; Willis, C. R. *J. Am. Chem. Soc.* **2012**, *134*, 1486.
- (278) Bellarosa, L.; Gutierrez-Sevillano, J. J.; Calero, S.; Lopez, N. *Phys. Chem. Chem. Phys.* **2013**, *15*, 17696.
- (279) Bellarosa, L.; Manuel Castillo, J.; Vlugt, T.; Calero, S.; Lopez, N. *Chem.—Eur. J.* **2012**, *18*, 12260.
- (280) De Toni, M.; Jonchiere, R.; Pullumbi, P.; Coudert, F.-X.; Fuchs, A. H. *ChemPhysChem* **2012**, *13*, 3497.
- (281) Duan, J.; Higuchi, M.; Horike, S.; Foo, M. L.; Rao, K. P.; Inubushi, Y.; Fukushima, T.; Kitagawa, S. *Adv. Funct. Mater.* **2013**, *23*, 3525.
- (282) Kolokolov, D. I.; Stepanov, A. G.; Guillerm, V.; Serre, C.; Frick, B.; Jobic, H. *J. Phys. Chem. C* **2012**, *116*, 12131.
- (283) Mondloch, J. E.; Katz, M. J.; Planas, N.; Semrouni, D.; Gagliardi, L.; Hupp, J. T.; Farha, O. K. *Chem. Commun.* **2014**, 274.
- (284) Murdock, C. R.; Hughes, B. C.; Lu, Z.; Jenkins, D. M. *Coord. Chem. Rev.* **2014**, *258*, 119.
- (285) Serre, C.; Bourrelly, S.; Vimont, A.; Ramsahye, N. A.; Maurin, G.; Llewellyn, P.; Daturi, M.; Filinchuk, Y.; Leynaud, O.; Barnes, P.; Ferey, G. *Adv. Mater.* **2007**, *19*, 2246.
- (286) Uemura, K.; Yamasaki, Y.; Komagawa, Y.; Tanaka, K.; Kita, H. *Angew. Chem., Int. Ed.* **2007**, *46*, 6662.
- (287) Uemura, K.; Yamasaki, Y.; Onishi, F.; Kita, H.; Ebihara, M. *Inorg. Chem.* **2010**, *49*, 10133.
- (288) Henke, S.; Schneemann, A.; Wuetscher, A.; Fischer, R. A. *J. Am. Chem. Soc.* **2012**, *134*, 9464.
- (289) Kitaura, R.; Seki, K.; Akiyama, G.; Kitagawa, S. *Angew. Chem., Int. Ed.* **2003**, *42*, 428.
- (290) Cheng, Y.; Kajiro, H.; Noguchi, H.; Kondo, A.; Ohba, T.; Hattori, Y.; Kaneko, K.; Kanoh, H. *Langmuir* **2011**, *27*, 6905.
- (291) Mu, B.; Li, F.; Huang, Y.; Walton, K. S. *J. Mater. Chem.* **2012**, *22*, 10172.
- (292) Han, S.; Huang, Y.; Watanabe, T.; Nair, S.; Walton, K. S.; Sholl, D. S.; Carson Meredith, J. *Microporous Mesoporous Mater.* **2013**, *173*, 86.
- (293) Han, S.; Huang, Y.; Watanabe, T.; Dai, Y.; Walton, K. S.; Nair, S.; Sholl, D. S.; Meredith, J. C. *ACS Comb. Sci.* **2012**, *14*, 263.
- (294) Hamon, L.; Leclerc, H.; Ghoufi, A.; Oliviero, L.; Travert, A.; Lavalle, J. C.; Devic, T.; Serre, C.; Ferey, G.; De Weireld, G.; Vimont, A.; Maurin, G. *J. Phys. Chem. C* **2011**, *115*, 2047.
- (295) Chavan, S.; Bonino, F.; Valenzano, L.; Civalleri, B.; Lamberti, C.; Acerbi, N.; Cavka, J. H.; Leistner, M.; Bordiga, S. *J. Phys. Chem. C* **2013**, *117*, 15615.
- (296) Saha, D.; Deng, S. *J. Colloid Interface Sci.* **2010**, *348*, 615.
- (297) Demessence, A.; D'Alessandro, D. M.; Foo, M. L.; Long, J. R. *J. Am. Chem. Soc.* **2009**, *131*, 8784.
- (298) Lu, Z.; Xing, H.; Sun, R.; Bai, J.; Zheng, B.; Li, Y. *Cryst. Growth Des.* **2012**, *12*, 1081.
- (299) Čelić, T. B.; Mazaj, M.; Mali, G.; Kaučič, V.; Logar, N. Z. *Proceedings of the 5th Serbian-Croatian-Slovenian Symposium on Zeolites 2013*, XX.
- (300) Yang, S.; Sun, J.; Ramirez-Cuesta, A. J.; Callear, S. K.; David, W. I. F.; Anderson, D. P.; Newby, R.; Blake, A. J.; Parker, J. E.; Tang, C. C.; Schroeder, M. *Nat. Chem.* **2012**, *4*, 887.
- (301) Akiyama, G.; Matsuda, R.; Sato, H.; Takata, M.; Kitagawa, S. *Adv. Mater.* **2011**, *23*, 3294.
- (302) Sindoro, M.; Jee, A.-Y.; Granick, S. *Chem. Commun.* **2013**, *49*, 9576.
- (303) Fateeva, A.; Chater, P. A.; Ireland, C. P.; Tahir, A. A.; Khimyak, Y. Z.; Wiper, P. V.; Darwent, J. R.; Rosseinsky, M. J. *Angew. Chem., Int. Ed.* **2012**, *51*, 7440.
- (304) Taddei, M.; Ienco, A.; Costantino, F.; Guerri, A. *RSC Adv.* **2013**, *3*, 26177.
- (305) Jia, Y.; Li, H.; Zhao, B.; Guo, Q.; Hou, H.; Fan, Y. *Eur. J. Inorg. Chem.* **2013**, *2013*, 438.
- (306) Taylor, J. M.; Dawson, K. W.; Shimizu, G. K. H. *J. Am. Chem. Soc.* **2013**, *135*, 1193.
- (307) Qian, X.; Yadian, B.; Wu, R.; Long, Y.; Zhou, K.; Zhu, B.; Huang, Y. *Int. J. Hydrogen Energy* **2013**, *38*, 16710.
- (308) Ma, D.; Li, Y.; Li, Z. *Chem. Commun.* **2011**, *47*, 7377.

- (309) Liu, H.; Zhao, Y.; Zhang, Z.; Nijem, N.; Chabal, Y. J.; Zeng, H.; Li, J. *Adv. Funct. Mater.* **2011**, *21*, 4754.
- (310) Yang, Q.; Guillerm, V.; Ragon, F.; Wiersum, A. D.; Llewellyn, P. L.; Zhong, C.; Devic, T.; Serre, C.; Maurin, G. *Chem. Commun.* **2012**, *48*, 9831.
- (311) Kandiah, M.; Nilsen, M. H.; Usseglio, S.; Jakobsen, S.; Olsbye, U.; Tilset, M.; Larabi, C.; Quadrelli, E. A.; Bonino, F.; Lillerud, K. P. *Chem. Mater.* **2010**, *22*, 6632.
- (312) Biswas, S.; Remy, T.; Couck, S.; Denysenko, D.; Rampelberg, G.; Denayer, J. F. M.; Volkmer, D.; Detavernier, C.; Van Der Voort, P. *Phys. Chem. Chem. Phys.* **2013**, *15*, 3552.
- (313) Xiang, S.; He, Y.; Zhang, Z.; Wu, H.; Zhou, W.; Krishna, R.; Chen, B. *Nat. Commun.* **2012**, *3*, 954.
- (314) Yoon, J. W.; Jhung, S. H.; Hwang, Y. K.; Humphrey, S. M.; Wood, P. T.; Chang, J.-S. *Adv. Mater.* **2007**, *19*, 1830.
- (315) Mohamed, M. H.; Elsaidi, S. K.; Wojtas, L.; Pham, T.; Forrest, K. A.; Tudor, B.; Space, B.; Zaworotko, M. J. *J. Am. Chem. Soc.* **2012**, *134*, 19556.
- (316) Gu, J.-Z.; Lu, W.-G.; Jiang, L.; Zhou, H.-C.; Lu, T.-B. *Inorg. Chem.* **2007**, *46*, 5835.
- (317) Nagarkar, S. S.; Chaudhari, A. K.; Ghosh, S. K. *Inorg. Chem.* **2012**, *51*, 572.
- (318) Zhai, F.; Zheng, Q.; Chen, Z.; Ling, Y.; Liu, X.; Weng, L.; Zhou, Y. *CrystEngComm* **2013**, *15*, 2040.
- (319) Santra, A.; Senkovska, I.; Kaskel, S.; Bharadwaj, P. K. *Inorg. Chem.* **2013**, *52*, 7358.
- (320) Li, Y.; Ju, Z.; Wu, B.; Yuan, D. *Cryst. Growth Des.* **2013**, *13*, 4125.
- (321) Xue, D.-X.; Cairns, A. J.; Belmabkhout, Y.; Wojtas, L.; Liu, Y.; Alkordi, M. H.; Eddaoudi, M. *J. Am. Chem. Soc.* **2013**, *135*, 7660.
- (322) Biswas, S.; Van Der Voort, P. *Eur. J. Inorg. Chem.* **2013**, *2013*, 2154.
- (323) Biswas, S.; Zhang, J.; Li, Z. B.; Liu, Y. Y.; Grzywa, M.; Sun, L. X.; Volkmer, D.; Van der Voort, P. *Dalton Trans.* **2013**, *42*, 4730.
- (324) Wissmann, G.; Schaafe, A.; Lilienthal, S.; Bremer, I.; Schneider, A. M.; Behrens, P. *Microporous Mesoporous Mater.* **2012**, *152*, 64.
- (325) Chmelik, C.; Mundstock, A.; Dietzel, P. D. C.; Caro, J. *Microporous Mesoporous Mater.* **2014**, *183*, 117.
- (326) Rezk, A.; Al-Dadah, R.; Mahmoud, S.; Elsayed, A. *Proc. Inst. Mech. Eng., Part C* **2013**, *227*, 992.
- (327) Karra, J. R.; Grabicka, B. E.; Huang, Y.-G.; Walton, K. S. *J. Colloid Interface Sci.* **2013**, *392*, 331.
- (328) Yoo, Y.; Varela-Guerrero, V.; Jeong, H.-K. *Langmuir* **2011**, *27*, 2652.
- (329) Liu, Z.; Fujita, N.; Miyasaka, K.; Han, L.; Stevens, S. M.; Suga, M.; Asahina, S.; Slater, B.; Xiao, C.; Sakamoto, Y.; Anderson, M. W.; Ryoo, R.; Terasaki, O. *J. Electron Microsc.* **2013**, *62*, 109.
- (330) Ameloot, R.; Vermoortele, F.; Hofkens, J.; De Schryver, F. C.; De Vos, D. E.; Roeffaers, M. B. *J. Angew. Chem., Int. Ed.* **2013**, *52*, 401.
- (331) Moh, P. Y.; Cubillas, P.; Anderson, M. W.; Attfield, M. P. *J. Am. Chem. Soc.* **2011**, *133*, 13304.
- (332) Kolokolov, D. I.; Jobic, H.; Stepanov, A. G.; Guillerm, V.; Devic, T.; Serre, C.; Fverey, G. *Angew. Chem., Int. Ed.* **2010**, *49*, 4791.
- (333) Springuel-Huet, M.-A.; Nossov, A.; Adem, Z.; Guenneau, F.; Volkringer, C.; Loiseau, T.; Ferey, G.; Gedeon, A. *J. Am. Chem. Soc.* **2010**, *132*, 11599.
- (334) Klein, N.; Herzog, C.; Sabo, M.; Senkovska, I.; Getzschmann, J.; Paasch, S.; Lohe, M. R.; Brunner, E.; Kaskel, S. *Phys. Chem. Chem. Phys.* **2010**, *12*, 11778.
- (335) Hoffmann, H. C.; Assfour, B.; Epperlein, F.; Klein, N.; Paasch, S.; Senkovska, I.; Kaskel, S.; Seifert, G.; Brunner, E. *J. Am. Chem. Soc.* **2011**, *133*, 8681.
- (336) Garcia-Ricard, O. J.; Fu, R.; Hernandez-Maldonado, A. J. *J. Phys. Chem. C* **2011**, *115*, 3595.
- (337) Hoffmann, H.; Debowski, M.; Muller, P.; Paasch, S.; Senkovska, I.; Kaskel, S.; Brunner, E. *Materials* **2012**, *5*, 2537.
- (338) Bordiga, S.; Bonino, F.; Lillerud, K. P.; Lamberti, C. *Chem. Soc. Rev.* **2010**, *39*, 4885.
- (339) Liu, M.; Wong-Foy, A. G.; Vallery, R. S.; Frieze, W. E.; Schnobrich, J. K.; Gidley, D. W.; Matzger, A. J. *Adv. Mater.* **2010**, *22*, 1598.
- (340) Bentrup, U. *Chem. Soc. Rev.* **2010**, *39*, 4718.
- (341) Lifson, S.; Hagler, A. T.; Dauber, P. *J. Am. Chem. Soc.* **1979**, *101*, 5111.
- (342) Greathouse, J. A.; Allendorf, M. D. *J. Am. Chem. Soc.* **2006**, *128*, 10678.
- (343) Han, S. S.; Choi, S.-H.; van Duin, A. C. T. *Chem. Commun.* **2010**, *46*, 5713.
- (344) van Duin, A. C. T.; Dasgupta, S.; Lorant, F.; Goddard, W. A. J. *Phys. Chem. A* **2001**, *105*, 9396.
- (345) Sauer, J.; Sierka, M. *J. Comput. Chem.* **2000**, *21*, 1470.
- (346) Torrie, G. M.; Valleau, J. P. *J. Comput. Phys.* **1977**, *23*, 187.
- (347) Mills, G.; Jonsson, H.; Schenter, G. K. *Surf. Sci.* **1995**, *324*, 305.
- (348) Bolhuis, P. G.; Chandler, D.; Dellago, C.; Geissler, P. L. *Annu. Rev. Phys. Chem.* **2002**, *53*, 291.
- (349) Ravon, U.; Savonnet, M.; Aguado, S.; Domine, M. E.; Janneau, E.; Farrusseng, D. *Microporous Mesoporous Mater.* **2010**, *129*, 319.
- (350) Park, T.-H.; Hickman, A. J.; Koh, K.; Martin, S.; Wong-Foy, A. G.; Sanford, M. S.; Matzger, A. J. *J. Am. Chem. Soc.* **2011**, *133*, 20138.
- (351) Goesten, M. G.; Kapteijn, F.; Gascon, J. *CrystEngComm* **2013**, *15*, 9249.
- (352) Yang, S. J.; Park, C. R. *Adv. Mater.* **2012**, *24*, 4010.
- (353) Castillo, J. M.; Vlugt, T. J. H.; Calero, S. *J. Phys. Chem. C* **2008**, *112*, 15934.
- (354) Wang, Z.; Cohen, S. M. *Chem. Soc. Rev.* **2009**, *38*, 1315.
- (355) Jiang, H.-L.; Makal, T. A.; Zhou, H.-C. *Coord. Chem. Rev.* **2013**, *257*, 2232.
- (356) Li, H.; Shi, W.; Zhao, K.; Li, H.; Bing, Y.; Cheng, P. *Inorg. Chem.* **2012**, *51*, 9200.
- (357) Szilagyi, P. A.; Serra-Crespo, P.; Dugulan, I.; Gascon, J.; Geerlings, H.; Dam, B. *CrystEngComm* **2013**, *15*, 10175.
- (358) Karagiariidi, O.; Bury, W.; Sarjeant, A. A.; Stern, C. L.; Farha, O. K.; Hupp, J. T. *Chem. Sci.* **2012**, *3*, 3256.
- (359) Bury, W.; Fairén-Jimenez, D.; Lalonde, M. B.; Snurr, R. Q.; Farha, O. K.; Hupp, J. T. *Chem. Mater.* **2013**, *25*, 739.
- (360) Takaishi, S.; DeMarco, E. J.; Pellin, M. J.; Farha, O. K.; Hupp, J. T. *Chem. Sci.* **2013**, *4*, 1509.
- (361) Kim, M.; Cahill, J. F.; Fei, H.; Prather, K. A.; Cohen, S. M. *J. Am. Chem. Soc.* **2012**, *134*, 18082.